Something To Chew On

Renders, G.A.P.

2017

document version
Publisher's PDF, also known as Version of record

Something to Chew on

The Neverending μCT Story of Bone and Cartilage

Greetje Renders

SOMETHING TO CHEW ON

THE NEVERENDING μCT STORY OF BONE AND CARTILAGE

Greetje A.P. Renders

The research in this thesis were carried out at the section of Oral Cell Biology and Functional Anatomy of the Academic Center for Dentistry Amsterdam (ACTA), University of Amsterdam and VU University Amsterdam, Research Institute MOVE, Amsterdam, the Netherlands. The studies were performed as part of the NWO Toptalent 2007 project "Consequences of mechanical interaction between cartilage and bone for development of osteoarthrosis", grant number 021.011.050.

The printing of this thesis was kindly supported by:

Academic Centre for Dentistry Amsterdam (ACTA)
The Dutch Society for Calcium and Bone Metabolism (NVCB)
Tandartsenpraktijk Vossers

Cover design:	Greetje Renders and Peter Vos
Interior design & layout:	Peter Vos (petervos1984@gmail.com)
Printing:	Proefschriftmaken, The Netherlands (2017)
ISBN:	978-94-6295-666-7
© Copyright 2017:	Greetje Anne Petronella Renders, Utrecht, The Netherlands, 2017

VRIJE UNIVERSITEIT

Something to chew on

The neverending story of bone and cartilage

ACADEMISCH PROEFSCHRIFT

ter verkrijging van de graad Doctor aan
de Vrije Universiteit Amsterdam,
op gezag van de rector magnificus
prof.dr. V. Subramaniam,
in het openbaar te verdedigen
ten overstaan van de promotiecommissie
van de Faculteit der Tandheelkunde
op vrijdag 30 juni 2017 om 11:45 uur
in Aula van de universiteit,
De Boelelaan 1105

door

Greetje Anne Petronella Renders

Geboren te Helmond

promotor: prof.dr. V. Everts

copromotor: dr. G.E.J. Langenbach

Voor Sas

committee members:	dr. M.N. Helder prof.dr. J. Klein-Nulend prof.dr. F. Lobbezoo dr.ir. L. Mulder prof.dr. T.H. Smit
paranymphs:	Catharina Rosalie Scheres Felix Paul Weijdema

CONTENTS

Chapter 1	General introduction	9
Chapter 2A	Degree and distribution of mineralization in the human mandibular condyle	21
Chapter 2B	Porosity of human mandibular condylar bone	35
Chapter 3A	Biomechanical effect of mineral heterogeneity in trabecular bone	53
Chapter 3B	Mineral heterogeneity affects predictions of intratrabecular stress and strain	67
Chapter 3C	Letter to the editor; Response to “letter to the editor”	79
Chapter 4A	Implications of high-dosage bisphosphonate-treatment on bone tissue in the knee and jaw joint	87
Chapter 4B	Bone-site-specific responses to zolendronic acid	103
Chapter 5	Contrast-enhanced μCT (EPIC-μCT) *ex vivo* applied to the mouse and human jaw joint	121
Chapter 6	General discussion	137
	General summary	145
	Algemene samenvatting	153
	References	163
	Dankwoord	187
	Over de auteur	203

CHAPTER 1

GENERAL INTRODUCTION

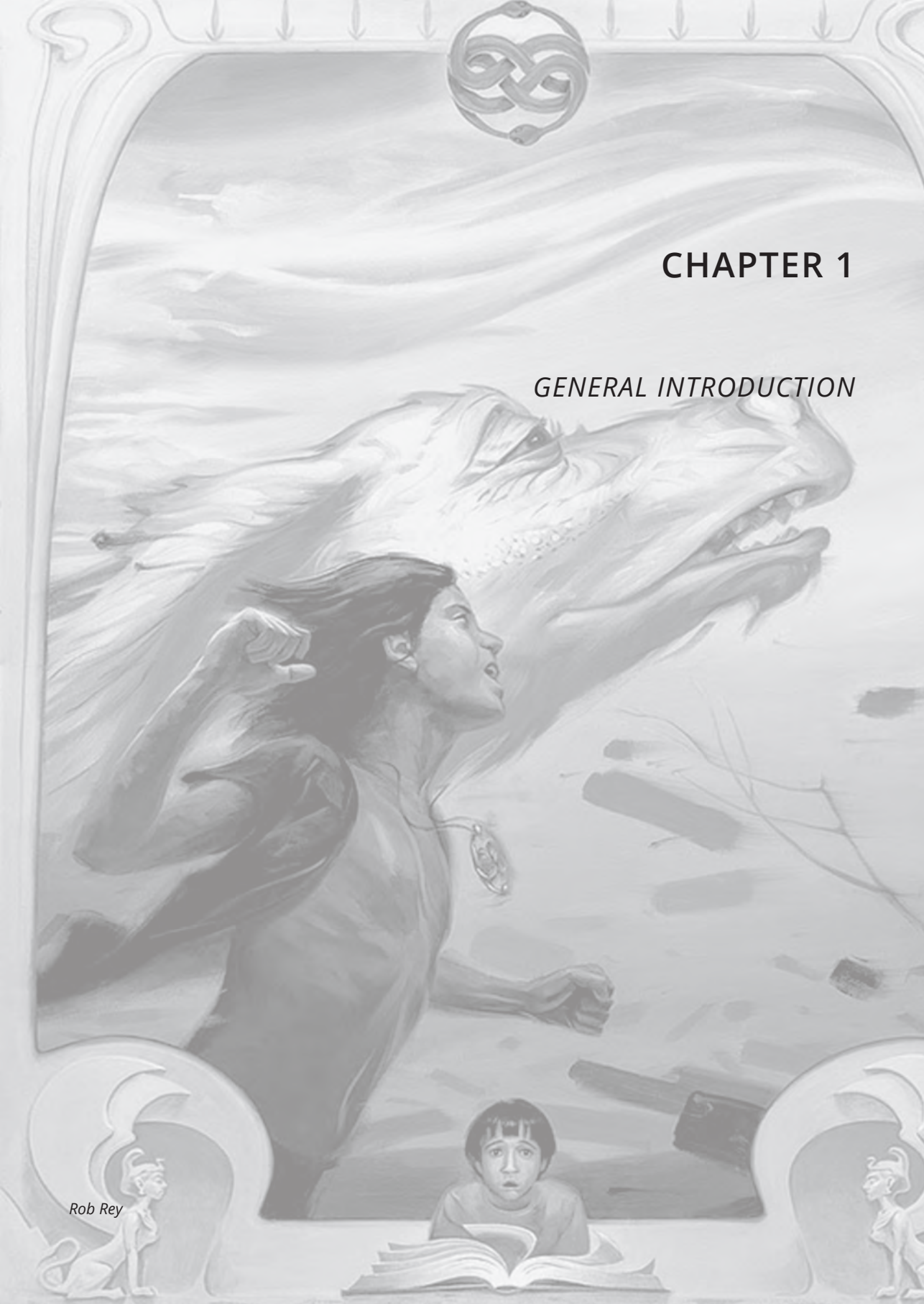

Rob Rey

Background of thesis

Osteoarthritis

Aetiology

Osteoarthritis (OA) is a multi-factorial disease that involves degradation of joints, including the articular cartilage and the underlying (*i.e.*, subchondral) bone. The risk of OA increases with age. In OA, normal functioning of a joint becomes impaired. A variety of causes (*e.g.,* mechanical, metabolic, developmental, and hereditary) may initiate processes that leads to loss of cartilage, ultimately causing bone exposure and damage. This results in decreased movement secondary to pain, regional muscles may atrophy, and ligaments may become more lax. The prime suspect in the etiology of this disease used to be the cartilage layer. A layer of articular cartilage lines each of the synovial joints. This tissue transmits loads and forces between skeletal elements, absorbs peak stress events, and assures (together with the synovial fluid) frictionless joint movement. Research indicates that bone is intimately involved in the progression of OA. For instance, a decrease in energy absorbing capacity of the subchondral bone could expose the overlying cartilage to increased impact and shear stress, leading to damage progressing to OA. Another factor is increased thickness of the subchondral bone, that was observed in advanced OA, related to an increased remodeling activity [1, 2]. This implies that the accumulated joint loads have created a local strain stimulus for bone adaptation in the subchondral bone [3, 4].

Clinical impact and relevance

Osteoarthritis is the most prevalent form of arthritis [5]. OA affects over 135 million people worldwide. It is the fourth most frequent cause of health problems in women and the eighth in men (The Bone and Joint Decade, 2010). In the Netherlands, the estimated prevalence is 1,189,000 persons; 440,000 men and 745,000 women (Rijksinstituut voor Volksgezondheid & Milieu, January 2011). All OA-types (*e.g.*, hip, knee, and other periphery types) are more prevalent in women than men, with knee-OA being the most common. In the Netherlands, the economic burden of this destructive joint disease was € 540.2 million in 2005. This corresponded to 12.8% of the total costs related to diseases of the locomotory system and connective tissues. A major increase in prevalence is expected between 2007 and 2040 [6] due to increasing population ageing.

Symptoms, problems, and treatment

Movement of the joint is painful and limited, and, in advanced disease stages, patients may complain of nocturnal or permanent pain. Treatment generally involves a combination

of exercise, analgesics and lifestyle modification. If pain becomes debilitating, joint replacement surgery may be used to improve the quality of life. Over the years, different strategies have been utilized to gather more knowledge on the initiation, development, and progression of osteoarthritis. These strategies are aimed toward eventually developing treatment targets to tackle the OA-problem.

Why bone tissue?

We were interested in the role of the underlying bone tissue. We know that both tissues can be seen as a functional unit during joint movement [7-9]. And when it comes to our knowledge about the interaction between these two important tissues, there is a gap in our general understanding of OA. Unraveling the relationship and interaction between subchondral bone and articular cartilage during the initiation, development and progression of OA is challenging. Various experiments have failed to explain the progression of cartilage damage because of the stiffening of the subchondral bone [10, 11]. However, these did not assess the mechanical environment necessary for repair and maintenance [12], the viscoelastic and hyperelastic nature of cartilage [13], and the mechanical behavior of the trabecular bone beneath the subchondral bone in relation to its loading history [3]. These factors are crucial for the deformations that are considered to be relevant for the development of OA [1]. The influence of the history of daily loading conditions on strain stimulus for bone adaptation was also disregarded [3]. As OA is considered an affliction mainly caused by a history of loading patterns, which can be characterized as overloading, this can be considered as a serious omission.

Combination of conventional with novel techniques

To unravel the relationship and interaction between subchondral bone and cartilage in the development of cartilage damage in OA, it is imperative to have a reliable, standardized and preferably 3D imaging method. Such a method would allow us to conduct a detailed assessment of both bone and cartilage properties in the healthy and diseased joint situation.

Conventional (micro) computed tomography

Conventional computed tomography (CT) is a non-destructive technique that provides 3D images of the internal structure of an object [14-17]. Because CT provides an excellent contrast of bone to soft tissue, new medical developments of this technique are often driven by the bone research field. Feldkamp *et al.* were first to build a microcomputed tomography (μCT or microCT) scanner for the evaluation of the 3D micro-structure of

trabecular bone [18]. At this stage, μCT was an experimental technique available to only a few research groups. However, with the presentation of the first commercially available bone μCT scanner in 1994, this technique quickly became a standard in bone research [19]. MicroCT is very suitable for determining and assessing the 3D morphology of bone samples [20], joint's bone components and complete small animals joints in high detail [21]. It can also be used to detect OA-related bone abnormalities like sclerosis, erosion and osteophytosis [22]. Interestingly, the use of μCT for TMJ-OA research has increased over the last couple of years [23-28]. However, it is difficult or virtually impossible to visualize the articular cartilage directly with conventional μCT due to the very low attenuation values of soft tissue such as the articular cartilage. The introduction of computed tomography in which these low attenuation are enhanced, provide a solution for this technical disadvantage.

Contrast-enhanced (micro) computed tomography

Interest in accurate 3D visualization of articular cartilage has increased immensely over the last decades. Currently, magnetic resonance imaging (MRI) is the golden standard for cartilage measurements [29-31], but the resolution of MRI is not sufficient to visualize very thin layers of cartilage [32, 33]. The enhancement of the attenuation of these soft tissue(s) in the μCT approach could provide a solution. Contrast-enhanced μCT would make it possible to overcome the low attenuation and resolution problems. Contrast-enhanced CT has been used for decades in various medical fields (*e.g.*, peripheral arteriography, cerebral angiography, excretory urography) and a wide range of clinical CT contrast-agents have been commercially available for years [34]. In 2006, the clinically available CT contrast-agent Hexabrix 320® [34, 35] was used for 3D imaging of articular cartilage layers for the first time [36]. The technique was called the 'Equilibrium Partitioning of an Ionic Contrast agent via micro Computed Tomography' (EPIC-μCT). In this novel imaging technique, the X-ray attenuation of cartilage is enhanced by treatment of samples with a contrast-enhancing ionic fluid containing the negatively charged hexaiodinated dimer ioxaglate. EPIC-μCT not only enables 3D imaging of cartilage morphology, but also qualification and quantification of the cartilage composition (*i.e.*, sulfated glycosaminoglycan [37, 38]) because the distribution of the contrast agent in the cartilage is inversely related to the amount of negatively charged glycosaminoglycans. Today, Hexabrix 320® is used as a contrast-agent in combination with a μCT system for osteoarthritis research [37-44]. This technique has been applied to evaluate numerous normal and osteoarthritic disease models, including rabbit [36], rat [45, 46], mouse [39], dog [47], and goat [48]. Because of the applicability of Hexabrix use in combination with μCT for OA research, this technique could also be very useful for our research.

Finite Element Analysis

MicroCT imaging offers unique capabilities for nondestructive reconstruction of microstructural features. Based on these detailed reconstructions, approaches such as Finite Element (FE) can be used to evaluate local biomechanical behavior under complex loading conditions of bone tissue and the overlying articular cartilage during (normal and pathological) loading. For a proper evaluation, the model used for such an analysis should be based on the actual 3D anatomy of both bone and cartilage tissue, rather than on assumptions or general values, and must be capable of estimating the deformations of the structures in 3D. By simulating different loading situations, FE analysis based on μCT-measured bone anatomy has proven to be a suitable and useful tool for determining the apparent mechanical properties of selected bone volumes [49-54]. The method enables one to analyze the effect of mechanical properties on, changes in loading, geometry, and bone distribution. Furthermore, it is possible to determine the influence of the degree and distribution of mineralization on the apparent mechanical properties. Part of the FE method is based on assumptions about the applied forces and distribution of bone properties. Yet, the material properties of the structure largely determine the relationship between the relative loads (stress) and the relative deformations (strain) inside a structure. For instance, the incorporation of mineral heterogeneity is likely of importance for the realistic performance of FE analysis applied to bone tissue. This component can be implemented in FE analysis if detailed information gathered by μCT is used as input.

Due to its relatively small size, the jaw joint is suitable for μCT and FE analysis. Furthermore, its high bone turnover rate and relatively large loads [55, 56] make it suitable to analyze bone adaptation. Such can be predicted from the history of global daily loading patterns by large-scale FE modeling [53, 57]. Consequently, the adaptive changes in the subchondral bone and underlying trabecular bone caused by changes in the functional behavior of a subject can be predicted [2, 4]. They can be compared to OA-like changes in the subchondral bone. The predicted mechanical behavior in healthy and diseased bone can be related to cartilage maintenance. This relationship may give insight into the initiation and progression of cartilage degradation as observed in osteoarthritis.

The techniques described above are applicable for OA-research in an *ex vivo* human model to gather fundamental data. Furthermore, it is possible to use the same techniques in an animal model. Different experimental interventions can be used to induce bone changes and study how this affects the cartilage in the synovial joints. An intervention used in this thesis was bisphosphonate treatment. Bisphosphonates (BPs) are bone antiresorption agents traditionally used for treatment of bone metastases or bone metabolic diseases [58]. But, since the early 2000s, there has been increased research in the field for the possible bone modifying effect of these agents for OA treatment [59].

The temporomandibular joint

The jaw joint or temporomandibular joint (TMJ) is a synovial ginglymoarthrodial joint, referring to the dual compartment structure (ginglymo) and function (arthrodial). The name is derived from the two bones that form the joint: the temporal bone that is part of the cranium (skull), and the lower jaw bone called the mandible [60, 61].

Cranial component

The temporal bone of the cranium forms the roof of the articular fossa and the tubercle. The temporal subchondral cortical bone is covered with a thin layer of articular cartilage. The structure of the cranial component is quite massive and consists mostly out of cortical bone tissue. The mandibular fossa is a concave depression in the squamous portion of the temporal bone (**Figure 1a**).

Mandibular component

Within the TMJ, the mandibular condyle is responsible for the transmission of loading forces from the mandible to the cranial component of the joint. It consists of a cortical shell, which envelops the trabecular bone (**Figure 1b**). The cortical bone is considered suitable for the transmission and dispersion of locally evoked forces. The subchondral cortical bone is primarily involved in shock absorption and the transmission of joint force from the articular cartilage to the trabecular bone [62]. Subsequent transmission of forces from the trabecular bone to the mandibular ramus is managed by the cortical bone of the condylar neck. Thus, the mandibular condyle plays an important role in the function of the masticatory system serving as a fulcrum between the mandible and the cranium.

The jaw joint as a functioning organ

The two TMJs on either side of the head work in unison. Together the joints form a bicondylar articulation, an ellipsoid variety of synovial joints similar to the knee articulation. The unique feature of the TMJ is the articular disc located between the bony components. The TMJ is like the knee joint one of the synovial joints in the human body with an articular disc. The disc divides the joint into an upper and lower joint compartment. The upper joint compartment, formed by the articular disk and the temporal bone, is involved in the secondary gliding motion of the jaw as it is opened widely (*i.e.,* translational movement). The lower joint compartment, formed by the mandible and the articular disc, is involved in the rotational movement of the jaw. Thus, the condyle articulates with the temporal bone in the mandibular fossa. The articular disc has a major role in shock absorption in the TMJ. However, the thin layers of articular cartilage on the bony surfaces also plays a role, and cannot be neglected [63].

Osteoarthritis in the temporomandibular joint

Temporary or prolonged excessive jaw joint loading initializes a cascade of events that may eventually lead to joint degradation. It is known that OA in the temporomandibular joint (TMJ-OA) is predominantly caused by such a mechanical joint imbalance [64, 65]. As in other joints, the disease process is characterized by deterioration and abrasion of articular cartilage and soft tissue surfaces, the occurrence of thickening and remodeling of the subchondral bone, and formation of marginal spurs (*i.e.,* osteophytes), and subarticular cysts [64, 66]. The frequency of TMJ bony degeneration related to OA (*e.g.*, cortical erosion, condylar flattening, and joint space alterations) in TMJ autopsy material can vary from 38% [67], or even to 85% in TMJ-OA patients [68]. If TMJ-OA is symptomatic, it can cause a lot of discomfort during daily usage of the masticatory system, such as talking, chewing, yawning etcetera.

Figure 1. a Sagittal view of a human skull. **b** Close-up of cranial and mandibular component of the temporomandibular joint. Drawing by Dr. Wilco de Jong ©

Outline of the thesis

Chapter 2 describes the application of the conventional μCT technique in the mandibular condyle of the human jaw joint for quantitative measurements of bone structural (*e.g.*, cortical and trabecular morphology) and material parameters (*e.g.*, mineral density and distribution).
Chapter 3 describes and discusses the application of μCT-based FE modeling to determine how mineral distribution in the trabecular bone of the mandibular condyle can influence apparent and intratrabecular biomechanical properties (*e.g.*, stress and strain).
Chapter 4 describes the different implications of high-dosage bisphosphonate treatment on bone tissue parameters (*e.g.,* mineral density, trabecular and cortical thickness) in the knee vs. jaw joint and mandible vs. humerus in a mouse model via μCT assessment and histological techniques.
Chapter 5 describes the introduction of a novel μCT technique called EPIC-μCT. Both conventional μCT and EPIC-μCT are applied *ex vivo* to both human and mouse jaw joint for 3D assessment of bone and cartilage morphology.
Chapter 6 is the general discussion of the thesis. This chapter first gives an overview of the most important findings, then evaluates the techniques that were used in the thesis, and lastly, provides an outlook for future research.

If we can apply conventional and contrast-enhanced μCT techniques in a successful manner to the jaw joint, our results could provide the means to produce μCT-based biomechanical computer models. In this thesis, the techniques were applied *ex vivo* to the complete human jaw joint. The dimension of the jaw joint is very suitable for this kind of research and was therefore our joint of interest. The combination of complimentary imaging techniques is promising for gaining more fundamental understanding of healthy and osteoarthritic joints as it permits the visualization of both bone and cartilage tissue. With the μCT-based biomechanical computer models that can be produced, it is possible to predict the biomechanical interaction of bone and cartilage tissue and the consequence of this interaction in a healthy and osteoarthritic human joint. Furthermore, an animal experiment can be used to induce bone changes allowing for detailed investigation into the influence of specific bone changes on the overlying articular cartilage in the animal jaw vs. knee joint. Combining both μCT techniques and an animal experiment will allow us to further investigate the influence of specific bone changes on the overlying cartilage *ex vivo*.

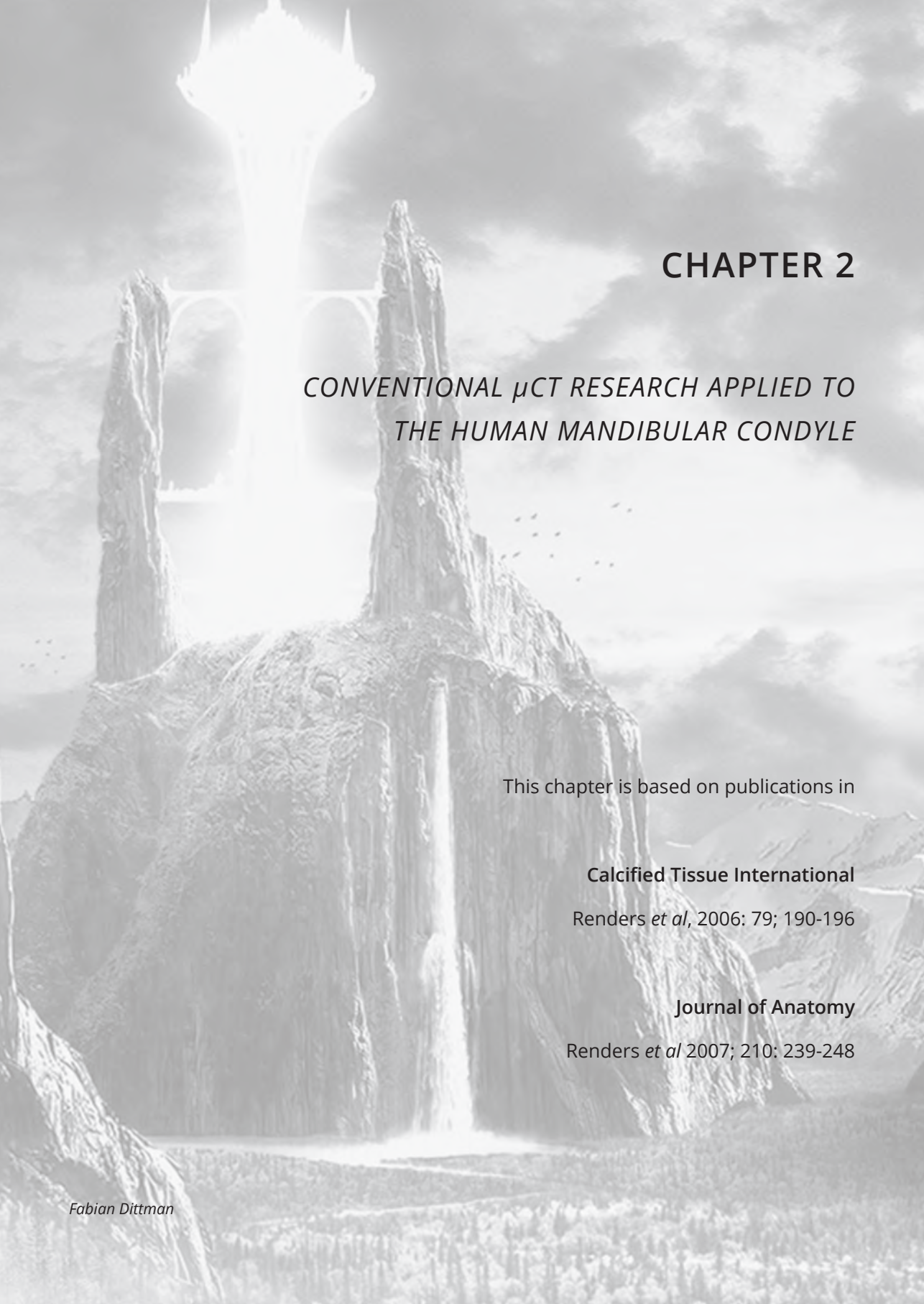

CHAPTER 2

CONVENTIONAL μCT RESEARCH APPLIED TO THE HUMAN MANDIBULAR CONDYLE

This chapter is based on publications in

Calcified Tissue International

Renders *et al*, 2006: 79; 190-196

Journal of Anatomy

Renders *et al* 2007; 210: 239-248

Fabian Dittman

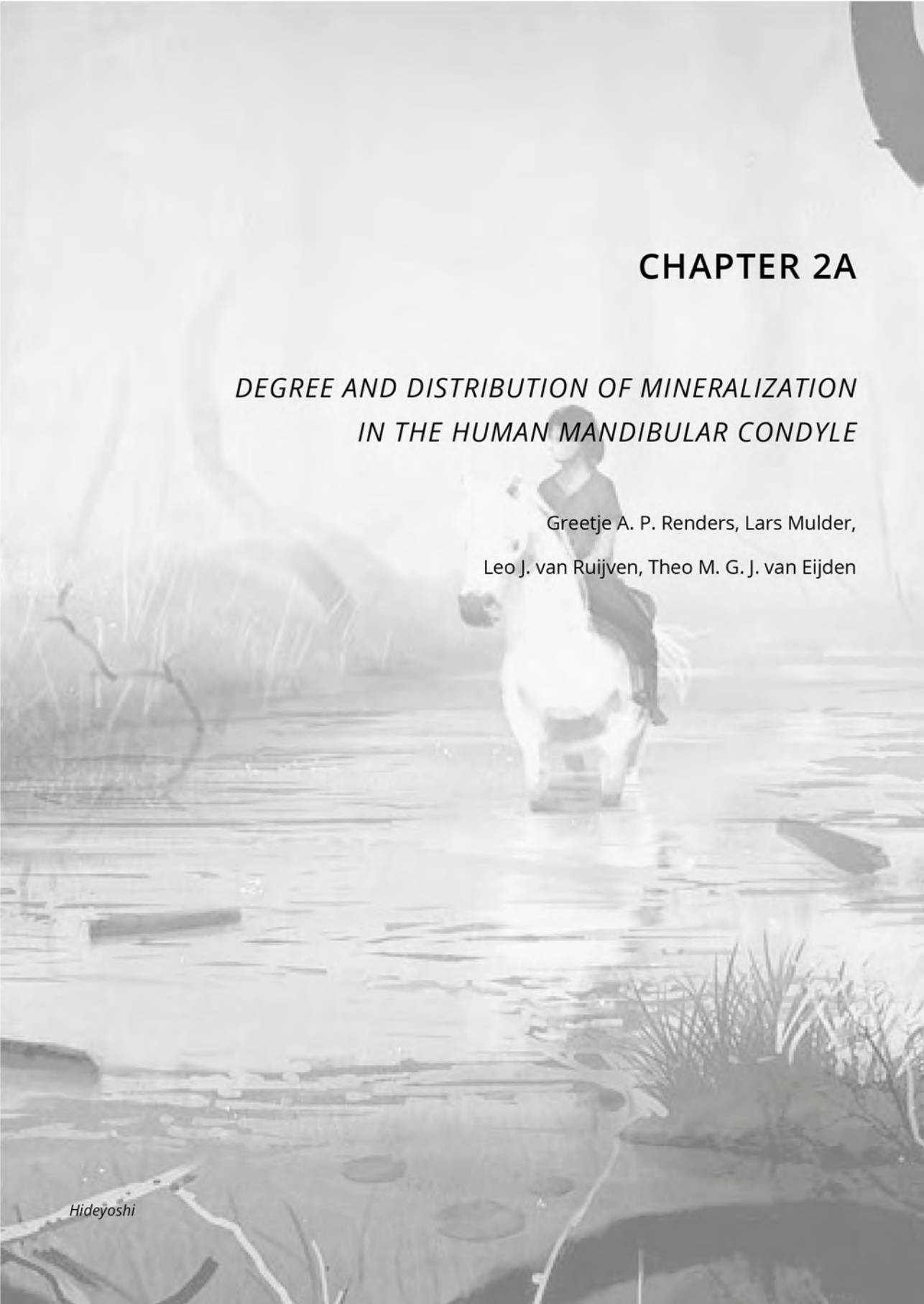

CHAPTER 2A

DEGREE AND DISTRIBUTION OF MINERALIZATION IN THE HUMAN MANDIBULAR CONDYLE

Greetje A. P. Renders, Lars Mulder,

Leo J. van Ruijven, Theo M. G. J. van Eijden

Hideyoshi

Introduction

The tissue mineral density of bone (TMD) strongly correlates with its mechanical properties. Together with porosity, variations in TMD may explain as much as 80% of the variation of mechanical properties [69]. Furthermore, as TMD depends on the remodeling rate of bone [70], the degree and distribution of mineralization can give information on bone formation or resorption rates [70-72]. In newly formed bone, the mineralization is much less than in older bone. In case of a high remodeling rate, the life span of bone is short and, consequently, the bone will be less mineralized. Thus, growth and a high remodeling rate will result in a low TMD, while aging and a low remodeling rate will result in a high TMD.

The remodeling rate of bone is assumed to be related to, *e.g.*, the amount of mechanical loading. In general, more heavily and/or frequently loaded bone is considered to have a higher remodeling rate and is therefore less mineralized and less stiff than bone that is loaded less. Earlier studies have demonstrated differences in TMD between different bone types (*e.g.*, trabecular vs. cortical bone [73-75]) and between different cortical regions of the same bone (*e.g.*, human femoral neck [76], equine radius [77], deer calcaneus [75, 78-81]). These differences have been related to, *e.g.*, differences in the amount of tensile/compressive stress.

Because of the active remodeling process, the cortical osteons and the trabecular packets in bone contain mineralized tissue with varying degrees of mineralization. Hence, the bone tissue is heterogeneous, *i.e.*, there are areas in which the process of mineralization has just started and areas in which this process has been carried out for longer periods of time (depicted in [82]). This heterogeneity in mineralization has certain topographical characteristics. As trabecular bone remodeling occurs at the trabecular surfaces, these surfaces are generally less mineralized than the trabecular cores [75, 79-81]. Comparably, in cortical bone, remodeling occurs by formation of the osteons. As the most recently formed bone is deposited on the surface of the cortical canals, the bone tissue near these canals is younger and thus less mineralized than peripheral osteonal bone and adjacent interstitial bone [71, 83].

Recently, desktop micro-computed tomography (μCT) and synchrotron radiation μCT have both been applied to evaluate the degree and distribution of mineralization of bone [84, 85]. The advantage of using μCT compared to microradiography [86] and backscattered electron imaging [72] is that it considers the three-dimensional structure and, thus, the true spatial distribution of the mineral content. In addition, μCT is largely available compared to synchrotron radiation μCT. The disadvantages are the relative large voxel size, the long scanning time, and partial volume effects at the bone surface. The partial volume effect is caused by the polychromatic character of the X-ray beam.

However, since the introduction of effective beam hardening correction algorithms the influence of this disadvantage on the measurements has significantly been reduced [84]. In the present study, a commercially available μCT system was used to study the degree and distribution of bone mineralization in the human mandibular condyle. We hypothesized a regional dependency of TMD. Previous work showed that during loading of the condyle the strain was higher in trabecular bone than in cortical bone and that they differed between various cortical regions [53, 87]. Therefore, concurrent differences in the degree and distribution of mineralization were expected. In addition, as remodeling in trabecular bone occurs at the trabecular surfaces and in cortical bone at the surfaces of the cortical canals, we examined whether this process was reflected by an increase in TMD with the distance from the surfaces of the trabeculae and cortical canals.

Materials and Methods

Condyles

Ten right mandibular condyles were obtained from ten embalmed human male cadavers (mean age ± SD: 69.8 ± 14.4 yrs, range: 43 to 92 yrs). Male subjects were used to eliminate any additional phenomena that might have resulted from postmenopausal osteoporosis in females. The number of teeth in the upper jaw was 10.2 ± 4.5, in the lower jaw 11.5 ± 2 .6. There were no signs of macroscopic bone pathologies. The use of the samples conforms to a written protocol that was reviewed and approved by the Department of Anatomy and Embryology of the Academic Medical Center of the University of Amsterdam. Condyles were separated from the mandible by a cut at the transition to the collum by a hand saw; condylar bone marrow was left *in situ*.

μCT

Three-dimensional reconstructions of the cortical and trabecular bone of the condyles were obtained using a commercially available high-resolution μCT system (μCT 40, Scanco Medical AG, Brüttisellen, Switzerland). For an extensive description of the scanning of mandibular condylar bone, we refer to earlier work [53, 87-90]. Condyles were mounted in cylindrical specimen holders (polyetherimide, outer diameter: 20 mm, wall thickness: 0.8 mm), secured with synthetic foam, and completely submerged in fixation fluid to avoid dehydration. Each condyle was positioned to be scanned sagitally. The scan resolution was 10 μm, the integration time 1200 ms, and the beam intensity was 45 kV, which corresponds to an effective energy of approximately 24 keV [84]. The mean duration of

scanning was 52.7 ± 4.0 hrs. The mean number of slices was 2080 ± 174.

The μCT system was equipped with an aluminum filter (0.5 mm) to remove the softest rays. The effect of beam hardening was further reduced by applying a correction algorithm that was developed by the manufacturer. To assess quantitatively the amount of noise and the effect of beam hardening, homogeneous K_2HPO_4 solutions (Merck, Darmstadt, Germany) with different concentrations were scanned [91] using the same settings as described above. Noise level and the effect of beam hardening appeared to be, respectively, maximally 6% and 7%, which was well below natural variations in mineralization.

The computed linear attenuation coefficient of the X-ray beam in each volume element (voxel) was stored in an attenuation map and represented by a gray value in the reconstruction. The attenuation coefficient can be considered proportional to the local TMD [84, 85]. TMD values for the bone-positive voxels were derived from the attenuation coefficients using a linear relation, which was calibrated with a phantom (QRM GmbH, Möhrendorf, Germany) containing hydroxyapatite densities of 0, 100, 200, 400, and 800 mg cm^{-3}.

Definition of Regions

In the center of the condyle, a cubic (size: 400 x 400 x 400 μm^3) volume of interest (VOI) of trabecular bone was selected, according to a similar method described previously [88]. In the cortical bone, three different regions were defined: subchondral cortex, anterior cortex, and posterior cortex (**Figure 1**). Within each of these cortical regions, six VOIs were chosen from medial to lateral to analyze mediolateral differences. Hence, the total number of cortical VOIs per condyle was 18 (three cortical regions x six mediolateral VOIs). As it was nearly impossible to distinguish unambiguously the three cortical regions at the condylar poles, the 15% most medial and 15% most lateral slices were excluded; the remaining slices were equally divided into 6 series of consecutive mediolateral slices (n = 243 ± 20).

After the VOIs were reconstructed three-dimensionally, they were segmented. In a segmented image, voxels with a linear attenuation value below a threshold (representing soft tissue or background) were made transparent and voxels above this threshold (representing bone) were made opaque. In trabecular bone, the threshold separated the bone tissue from the marrow spaces; in cortical bone, it separated the bone tissue from the intracortical canals and spaces. For the trabecular bone, an adaptive thresholding procedure (Scanco Medical AG, Brüttisellen, Switzerland) was used to determine the optimal threshold; the same threshold was applied to all trabecular VOIs. For cortical bone, the adaptive thresholding procedure could not be used, because of the relatively

large amount of bone tissue compared to the small amount of cortical canals and spaces (about 3%). For this reason, in cortical bone, the threshold was determined by varying it first in steps of 1.5% and comparing the outcome of each step with the original CT scan. The resulting thresholds for the subchondral, anterior, and posterior cortex were, respectively, 65.2 ± 3.4%, 57.8 ± 3.8%, and 61.8 ± 3.7% of the maximum gray value. The segmented VOIs were used to calculate bone architectural parameters (including bone volume fraction, BV/TV: *i.e.*, percent of bone) using morphometric software (Version 3.2, Scanco Medical AG).

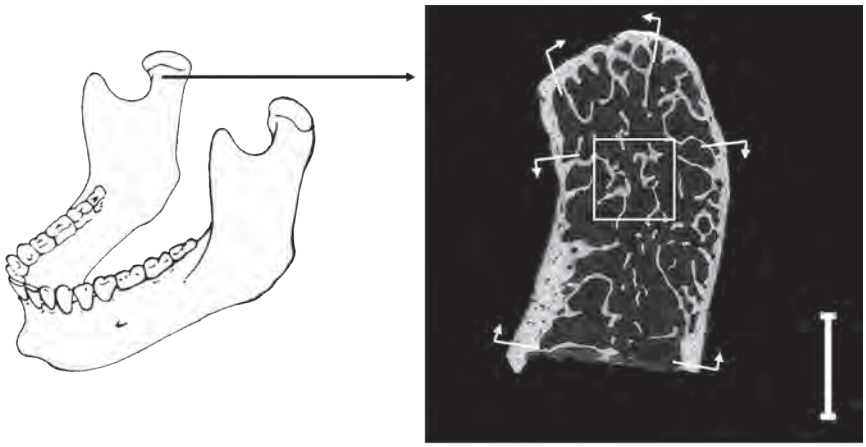

Figure 1. After the condyle was separated from the mandible, it was scanned in a µCT system. The µCT slice (*left,* anterior; *right*, posterior) shows the selected three cortical regions (*SC,* subchondral bone; *AC*, anterior cortex; *PC,* posterior cortex) and the trabecular volume of interest. *Bar* 5 mm.

Degree and distribution of mineralization

The tissue mineral density and its distribution of the trabecular bone were determined for a 3-D sample (dimensions: 200 x 200 x 200 µm^3) extracted from the center of the trabecular VOI. Similarly, a sample (dimensions: 2 x 0.5 mm x cortical thickness) was extracted from the center of each of the eighteen cortical VOIs.

The previously determined thresholds were applied to these samples to segment bone tissue. For this analysis, the voxels exceeding the threshold kept their original gray value. The outermost two layers of the trabecular bone (*i.e.*, transition between bone marrow and trabeculae) and the inner layers of the cortical bone (*i.e.*, transition between

cortical canals and bone) were disregarded as these layers were likely to be corrupted by partial volume effects.

To further investigate the 3-D distribution of the tissue mineral density, a specifically designed algorithm was used [75, 80]. From the surface of the trabeculae to their centers, layers of bone-containing voxels (10 µm; average layer thickness: 7-8 µm) were consecutively peeled from the surface of the reconstructed bone. After a layer had been peeled off, its average degree and variation of mineralization were calculated. A similar stepwise procedure was used to examine the tissue mineral density from the surface of the cortical bone adjacent to the cortical canals towards the periphery.

Statistical analysis

For each condyle, mean value and standard deviation (SD) of TMD and frequency distributions were determined for the trabecular bone sample and for the 18 cortical bone samples. To obtain mean and SD values and frequency distributions of TMD for the whole cortical bone, the latter 18 samples were combined. The width of every distribution curve was defined as 2 x SD value. Similarly, these parameters and frequency distributions were determined for the three condylar regions (subchondral, anterior, posterior) by combining the six regional samples. Finally, grand means were calculated over the ten mandibular condyles.

Differences in TMD between trabecular and cortical bone and between the three cortical regions were tested using paired *t*-tests. Regression analyses were performed to identify relationships between (1) TMD of cortical and trabecular bone, (2) TMD and age, (3) TMD and bone volume fraction. A general linear model (repeated measures) was used to test whether there was a significant increase or decrease in TMD with the distance from the surface of the trabeculae or cortical canals; because of partial volume effects the first two bone layers were not included in these analyses. In all tests a *p*-value of less than 0.05 was considered statistically significant. Statistical tests were performed using SPSS statistical software package (SPSS Inc., Chicago, IL, USA, version 11.5.1).

Results

BV/TV and TMD values for the trabecular and cortical bone and for the 3 cortical regions are given in **Table 1**. TMD in cortical bone (1045 mg hydroxyapatite [HA] cm^{-3}) was significantly higher ($p < 0.001$) than that in trabecular bone (857 mg HA cm^{-3}). There was no correlation between trabecular TMD and cortical TMD. Furthermore, TMD was not affected significantly by age or bone volume fraction in either the trabecular or cortical

bone. The distribution curves of TMD (**Figure 2**, upper panel) show that the higher TMD in cortical compared to trabecular bone was primarily due to a shift of the distribution to higher TMD values. The width of the two curves (**Table 1**) did not differ significantly, indicating that the amount of TMD heterogeneity (variation) was similar in cortical and trabecular bone. Irrespective of the bone type or region, inter-individual variations for the degree and distribution of mineralization were relatively low (5-7%, SD values in **Table 1**).

Table 1. BV/TV and TMD of trabecular and cortical condylar bone: mean ± SD[a]

	BV/TV[b] (%)	TMD (mg HA/cm^3)	Width[c] of TMD distribution curve (mg/cm^3)
Trabecular	20.70 ± 5.07	875 ± 41	210 ± 9
Cortical total	96.47 ± 1.19	1,045 ± 57	220 ± 17
Subchondral cortex	96.65 ± 1.77	1,120 ± 52	176 ± 12
Anterior cortex	96.73 ± 1.13	987 ± 66	216 ± 9
Posterior cortex	96.02 ± 1.68	1,028 ± 68	162 ± 8

HA, hydroxyapatite

[a] SD values are a measure for interindividual variation (n = 10)

[b] Bone volume fraction, *i.e.*, without marrow (trabecular bone) or canals and spaces (cortical bone)

[c] Width is defined as 2 x SD value of the distribution curve

TMD was highest in the subchondral cortex (1120 mg HA cm^{-3}), intermediate in the posterior cortex (1028 mg HA cm^{-3}), and lowest in the anterior cortex (987 mg HA cm^{-3}); the differences in TMD between the regions were significant (subchondral vs. anterior: p < 0.001; subchondral vs. posterior: p < 0.001, anterior vs. posterior: p = 0.037). In addition, TMD in the three regions correlated positively (subchondral vs. anterior: r = 0.8, p = 0.005; subchondral vs. posterior: r = 0.82, p = 0.003; anterior vs. posterior: r = 0.68, p = 0.03). No significant mediolateral TMD differences were found within each of the three cortical regions (data not shown).

Comparison of the distribution curves of the three regions showed that their relative positions and widths differed (**Figure 2**, lower panel; **Table 1**). Compared to the subchondral and posterior cortex, the distribution curve of the anterior cortex was shifted to lower TMD values, while the width of the curve was also significantly larger (anterior vs. subchondral and posterior: p < 0.001). The posterior cortex had the narrow most curve (posterior vs. subchondral: p = 0.029). The tissue mineral density showed a clear topographical gradient (**Figure 3**). In all cortical regions, mineralization was lowest in the bone adjacent to the cortical canals and increased gradually and significantly (p < 0.001 for the three regions) with the distance from these canals (**Figure 4**). In trabecular bone, mineralization increased significantly (p < 0.001) with the distance from the surface of the trabeculae. In trabecular bone the increase was much steeper than in cortical bone.

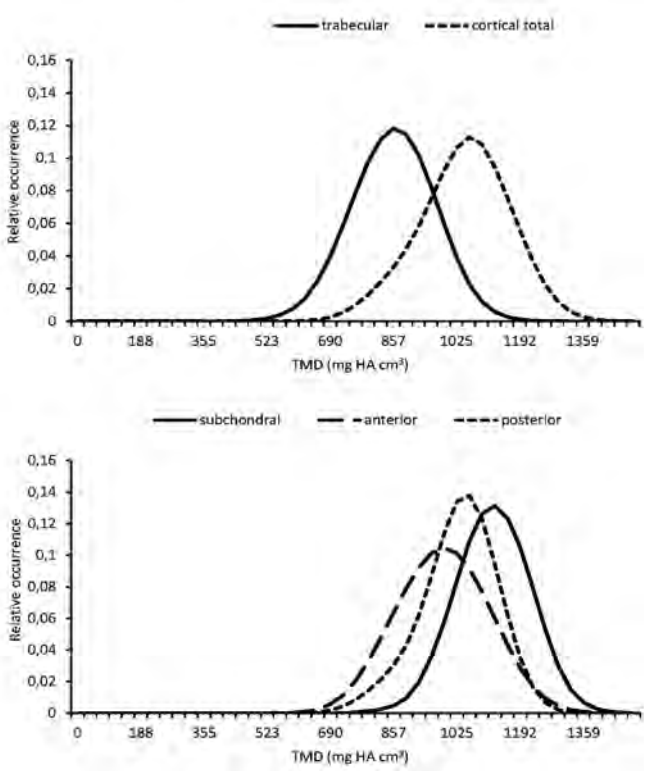

Figure 2. Mean distributions of TMD of trabecular and total cortical bone and the three separate cortical regions (*n* = 10). *HA*, hydroxyapatite.

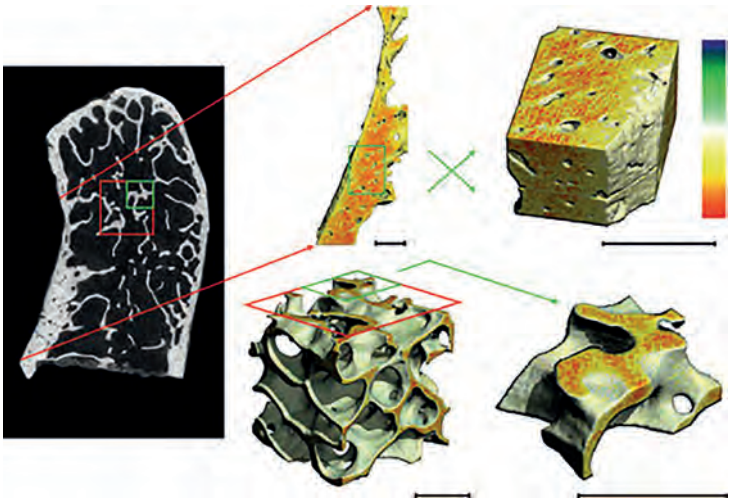

Figure 3. Three-dimensional reconstructions of trabecular and cortical bone. Note the increasing tissue mineral density from the surface of the trabeculae to the cores and from the surface of the cortical canals to the periphery. *Bar* 1 mm; *color scale*, increasing tissue mineral density from blue to red.

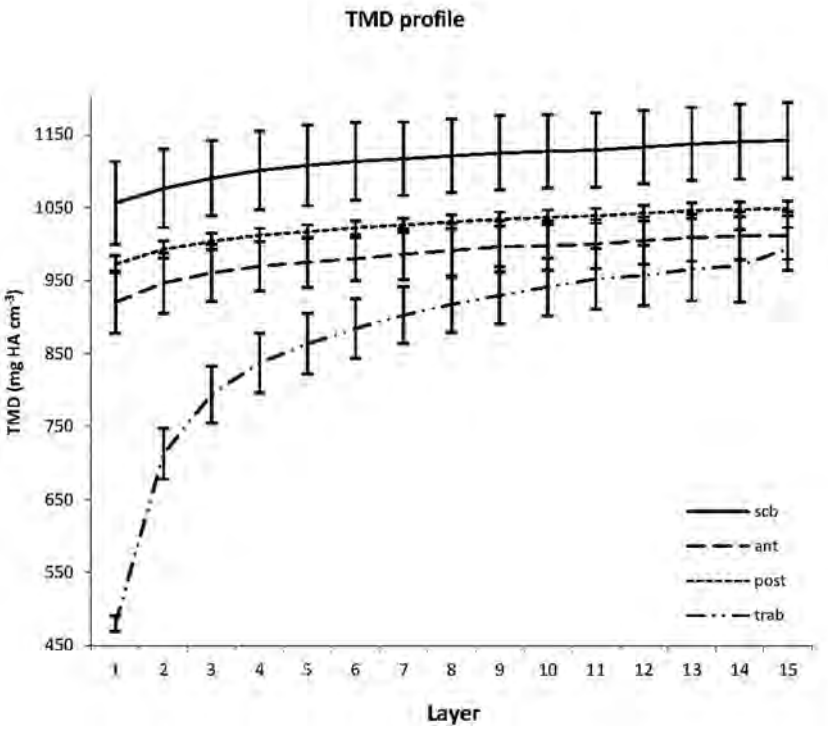

Figure 4. Mean TMD within trabecular bone and three cortical regions as a function of the distance from the surface of the trabecular elements and cortical canals, respectively. Layers of bone-containing voxels (10 µm) were consecutively peeled off (average layer thickness 7-8 µm). TMD increased with the distance from the surface (layer 1). SD bars are a measure for interindividual variation (n = 10). *HA*, hydroxyapatite.

Discussion

The present study is the first one that examined the degree and distribution of mineralization in cortical and trabecular bone of the human mandibular condyle. The results show that tissue mineral density (TMD) in the mandibular condyle is significantly lower in its trabecular than in cortical bone. Thus, the mineral density of cortical bone in the condyle is higher not only because of its higher volume fraction but also because of its higher TMD. The lower TMD in trabecular bone compared to cortical bone could point to a higher bone remodeling rate in trabecular bone, which is consistent with the reported higher strains in the trabecular bone [53, 87]. Thus, mineral deposition in the condyle is less advanced in trabecular bone than in cortical bone and, consequently, trabecular

bone has an increased proportion of less mineralized bone and a decreased proportion of more mineralized bone compared to cortical bone. Thus far, it is not clear how, on a molecular level, differences in mechanical loading affect the degree and distribution of mineralization. We speculate that differences in mechanical loading result in differences in sensitivity to, *e.g.*, stimulators of bone formation, such as parathyroid hormone, growth hormone, and insulin-like growth factor [92], or inhibitors of bone resorption, such as estrogen [93].

TMD values of the mandibular condyle reported in the present study fall within the range of values reported in other studies, which were obtained from ashed bone samples of various species and sites [74] or by applying computerized quantitative contact microradiography on human iliac crest [86] and human calcaneus [94]. Using quantitative backscattered electron (BSE) imaging, it has been found that the mineralization density of the mandibular body is higher than that of postcranial bones like lumbar vertebra, iliac crest, and femoral neck [95]. Consequently, it is likely to be also higher than that of the mandibular condyle. Such a difference in TMD between the mandibular body and condyle has been observed in developing pig specimens using μCT [75]. However, the resolving power of μCT for TMD is less than that of BSE and microradiography. This means that these methods enable localization and identification of regions of, for instance, calcified cartilage remnants [86, 96]. However, when a non-destructive and 3-D technique is of importance, μCT can be regarded as a reliable alternative.

A higher TMD in cortical bone than in trabecular bone has also been reported earlier [73, 74] and is consistent with the higher elastic moduli that have been reported for cortical bone compared to trabecular bone [97, 98]. Similar to earlier studies we did not find that TMD changed with age [86, 94].

The widths of the distribution curves did not differ significantly between trabecular and cortical bone, indicating that the variation in mineralization (heterogeneity) is similar for both bone types. Irrespective of bone type, inter-individual variation of TMD was relatively low (5-7%). This is in agreement with other studies (human rib [72]; human iliac crest [96]). The low inter-individual variation indicates that under physiological situations the rate of bone remodeling at a particular skeletal site can be considered as a constant biological parameter. However, the results of the present study also demonstrate that the TMD, and probably the rate of remodeling, can be very different between different types of bone (trabecular vs. cortical) and different sites.

The degree and distribution of mineralization differed significantly between cortical regions. The anterior cortex of the mandibular condyle had a significantly lower TMD and a wider distribution curve than the subchondral and posterior cortex. Hence, in the anterior cortex, not only the rate of remodeling, and consequently the proportion of less mineralized bone, but also the heterogeneity was higher (about 30%). Differences

in TMD between various cortical regions of the same bone have also been described for other bones [76-78]. These differences have been related to suggested differences in occurring tensile/compressive stress. Whether such an explanation also applies to the mandibular condyle must be further examined, *e.g.*, by finite element analysis. Alternatively, a possible role of the attachment of the lateral pterygoid muscle to the anterior cortex can be considered.

We provide for the first time quantitative information on topographical variation of TMD in cortical bone and trabecular bone of the human mandibular condyle. As we used condyles from embalmed cadavers, one might argue that this variation resulted from the formalin fixation. It has, however, been demonstrated that mineral content in hard tissues is not affected by such a fixation [99]. With respect to cortical bone, the inner lamellae in an osteon represent the youngest bone, the peripheral lamellae the older bone, whereas the oldest bone is present in the interstitial bone adjacent to the osteons [71, 83]. Hence, an increase in TMD can be expected going from the center towards the periphery. Such an increase was indeed found in the present study. A similar radial distribution was found in studies, in which Fourier transformed infrared microspectroscopic analysis of human iliac crest samples was performed [81, 83]. However, in the human femoral neck the opposite tendency was observed using BSE [99]. Early microradiographic studies showed that, in growing osteons, the tissue mineral density increases from the center towards the cement line, whereas the opposite occurs in old, completed osteons. Moreover, in the latter, a ring of hypermineralized matrix forms along the wall of the Haversian canal [100].The higher mineralization towards the periphery agrees with differences in elastic moduli (10-30%) found between interstitial regions and more recently formed osteons [97, 101, 102].

With respect to the trabeculae, we found that interior trabecular regions have higher mineralization than superficial regions. This indicates that remodeling occurs at the surfaces and that the youngest bone is present at these surfaces and the oldest bone at the cores. The steeper increase in trabecular mineralization than in cortical bone as a function of distance implies that the age difference between the various layers in the trabeculae is larger than that between the layers in the osteons. A higher tissue mineral density in the cores of the trabeculae relative to their surfaces may be important when the trabeculae are loaded in bending. When trabeculae are loaded in bending and there are increased surface strains, the less mineralized surface would demonstrate greater ability to withstand the strains without breaking, and hence the trabeculae are less prone to fracture.

From a mechanical point of view, it should be noted that the bone mineral provides rigidity to the bone [69]. Bone tissue with a higher TMD can be expected to be stiffer and more brittle, while it will likely have reduced fracture toughness. In addition,

heterogeneity in bone mineralization has an important influence on crack initiation and propagation behavior and is therefore essential for the bone toughness [79]. Loss of heterogeneity will probably result in a decrease in stiffness and will therefore favor the appearance of microcracks.

Some remarks have to be made with respect to the methods used in the present study. Firstly, because the superficial voxels are likely to be corrupted by partial volume effects, the superficial bone layers were disregarded in the calculation of the mean TMD values and in the statistical analyses. This exclusion results in an overestimation of mean TMD. As the overestimation will be larger for trabecular than for cortical bone, it will result in an underestimation of the difference in TMD between trabecular and cortical bone. Secondly, the gray value of a voxel is not only determined by the TMD of a point located in the center of that voxel but also by the TMD of the points in the neighborhood of that voxel (resolving power). This influence decreases with an increase in distance from the voxel and can be described by a probability distribution. At a resolution of 10 μm its standard deviation is approximately 10 μm and its 95% confidence interval approximately 20 μm (Scanco Medical AG, Brüttisellen, Switzerland). Assuming a Gaussian distribution, this implies that the contribution of voxels at a distance > 20 μm is < 5%, and at a distance > 33 μm, < 0.1%. Thus, it can be expected that the gray level of the voxels from the second bone layer are still underestimated by several percentage points due to the presence of empty voxels in their neighborhood. For this reason, we removed the two surface layers before we did the statistical analyses. In the deeper layers, the effect of the resolving power becomes < 1% and is therefore not responsible for the observed increase in mineralization from the surface towards the cores (**Figure 4**). Also, the difference in mean TMD between cortical and trabecular bone is much larger (about 25%) than could possibly be ascribed to an artifact due to the resolving power; in addition, the two superficial layers were not included in the analysis. Finally, in the present study, heterogeneity was defined as the amount of variation in TMD. It might be expected that heterogeneity also depends on the rate of remodeling. For example, if remodeling has stopped for a considerable time, the mean TMD would be high while heterogeneity would be low because all bone tissue would have a relatively high age. In comparison, in very young bone, both the mean TMD and heterogeneity will be relatively low. As TMD in trabecular bone was lower than that in cortical bone, we speculate that the remodeling rate in trabecular bone was higher than in cortical bone. In the present study, differences in heterogeneity were small. Therefore, we did not draw conclusions with respect to remodeling rate from the heterogeneity observations.

In conclusion, for the mandibular condyle, this study reveals that TMD is 25% higher in cortical than in trabecular bone. This difference is much larger than inter-individual variations (5-7%) and it suggests a much higher remodeling activity in

the trabecular bone. Also, this difference probably has a large influence on the Young's modulus. Using to the empirical equation of Currey [69], the calculated Young's moduli are 2.8 GPa and 6.3 GPa, respectively, for trabecular and cortical bone. This will certainly result in much higher strain in trabecular than in cortical bone during condylar loading.

Acknowledgements

We are grateful to Irene Aartman for statistical advice, to Peter Brugman for technical assistance, and to Jan Harm Koolstra and Geerling Langenbach for their comments on the manuscript. This research was institutionally supported by the Inter-University Research School of Dentistry, through the Academic Center for Dentistry Amsterdam.

CHAPTER 2B

POROSITY OF HUMAN MANDIBULAR CONDYLAR BONE

Greetje A.P. Renders, Lars Mulder, Leo J. van Ruijven, Theo M.G.J. van Eijden

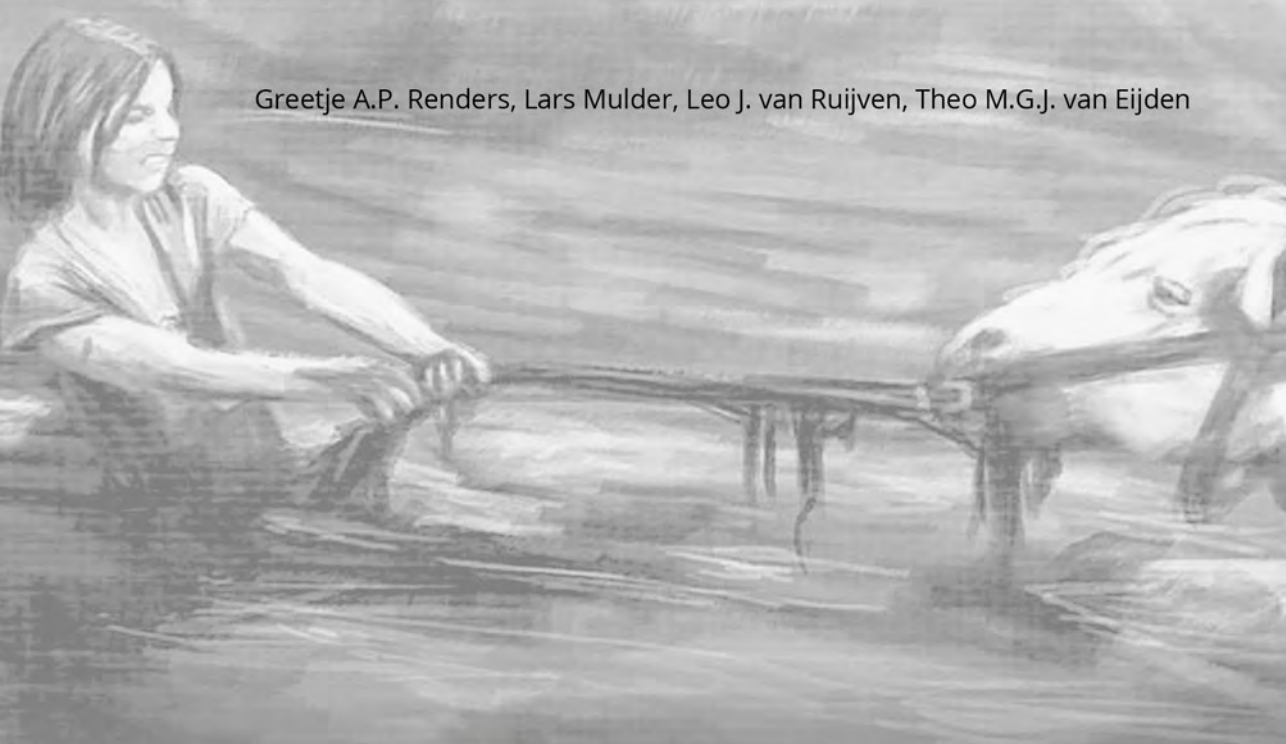

Ali Phelps

Introduction

The porosity of bone is the volume fraction of bone which is not occupied by bone tissue. Cortical porosity is due to a complex network of intracortical canals and spaces, whereas trabecular porosity is due to the intratrabecular marrow spaces. Porosity is considered to be inversely proportional to several mechanical properties, such as bone strength and stiffness [103-108]. Regional variation in porosity has been linked to differences in loading [109-112]. Within the human femur, *e.g.*, Bell *et al*. [109] found a lower porosity in the compression cortex than in the tension cortex.

Apart from porosity, the orientation of the cortical canals may give clues with respect to the loading history of the cortical bone. The orientation of the osteons, and therefore the cortical canals, varies within and among bones. It is believed that this variation reflects the mechanical environment, as osteons are generally preferentially oriented parallel to the main loading direction [113].

The tissue mineral density of bone is, like porosity, possibly influenced by loading. In general, more heavily loaded bone is considered to have a higher remodeling rate and is therefore less mineralized and less stiff than bone that is loaded less. Because of regional differences in loading, the tissue mineral density is also likely to vary regionally [111, 114].

Cortical bone remodeling occurs by formation of osteons. As the most recently formed bone is deposited on the surface of the cortical canals, the bone tissue near these canals is younger and thus less mineralized than peripheral osteonal bone and adjacent interstitial bone [71, 83]. Trabecular bone remodeling occurs at the trabecular surfaces, and therefore these surfaces are generally less mineralized than the trabecular cores [80, 81, 115]. Trabecular bone is considered to have a higher turnover rate and appears to respond more rapidly to changes in mechanical loading and unloading [116]. This may partially be due to the larger bone surface area available in trabecular bone than in cortical bone for osteoblastic and osteoclastic activity. It might thus be expected with a higher porosity the surface area of the cortical canals and trabeculae is larger, which in turn might result in a higher remodeling rate and consequently a lower tissue mineral density. For cortical bone, an increase in porosity has indeed been found to coincide with a decrease in mineralization [117, 118].

The present study concerns the porosity and tissue mineral density of the cortical and trabecular bone of the human mandibular condyle. The subchondral cortex of the condyle is primarily involved in shock absorption and the transmission of joint force from the articular cartilage to the trabecular bone in the condyle [110, 119]. The anterior and posterior cortexes of the condyle are important in the subsequent transmission of force to the mandibular ramus. In addition, the anterior and posterior cortex are probably

loaded differently, *i.e.* the concave anterior cortex is primarily subjected to compressive strain, whereas the convex posterior cortex is primarily subjected to tensile strain [53].

Thus far, no studies have been published on the 3-D structure of the cortical canals in the human mandibular condyle. The advantage of using μCT is that it considers the 3-D structure and has the potential to analysis the cortical canal network in 3 dimensions [120]. Scan resolutions up to 6 μm are possible, providing a high level of detail without complete destruction of the bone sample. Recently, μCT has also been applied to evaluate the degree and distribution of mineralization of bone [75, 84, 115].

In the present study μCT was used to study porosity in cortical and trabecular bone of the human mandibular condyle. We set out, first, to give a 3-D description of the cortical canalicular network in the condyle in order to obtain more information about the principal directions of stress and strain during loading. Our second aim was to determine whether the amount of remodeling was larger in the trabecular bone than in cortical bone of the condyle, and to establish whether the variation in amount of remodeling was related to the surface area of the cortical canals and trabeculae. We hypothesized that there would be differences in the amount of porosity and orientation of cortical canals between various cortical regions. In addition, a greater cortical and trabecular porosity is likely to coincide with a greater surface area of cortical canals and trabeculae, we hypothesized that this surface area is related to the tissue mineral density of cortical and trabecular bone, respectively.

Materials and methods

Condyles

Ten right mandibular condyles were obtained from ten embalmed human male cadavers (mean age ± SD: 69.8 ± 14.4 yrs, range: 43 to 92 yrs). The number of teeth in the upper jaw was 10.2 ± 4.5, in the lower jaw 11.5 ± 2.6. The use of the condyles conforms to a written protocol that was reviewed and approved by the Department of Anatomy and Embryology of the Academic Medical Center of the University of Amsterdam. The condyles were separated from the mandible by a hand saw.

μCT

Three-dimensional reconstructions of the cortical and trabecular bone of the condyles were obtained using a high-resolution μCT system (μCT 40, Scanco Medical AG, Brüttisellen, Switzerland). The condyles were mounted in cylindrical specimen holders

(polyetherimide, outer diameter: 20 mm, wall thickness: 0.8 mm), secured with synthetic foam and completely submerged in fixation fluid. The scan resolution was 10 µm, the integration time 1200 ms, and the beam intensity 45 kV, which corresponds to an effective energy of approximately 24 keV [84].

The µCT system was equipped with an aluminum filter (0.5 mm) to remove the softest rays. The effect of beam hardening was further reduced by applying a correction algorithm that was developed by the manufacturer. To assess quantitatively the amount of noise and the effect of beam hardening, homogeneous K_2HPO_4 solutions (Merck, Darmstadt, Germany) with different concentrations were scanned [91] using the same settings as described above. Noise level and the effect of beam hardening appeared to be, respectively, maximally 6% and 7%, which was well below natural variations in mineralization.

The computed attenuation in each volume element (voxel) was stored in an attenuation map and represented by a gray value in the reconstruction. The attenuation coefficient can be considered proportional to the local tissue mineral density [84, 85]. tissue mineral density values for the bone-positive voxels were derived from the attenuation coefficients using a linear relation, which was calibrated with a phantom containing hydroxyapatite (HA) densities of 0, 100, 200, 400, and 800 mg HA cm^{-3}. It is important to recognize the difference between two mineralization parameters. The second parameter is the so-called mineral density of bone and is not used in this study; it is the mass of the mineralized bone tissue relative to the total volume of the selected volume of interest (BV/TV); this latter parameter is therefore dependent on both the tissue mineral density and the amount of bone present in the volume of interest.

Definition of regions

In the center of the condyle a cubic (size: 400 x 400 x 400 μm^3) volume of interest (VOI) of trabecular bone was selected (**Figure 1**), according to a similar method described previously [115, 119]. In the cortical bone three different regions were defined, *i.e.* subchondral cortex, anterior cortex, and posterior cortex. Within each of these cortical regions, six VOIs were chosen from medial to lateral to analyze mediolateral differences. Hence, the total number of cortical VOIs per condyle was 18 (three cortical regions x six mediolateral VOIs). To define the cortical VOIs, first the 15% most medial and 15% most lateral slices of the condyle were excluded; the remaining slices were equally divided into six series of consecutive mediolateral slices (n = 243 ± 20).

Once the VOIs were defined, they were segmented. In a segmented image, voxels with a linear attenuation value below a threshold represent soft tissue or background while voxels above this threshold represent bone. In case of trabecular bone the threshold

separated the bone tissue from the marrow spaces; in case of cortical bone it separated the bone tissue from the intracortical canals and spaces. For the trabecular bone an adaptive thresholding procedure (Scanco Medical AG, Brüttisellen, Switzerland) was used to determine the optimal threshold. For cortical bone, the adaptive thresholding procedure could not be used, because of the relatively large amount of bone tissue

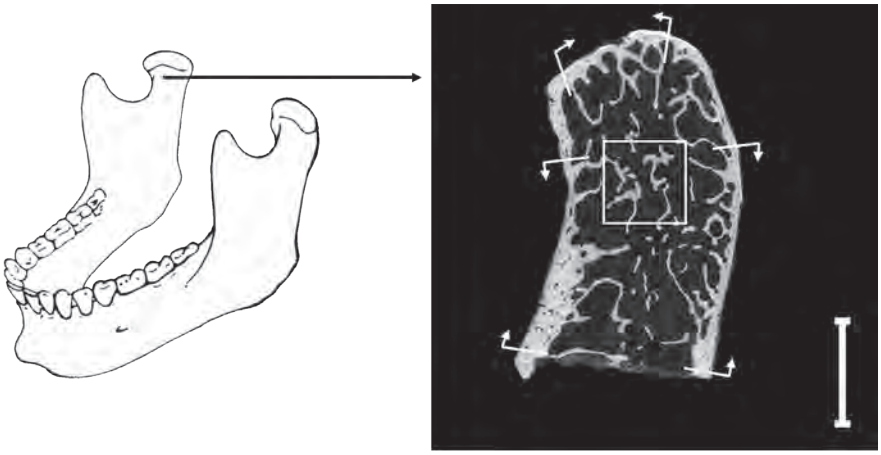

Figure 1. After the condyle was separated from the mandible, it was scanned in a μCT system. The μCT slice (*left*, anterior; *right*, posterior) shows the selected three cortical regions (*SC*, subchondral bone; *AC*, anterior cortex; *PC*, posterior cortex) and the trabecular volume of interest. *Bar* 5 mm.

compared to the small amount of cortical canals and spaces (about 3%). For this reason in cortical bone the threshold was determined by varying it in steps of 1.5% and comparing the outcome of each step with the original CT scan.

After determination of the threshold small fragments could be seen in the reconstructed cortical canal network, which were remnants of the smallest cortical canals which we were not able to visualize due to the applied resolution of 10 μm. These fragments were excluded before the actual determination of morphometric parameters and tissue mineral density.

Morphometric parameters

The segmented VOIs of the trabecular bone samples were used to calculate the following bone architectural parameters: bone volume fraction (BV/TV; trabecular porosity = 1 – BV/TV), trabecular thickness (Tb.Th), trabecular separation (Tb.Sp), trabecular number (Tb.N),

bone surface to volume ratio (BS/BV), and degree of anisotropy, using morphometric software (Version 3.2, Scanco Medical AG, Brüttisellen, Switzerland).

To describe morphometric characteristics of the cortical canal network, various canal parameters were calculated for each VOI. Cortical porosity (Ca.V/TV) is the relative volume of cortical canals, which is determined by dividing the number of canal voxels in the VOI by the total number of voxels in the VOI; thus porosity is defined by void volume/tissue volume. Canal diameter (Ca.Dm) is the mean diameter of the canals. Canal separation (Ca.Sp) is the mean distance that separates the canals within the canal network. Canal number (Ca.N) is the mean number of canals per mm. Canal surface to volume ratio (Ca.S/Ca.V) is the surface of the cortical canals per unit volume of canals; to relate the canal surface area to the amount of cortical bone, in the present study it was expressed per unit volume of cortical bone (Ca.S/BV). Degree of anisotropy is a measure of preference of orientation of the canal network; for this purpose, a mean intercept length tensor was calculated [121]. All canal architectural parameters were calculated using the software morphometric package at the µCtT system (Software Version 3.2, Scanco Medical AG, Brüttisellen, Switzerland).

Tissue mineral density

The tissue mineral density of trabecular bone (TMD) was determined for a three-dimensional sample (dimensions: 200 x 200 x 200 μm^3) extracted from the center of the trabecular VOI. Similarly, to determine the tissue mineral density of cortical bone a sample (dimensions: 2 x 0.5 mm x cortical thickness) was extracted from the center of each of the 18 cortical VOIs. The previously determined thresholds were applied to these samples to separate bone from background. For this analysis, the voxels exceeding the threshold kept their original gray value. The outermost two layers of the trabecular bone (*i.e.* transition between bone marrow and trabeculae) and the inner layers of the cortical bone (*i.e.* transition between cortical canals and bone) were disregarded as these layers were likely to be corrupted by partial volume effects.

Statistical analysis

Descriptive statistics included the mean, standard deviation, and range of the various morphometric parameters and tissue mineral density. For the trabecular bone samples the values were calculated over the ten condyles. To obtain values for the cortical canal parameters and tissue mineral density of the entire cortical bone of the condyle, the 18 cortical samples were combined. Similarly, these parameters were determined for the three separate condylar regions (subchondral, anterior, posterior) by combining the six

regional samples. Finally, grand means were calculated over the ten condyles. Differences in parameters between the three cortical regions were tested using paired *t*-tests. Regression analyses were performed to identify relationships (1) among the trabecular bone parameters, (2) among the cortical canal parameters (for the entire cortical bone), (3) between cortical and trabecular porosity, (4) between cortical and trabecular tissue mineral density, (5) between age and porosity, and age and tissue mineral density, (6) between number of teeth and porosity, and number of teeth and tissue mineral density. In all tests a *p*-value of less than 0.05 was considered statistically significant. Statistical tests were performed using the SPSS statistical software package (SPSS Inc., Chicago, IL, USA, version 11.5.1).

Results

The cortical canal network of the condyle has many longitudinal canals with relatively few perpendicular and oblique connections. The overall orientation of the cortical canals differed between the three cortical regions. The main direction was mediolateral in the subchondral cortex, whereas it was superoinferior in the anterior and posterior cortex (**Figure 2**). Within the anterior and posterior cortex the canals also diverged superomedially and superolaterally in a fan-like way. The degree of anisotropy of the canals was significantly higher ($p < 0.05$) in the posterior cortex (2.30) than in the subchondral (1.85) and anterior cortex (2.01).

Cortical canal parameters and tissue mineral density values for the entire cortical bone and for the three separate cortical regions are given in **Table 1**. The average porosity in cortical bone was 3.5%. No significant differences in porosity were found between the three cortical regions. The diameter of the cortical canals (average: 0.053 mm) was significantly lower in the subchondral cortex (0.048 mm) than in the posterior ($p < 0.01$; 0.058 mm) or anterior cortex ($p < 0.05$; 0.053 mm). The canal separation (average: 0.52 mm), canal number (average: 2.05 mm^{-1}), and canal surface to volume ratio (average: 1.88 mm^{-1}) did not differ significantly between the three cortical regions. The tissue mineral density of cortical bone (average: 1045 mg hydroxyapatite [HA] cm^{-3}) was highest in the subchondral cortex (1120 HA mg cm^{-3}), and lowest in the anterior cortex; the differences in tissue mineral density between the cortical regions were significant (subchondral vs. anterior: $p < 0.001$, subchondral vs. posterior: $p < 0.01$, anterior vs. posterior: $p < 0.05$). No significant mediolateral differences in canal parameters and tissue mineral density were found within each of the three cortical regions (data not shown).

A large number of significant correlations were found among the canal parameters (**Table 2**). For example, porosity was positively correlated with the diameter and number

of canals, and negatively correlated with the separation of the canals. None of the canal parameters, including canal surface to volume ratio, correlated significantly with the tissue mineral density of cortical bone.

Morphometric parameters of the trabecular bone are summarized in **Table 3**; correlation coefficients among the parameters are given in **Table 4**. Average porosity of trabecular bone was 79.3% and its average tissue mineral density was 857 HA mg cm^{-3}. Note, trabecular porosity correlated positively with, *e.g.*, the bone surface to bone volume ratio of the trabeculae, and negatively with their thickness and number (**Table 4**). There was a significant negative correlation between the trabecular bone surface to volume ratio and the tissue mineral density of trabecular bone. Thus, a larger trabecular surface coincided with a lower tissue mineral density.

The tissue mineral density of trabecular bone was significantly ($p < 0.001$) lower than that of cortical bone. There was no significant correlation between trabecular and cortical porosity, nor between trabecular and cortical tissue mineral density. Porosity and tissue mineral density were not affected significantly by age or number of teeth in either trabecular or cortical bone.

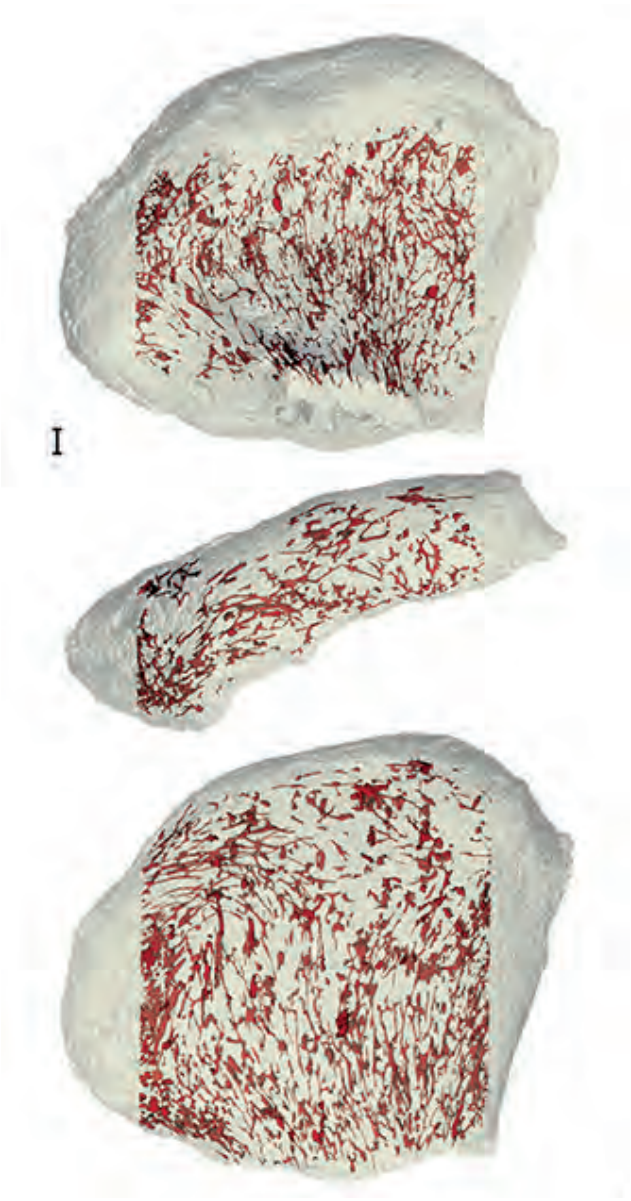

Figure 2. Cortical canal system of the human mandibular condyle. *Top*, view of anterior cortex; *middle*, subchondral cortex; *bottom*, posterior cortex. Note the predominantly mediolateral orientation of the canals in the subchondral cortex and their fan-like superoinferior orientation in the anterior and posterior cortex. *Solid red*, canals; *transparent*, cortical bone. *Bar* 1 mm.

Table 1. Descriptive statistics of cortical canal parameters of the human mandibular condyle

	Mean ± SD	Range
Cortical porosity (%)		
Cortical total	3.53 ± 1.19	2.26 - 5.52
Subchondral cortex	3.35 ± 1.77	1.11 - 6.27
Anterior cortex	3.27 ± 1.13	1.41 – 4.80
Posterior cortex	3.98 ± 1.68	2.06 – 7.01
Canal diameter (mm)		
Cortical total	0.053 ± 0.005	0.044 – 0.062
Subchondral cortex	0.048 ± 0.007	0.040 – 0.060
Anterior cortex	0.053 ± 0.004	0.045 – 0.059
Posterior cortex	0.058 ± 0.008	0.043 – 0.074
Canal separation (mm)		
Cortical total	0.52 ± 0.08	0.43 – 0.66
Subchondral cortex	0.50 ± 0.12	0.39 – 0.73
Anterior cortex	0.56 ± 0.10	0.49 – 0.83
Posterior cortex	0.51 ± 0.10	0.34 – 0.68
Canal number (mm^{-1})		
Cortical total	2.05 ± 0.28	1.66 – 2.44
Subchondral cortex	2.16 ± 0.46	1.39 – 2.65
Anterior cortex	1.87 ± 0.28	1.24 – 2.18
Posterior cortex	2.10 ± 0.40	1.51 – 2.89
Canal surface area (mm^{-1})		
Cortical total	1.88 ± 0.56	1.22 – 2.69
Subchondral cortex	1.84 ± 0.87	0.67 – 3.26
Anterior cortex	1.79 ± 0.56	0.81 – 2.57
Posterior cortex	2.03 ± 0.72	1.17 – 3.32
Canal degree of anisotropy		
Cortical total	2.05 ± 0.17	1.77 – 2.34
Subchondral cortex	1.85 ± 0.20	1.57 – 2.24
Anterior cortex	2.01 ± 0.21	1.65 – 2.21
Posterior cortex	2.30 ± 0.23	1.96 – 2.63
Mineralization bone (mg HA cm^{-3})		
Cortical total	1045 ± 57	922 - 1110
Subchondral cortex	1120 ± 52	1026 - 1201
Anterior cortex	987 ± 66	884 - 1077
Posterior cortex	1028 ± 68	857 - 1082

Cortical values: values of all 18 VOIs of the three subregions combined; SD values are a measure for interindividual variation (n = 10); *HA*, hydroxyapatite.

Table 2. Correlation coefficients between all canal parameters and mineralization

	Ca.Dm	Ca.Sp	Ca.N	Ca.S/BV	DA	TMD
Ca.V/TV	0.77***	-0.91****	0.95****	0.99****	-0.27	0.03
Ca.Dm		-0.52	0.55*	0.68**	-0.12	-0.26
Ca.Sp			-0.98****	-0.93****	0.26	-0.01
Ca.N				0.96****	-0.30	0.16
Ca.S/BV					-0.31	0.08
DA						0.35

Ca.V/TV, cortical porosity; *Ca.Dm*, canal diameter; *Ca.Sp*, canal separation; *Ca.N*, canal number; *Ca.S/BV*, canal surface area per unit volume of cortical bone; *DA*, degree of anisotropy; *TMD*, tissue mineral density of cortical bone. Significance of correlations: *$p < 0.1$, ** $p < 0.05$, *** $p < 0.01$, **** $p < 0.001$.

Table 3. Descriptive statistics of trabecular bone parameters of the human mandibular condyle

	Mean ± SD	Range
Trabecular porosity (%)	79.3 ± 5.1	72.6 – 87.4
Trabecular thickness (mm)	0.15 ± 0.03	0.11 – 0.22
Trabecular separation (mm)	0.70 ± 0.10	0.56 – 0.85
Trabecular number (mm^{-1})	1.44 ± 0.15	1.16 – 1.67
Trabecular bone surface area (mm^{-1})	16.44 ± 3.28	12.05 – 22.46
Degree of anisotropy	1.94 ± 0.21	1.71 – 2.23
Tissue mineral density (mg HA cm^{-3})	857 ± 41	790 – 906

SD values are a measure for interindividual variation ($n = 10$); *HA*, hydroxyapatite.

Table 4. Correlation coefficients between all trabecular bone parameters and mineralization

	Tb.Th	Tb.Sp	Tb.N	BS/BV	DA	TMD
Porosity	-0.79***	0.49	-0.63**	0.88****	0.47	-0.54
Tb.Th		-0.16	0.26	-0.86***	-0.46	0.60*
Tb.Sp			-0.85***	0.32	0.08	-0.09
Tb.N				-0.57*	-0.12	0.21
BS/BV					0.49	-0.67**
DA						-0.29

Porosity, 1 – BV/TV; *Tb.Th*, trabecular thickness; *Tb.Sp*, trabecular separation; *Tb.N*, trabecular number; *BS/BV*, bone surface area; *DA*, degree of anisotropy; *TMD*, tissue mineral density of trabecular bone. Significance of correlation:
* $p < 0.01$, ** $p < 0.05$, *** $p < 0.01$, **** $p < 0.001$.

Discussion

Recently, μCT has been applied in a few studies to quantify non-destructively the three-dimensional cortical canal network (desktop μCT: [120]; synchrotron radiation μCT: [122-124]. We provide for the first time quantitative information on topographical variation in orientation of the cortical canals in the human mandibular condyle using a μCT system. In addition, we have been able to examine porosity in relation to the tissue mineral density of the condyle. Together with porosity, the tissue mineral density is crucial for bone quality [69].

The orientation of the cortical canals was clearly anisotropic, *i.e.* the main direction was mediolateral in the subchondral cortex while it was superoinferior in both the anterior and posterior cortex. It is generally assumed that the osteons, and hence the cortical canals, are preferentially oriented along the main direction of loading [113, 125, 126]. Thus, the direction of cortical canals in the condyle might provide information about the loading history of the condyle.

So far, no information is available on the magnitudes and principal directions of stress and strain in the cortical bone during loading of the condyle. The direction of the cortical canals suggests that the principal directions of stress and strain are oriented mediolaterally in the subchondral cortex and superoinferiorly in the anterior and posterior cortex. The anisotropic orientation of cortical canals also suggests that the stiffness of the cortical bone is anisotropic, *i.e.* the subchondral cortex is probably stiffer mediolaterally than anteroposteriorly, while the anterior and posterior cortexes are stiffer superoinferiorly than mediolaterally. This anisotropy implies that the subchondral bone is more capable of sustaining loads in mediolateral direction, whereas the anterior and posterior cortexes are more capable of sustaining loads in superoinferior direction. A possible explanation for the anisotropy within the subchondral cortex is the direction of loading forces occurring during movement of the mandible. Koolstra & Van Eijden [55] reported a mediolateral shift of stress along the articular surfaces of the temporomandibular joint during open-close movements of the jaw. A similar mediolateral shift of stress is likely to occur within the subchondral cortex. The mediolateral orientation of the osteons within the subchondral cortex might be considered as an adaptation to this loading. Another possible explanation is related to mediolateral and anteroposterior differences in bending during loading [52]. Owing to the shape of the subchondral cortex, *i.e.* its convexity is less in the frontal than in the sagittal plane, the amount of bending is probably larger mediolaterally than anteroposteriorly. Mediolaterally oriented osteons might be more capable of resisting these larger bending forces. Comparably, the superoinferior orientation of the osteons in the anterior and posterior cortex might be optimal to resist the superoinferiorly directed forces that are transmitted from the

subchondral cortex and trabecular bone to the mandibular ramus.

The cortical porosity in the mandibular condyle (3.5%) reported in the present study is consistent with values reported for other sites of the human mandible [127, 128]. Cortical porosity in the human mandible seems relatively low compared to other human bones (*e.g.* femoral shaft: >5 %, [129]; femoral neck: > 10% [109]). The average diameter of the cortical canals (0.053 mm) in the condyle is also consistent with other sites of the mandible [128, 130]. Canal diameter and number have been reported to vary considerably across age, sex, and sampling site [129, 131]. We found that both these parameters correlated positively with cortical porosity.

In the condyle, cortical porosity did not change with age. By contrast, a positive correlation between cortical porosity and age has frequently been reported (human femur: [112, 131]; human mandible: [128]). The lack of influence of age in the present study might be due to the relative small number of condyles (n = 10) in comparison to the study of Verna *et al*. (n = 50). In the latter study both male and female samples were examined, without taking into account a possible effect of postmenopausal osteoporosis on cortical porosity [132, 133]. In the present study only samples from male subjects were examined to eliminate any additional phenomena that might have resulted from postmenopausal osteoporosis in females.

No significant differences in porosity between the three cortical regions of the condyle were found. This is in contrast with other studies; for example, within the human femoral neck differences were found between the inferior and superior cortex [109]. The anterior cortex of the mandibular condyle had a significantly lower tissue mineral density than the subchondral and posterior cortex, indicating that the proportion of less mineralized bone is higher in the anterior cortex. These differences are probably due to differences in occurring tensile/compressive stress [109, 111].

The reported values for the trabecular morphometric parameters where consistent with values reported by Giesen & Van Eijden [110]. We found no relationship between trabecular and cortical porosity, or between trabecular tissue mineral density and cortical tissue mineral density. This suggests that adaptive remodeling is independent and different between trabecular and cortical bone. The lower tissue mineral density of trabecular bone points to a higher remodeling rate, which is consistent with the higher surface to volume ratio available for remodeling in trabecular bone (16.44 mm^{-1}) compared to that in cortical bone (1.88 mm^{-1}). Mineral maturation in the condyle is less advanced in trabecular bone than in cortical bone and consequently the trabecular bone has an increased proportion of less mineralized bone and a decreased proportion of more mineralized bone compared to cortical bone. The present results indicate that larger trabecular porosity, and thus a larger trabecular surface area, coincides with a larger surface for remodeling and thus a lower tissue mineral density. Such a correlation

was not found between the surface area of cortical bone and cortical tissue mineral density. Although bone formation occurs at the surfaces of the cortical canals, the absence of a significant correlation is presumably due to the relatively small remodeling surface compared to the large cortical bone volume. In trabecular bone the remodeling surface is much larger.

The higher tissue mineral density in the cortical bone compared with that in the trabecular bone indicates that the tissue stiffness is higher in the cortical bone than in the trabecular bone, as the tissue mineral density is related to tissue stiffness [134]. From a mechanical point of view it should be noted that bone mineral provides rigidity to the bone. Bone tissue with a high tissue mineral density can be expected to be relatively stiff and brittle, which is likely to have reduced fracture toughness [79]. The relatively low tissue mineral density of the trabecular bone makes the trabecular bone of the condyle more compliant to bending than its cortical bone. Moreover, due to the relatively low tissue mineral density, the accompanying stress remains relatively low. The higher tissue mineral density in the cortex results in higher stress.

Some remarks about the methods used in the present study have to be made. First, μCT is superior in non-invasively visualizing and quantifying cortical canals in three dimensions. In the present study we did not compare our μCT data with those obtained from histological or microradiographic bone sections. Such comparisons have been reported for porosity measurements from μCT and histological sections [135, 136]. These studies showed strong correlations between the techniques. Second, the resolution used in the present study (10 μm) was relatively high compared to the mean diameter of cortical canals (53 μm). Therefore, we expected to be able to visualize the majority of cortical canals in the bone of the mandibular condyle, and subsequently quantify their orientation and the cortical porosity. However, with the resolution we used, the smallest cortical canals could not be visualized. According to Dempster & Enlow [130] about 7% of the canals in the mandible are 15 μm or less in diameter. Thus, the resolution used in the present study will inevitably result in an underestimation of the porosity and number of canals. This was also evident from the 3-D reconstructions, where the smallest canals had been broken up as the resolution was insufficient to resolve them. Cooper *et al.* [135] found that μCT underestimated porosity by about 0.5% and the number of pores (canals viewed in cross-section) by about 14%. The use of a higher resolution might decrease the amount of underestimation. A disadvantage of using higher resolution is the decrease of the field of view and consequently the requirement of relatively small bone samples; for the highest resolution possible with our scanner (6 μm), the maximum width of the samples would be 12 mm. Finally, the choice of the threshold influences the values of the morphometric and mineralization parameters. For example, if the chosen threshold was too low, it may be expected that this results in an underestimation of the cortical

porosity. In a separate sensitivity analysis we found that an increase or decrease in the threshold of 1.5% relative to the optimal threshold resulted in, respectively, an increase and decrease of about 7% of cortical porosity and of about 3.5% in diameter and number of canals (unpublished results). The error in the visually checked threshold was much smaller than the 1.5% variation that was used in this sensitivity analysis.

We conclude (1) that the principal directions of stress and strain are presumably directed mediolaterally in the subchondral cortex and superoinferiorly in the anterior and posterior cortex, and (2) that the amount of remodeling is presumably larger in the trabecular than in the cortical bone of the mandibular condyle; in trabecular bone variation in the amount of remodeling is related to the available surface area of the trabeculae.

Acknowledgements

We are grateful to Irene Aartman for statistical advice, to Peter Brugman for technical assistance, and to Jan Harm Koolstra and Geerling Langenbach for their comments on the manuscript. This research was institutionally supported by the Inter-University Research School of Dentistry, through the Academic Center for Dentistry Amsterdam.

CHAPTER 3

μCT-BASED BIOMECHANICAL MODELS APPLIED TO THE HUMAN MANDIBULAR CONDYLE

This chapter is based on publications in

Journal of Biomechanics

Renders *et al*, 2008: 41: 2793-2798

Journal of Biomechanics

Renders *et al*, 2011; 44: 402-407

Journal of Biomechanics

Renders *et al*, 2011; 44: 1826-1827

Byzko

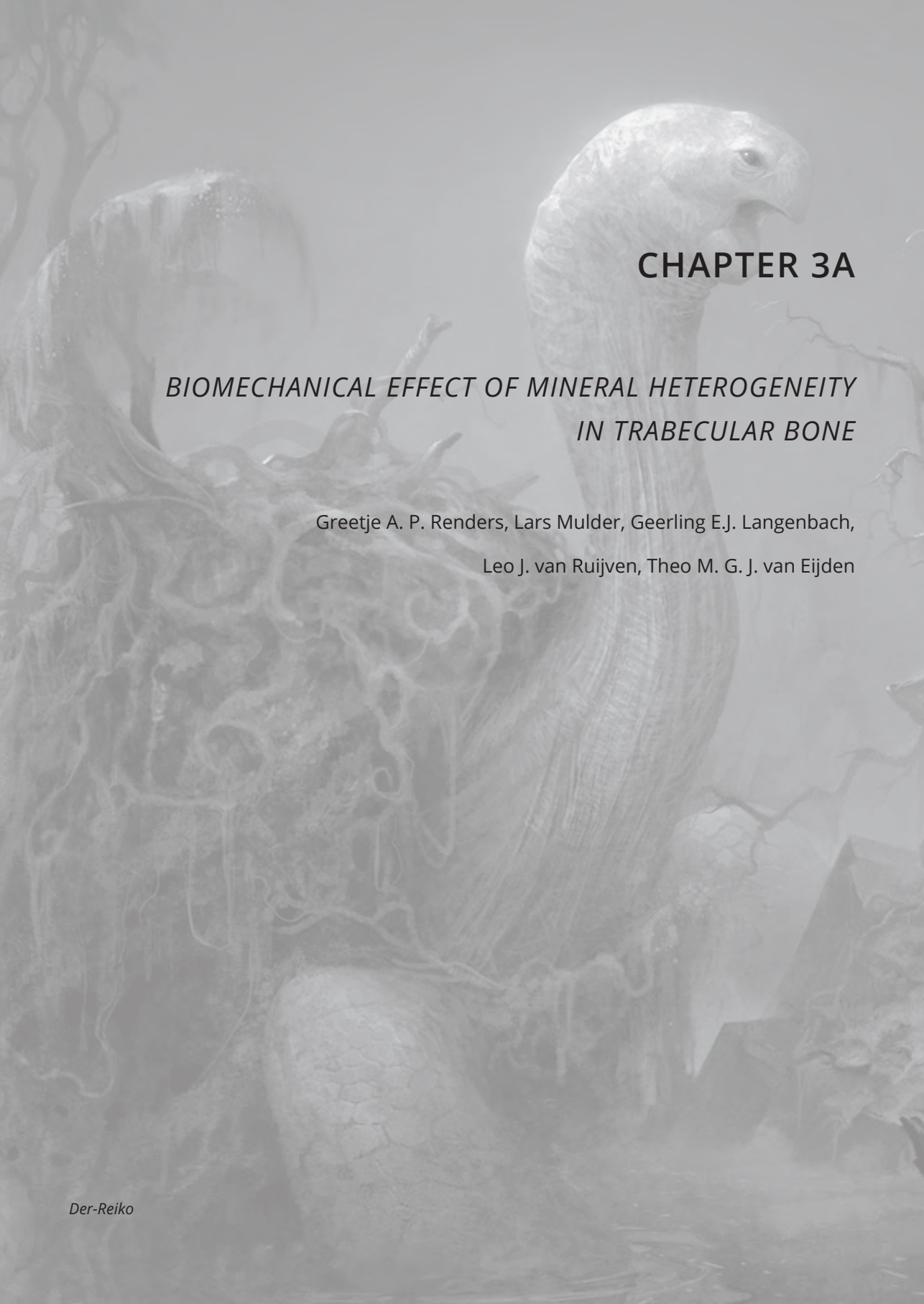

CHAPTER 3A

BIOMECHANICAL EFFECT OF MINERAL HETEROGENEITY IN TRABECULAR BONE

Greetje A. P. Renders, Lars Mulder, Geerling E.J. Langenbach,

Leo J. van Ruijven, Theo M. G. J. van Eijden

Der-Reiko

Introduction

The human mandibular condyle plays an important role in the function of the masticatory system, serving as a fulcrum between the mandible and the cranium. It is subjected to a wide range of mechanical loads both in direction and in amplitude. As a consequence it endures various deformations (*i.e.*, strain), which in turn lead to stress patterns in the bone tissue [137]. The relationship between bone loading (stress) and deformation (strain) depends mainly on bone properties like tissue mineral density and architecture [69]. As the condyle consists of a trabecular bone core with a relatively thin cortex, the properties of the former can be considered dominant.

Variations in the tissue mineral density of bone (TMD) are the product of the remodeling process, which occurs at the trabecular bone surfaces. Remodeling is also responsible for adaptation of the bone structure to make it effectively withstand the variety of applied forces during normal function [3, 90, 105, 138-141]. TMD is low in newly formed bone, and increases with the maturation of the bone tissue. Consequently, the TMD increases from the outer layers of trabeculae towards their centers [80, 81, 115]. Bone tissue with a high TMD is relatively stiff and brittle [79] whereas bone with a relatively low TMD is more compliant, leading to relatively low stress [53, 142, 143]. Therefore, mineral heterogeneity implicates heterogeneity of tissue stiffness, which may influence the apparent mechanical properties of the complete trabecular structure [75, 89, 90, 144-146]. Since mineral heterogeneity is a product of bone remodeling and caused by the bone loading history, it may contribute to the bone's capability to effectively withstand habitual loading.

The consequences of variation in microarchitecture for the apparent bone stiffness have been predicted by finite element (FE) analysis of trabecular bone [50, 147, 148] and cortical bone [149]. In addition, they have increased our understanding of the mechanical properties of the trabecular bone in the human mandibular condyle [88, 150]. However, the effect of mineral distribution has so far not been taken into account. Recently, it has been demonstrated that in developing porcine bone the estimation of apparent mechanical behavior using FE modeling are considerably influenced when the effects of mineral heterogeneity are ignored [142]. When these variations are artificially incorporated, FE methods may be used to predict the mechanical properties of bone with more accuracy [151]. Therefore, the purpose of the present study was to investigate to what extent the distribution of mineralization affects bone stiffness (*i.e.*, apparent Young's and shear moduli of the trabecular structure) in human mature trabecular bone. Using FE analyses, we compared the apparent Young's and shear moduli in simulated compression and shear tests of models where heterogeneity of mineral distribution was incorporated or disregarded. We hypothesized that incorporation of mineral heterogeneity evidently

can influence the predicted outcome of FE modeling.

Materials and methods

Bone samples

The study was performed on nine right condyles of nine dentate mandibles recently used in two other studies [115, 152], which were obtained from nine embalmed male human cadavers. Mean age was 68.1 years (± 14.2), range: 43-92 years, the number of teeth in the upper jaw 10.0 (± 4.7) and in the lower jaw 11.9 (± 2.4). The cause of death of the subjects was unknown. There were no signs of macroscopic pathologies. The cadavers were embalmed with a mixture of formalin, glycerol, alcohol, and phenol. The use of human specimens conforms to a written protocol that was reviewed and approved by the Department of Anatomy and Embryology of the Academic Medical Center of the University of Amsterdam.

µCT

Three-dimensional reconstructions of trabecular bone cubes were obtained by using a high-resolution µCT system (µCT 40, Scanco Medical AG, Brüttisellen, Switzerland). The condyles were mounted with their lateral pole facing down in cylindrical specimen holders (polyetherimide, 20.0 mm outer diameter, 1.5 mm wall thickness) and secured with synthetic foam. The samples were completely submerged in fixation fluid to avoid dehydration and scanned at 10 µm resolution. A 45 kV peak voltage was used, which corresponds to an effective energy of approximately 24 keV. An integration time of 1200 ms was applied to reduce noise substantially and to facilitate the discrimination between bone and background. The µCT was equipped with an aluminum filter and a correction algorithm that reduces the effects of beam hardening [84]. The scan time was 51.7 ± 4.0 hours for each sample. The number of slices was 2090 ± 182. The computed linear attenuation coefficient of the X-ray beam in each volume element (voxel) was stored in an attenuation map and represented by a gray value in the reconstruction.

Cubic volumes of interest (300 x 300 x 300 μm^3) were selected in 4 quadrants of each condyle: superolateral, superomedial, inferolateral, and inferomedial (respectively: SL, SM, IL, and IM; **Figure 1**). To discriminate between bone and background, the reconstructions were segmented using an adaptive threshold determination procedure supplied by the manufacturer. In order to facilitate segmentation, this procedure pursues a clear distinction between two peaks in the gray values histogram, one representing

bone and another background. Thus, in segmented images every voxel with a linear attenuation below the threshold (representing soft tissue or background) was made transparent and voxels above this threshold (representing bone) kept their original gray

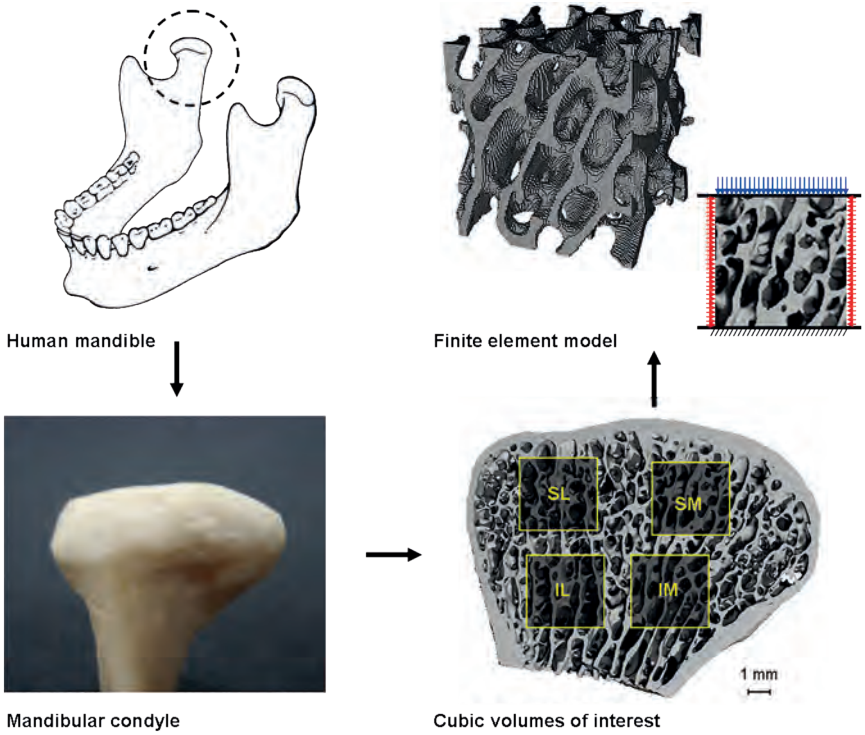

Figure 1. A schematic overview of the different steps in sample preparation. After the right condyle was separated from the mandible, it was scanned (resolution: 10µm) in a µCT system. Within each condyle four cubic volumes of interest (*i.e.,* SL, SM, IL, and IM) were selected and used for the construction of finite element models. The FE model and boundary conditions are shown in the top right panel (*blue arrows*: prescribed displacement on the top surface; *red arrows*: the displacements of nodes at the vertical surfaces were suppressed in the direction normal to the face; *black hatching*: the bottom surface was fixed).

value. Gray values were considered proportional to the local tissue mineral density (TMD). This is equivalent to the concentration of hydroxyapatite (HA) [84, 85] and quantified by comparing the attenuation coefficient with reference measures of a phantom containing HA of 0, 200, 400, 600, and 800 mg cm^{-3}. The obtained threshold was 39.7% of the maximum gray value (*i.e.,* 477 mg HA cm^{-3}, [153]), which was visually checked. To determine the radial distribution of TMD in the trabeculae a peeling algorithm was used. For description of this algorithm see Mulder et al. [80] and Renders et al. [115]. Relevant bone architectural parameters (BV/TV: bone volume fraction, Tb.N: trabecular number, Tb.Th: trabecular thickness, Tb.Sp: trabecular separation, SMI: structure model index, DA:

degree of anisotropy) were calculated with morphometric software (Scanco Medical AG).

Finite Element Analysis

Three-dimensional μCT reconstructions were used to create heterogeneous and homogeneous FE models for all nine condyles (*i.e.*, 36 condylar specimens). The voxels were directly converted into 8-node brick elements. The tissue modulus (E_t; expressed in GPa) for each element of the heterogeneous FE models was approximated from the TMD value of the corresponding μCT voxel according to ^{10}log E_t = -8.58 + 4.05 * log [Ca] [134], where [Ca] = (0.4 * [HA])/2.0 mg/g as approximately 40% of HA consists of calcium [98] and the specific density of trabecular bone tissue is 2.0 g cm^{-3} ([53, 89]. In the homogeneous FE models a standard E_t of 9.0 GPa was used for each element. The resulting apparent moduli of the homogeneous models were scaled afterwards so the tissue stiffness matched the averages measured in the heterogeneous models: scaling factor = ($E_t^{heterogeneous}$ / $E_t^{homogeneous}$). The bone tissue in all FE models was assumed to be isotropic with a Poisson's ratio of 0.3 [50, 87].

The apparent mechanical properties were estimated using an element-by-element FE-solver [50]. This program was modified to permit the assignment of different Young's moduli to each individual element. Six load cases were simulated for each volume of interest, comprising three compressive and three shear tests. From the results of these analyses, the complete elastic stiffness matrix was calculated [154, 155]. The best orthotropic representation of the apparent stiffness matrix of the specimen was calculated using a numerical optimization procedure. This procedure enabled the rotation of the original condylar coordinate system until the principal mechanical directions were found for which the Young's moduli and the shear moduli were greatest. The Young's moduli (E_1, E_2, E_3) and shear moduli (G_{23}, G_{13}, G_{12}) were approximated relative to these directions. Together, these directions constitute an orthogonal coordinate system. They were sorted such that $E_1 > E_2 > E_3$. The degrees of mechanical anisotropy (DA) were defined as E_1/E_3, E_1/E_2, and E_2/E_3. To determine the orientation of the principal mechanical directions relative to the condyle, they were projected on the sagittal and frontal planes.

Statistics

A general linear model for repeated measures was used to test for differences in architecture and TMD between the condylar subregions. As no significant differences were found between the trabecular subregions, the components of the global stiffness matrix (E_1, E_2, E_3, G_{23}, G_{13} G_{12}) and mechanical anisotropies (DA_{23} DA_{13}, DA_{12}) were averaged

per condyle for further analysis. A general linear model for repeated measures was used to test for differences between the homogeneous and heterogeneous models. Correlations between architectural and mechanical properties were explored by taking all specimens into account. SPSS 14.0 software (SPSS Inc., Chicago, IL, USA) was used to perform all statistical analyses. In all tests a *p*-value of less than 0.05 was considered statistically significant.

Results

The descriptive statistics of the architecture and TMD of the specimens are summarized in **Table 1**. The average TMD in the trabecular bone was 834 ± 52 mg HA cm^{-3}. Within the individual trabeculae a significant increase in TMD ($p < 0.001$) was seen with the distance from the surface towards the core (**Figure 2**). No significant correlation was found between bone volume fraction of the specimens and their average TMD.

The predicted average E_t for the heterogeneous model was 2.8 ± 0.6 GPa. When the mineralization heterogeneity was disregarded the approximated outcome of apparent mechanical properties after scaling for tissue stiffness was influenced considerably (**Table 2**). The apparent Young's moduli (E_1, E_2, E_3) and apparent shear moduli (G_{23}, G_{13}, G_{12}) of the homogeneous trabecular bone models were overestimated by maximally 21% (**Figure 3**) but on average by approximately 20%.

In both models resistance against shear was largest in the sagittal plane (G_{12} heterogeneous: 56 MPa; homogeneous: 68 MPa), and was relatively small in the transverse (G_{23} heterogeneous: 25 MPa; homogeneous: 31 MPa) and frontal planes (G_{13} heterogeneous: 31 MPa; homogeneous: 38 MPa). The degree of mechanical anisotropy was not significantly affected by TMD heterogeneity.

The relationships between bone volume fraction, TMD, and the various moduli are shown in **Figure 4**. The apparent Young's and shear moduli correlated positively with bone volume fraction ($p < 0.001$). This correlation differed for the various principal directions. Furthermore, in four occasions Young's and shear moduli were positively related to the average TMD of the samples (E_1, E_3, and G_{13}: $p < 0.05$, G_{23}: $p < 0.001$; **Table 3**). Interestingly, bone volume fraction accounted for up to 82% of the variation in apparent moduli whereas TMD accounted up to 29% of this variation. The large amount of scatter seen is probably due to the high inter-individual variation.

Table 1. Descriptive statistics of the trabecular bone of the human mandibular condyle

	Average ± SD	Range
Bone volume fraction (%)	17.0 ± 4.5	9.0 – 28.0
Trabecular number (mm^{-1})	1.34 ± 0.14	1.02 – 1.77
Trabecular thickness (mm^{-1})	0.14 ± 0.03	0.08 – 0.22
Trabecular separation (mm)	0.71 ± 0.08	0.53 – 0.93
Structure model index	0.62 ± 0.41	-0.2 – 1.49
Degree of anisotropy	2.26 ± 0.38	1.57 – 2.99
TMD (mg HA cm^{-3})	834 ± 52	672 - 922

SD: standard deviations are a measure for interindividual variation (*n* = 9); *TMD*: tissue mineral density; *HA*: hydroxyapatite.

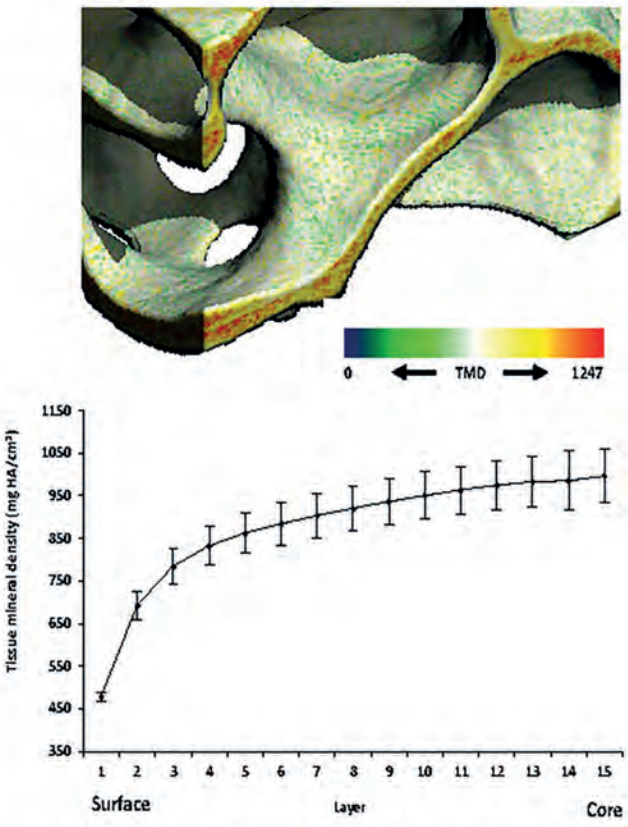

Figure 2. Mean TMD within the trabecular bone as a function of the distance from the surface of the trabecular elements. Layers of bone-containing voxels were consecutively peeled off (average layer thickness 7-8 µm). TMD increased from the surface (layer 1) towards the cores (layer 15), which can also be seen in a three-dimensional reconstruction of the trabecular elements. Standard deviations are a measure for interindividual variation (*n* = 9). *HA*, hy-droxyapatite; *color scale,* increasing TMD from blue to red.

Table 2. Influence of TMD distribution on mechanical properties[a] in the trabecular bone of the human mandibular condyle

	Heterogeneous model[b]	Homogeneous model
E_t (GPa)	2.8 ± 0.6	9.0
E_1 (MPa)	145 ± 54	182 ± 65***
E_2 (MPa)	98 ± 42	125 ± 52***
E_3 (MPa)	35 ± 19	46 ± 25**
G_{23} (MPa)	25 ± 11	31 ± 14**
G_{13} (MPa)	31 ± 12	38 ± 15**
G_{12} (MPa)	56 ± 22	68 ± 25***
DA_{23}	3.04 ± 0.76	2.96 ± 0.65
DA_{13}	4.74 ± 1.49	4.57 ± 1.44
DA_{12}	1.58 ± 0.47	1.53 ± 0.36

The apparent Young's and shear moduli of homogeneous model was scaled; so the tissue stiffness matched between both models; scaling factor = ($E_t^{heterogeneous}/E_t^{homogeneous}$). *TMD*: tissue mineral density; E_t: apparent tissue stiffness; $E_{1\text{-}3}$: apparent Young's moduli; G_{23}, G_{13}, G_{12}: apparent shear moduli; DA_{23}, DA_{13}, DA_{12}: degrees of anisotropy.

[a] Apparent Young's and shear moduli.

[b] Isotropic, heterogeneously distributed, specimen-specific tissue modulus distribution.

** Significance difference between heterogeneous and homogeneous models ($p < 0.005$), $n = 9$; *** Significance difference between heterogeneous and homogeneous models ($p < 0.001$), $n = 9$.

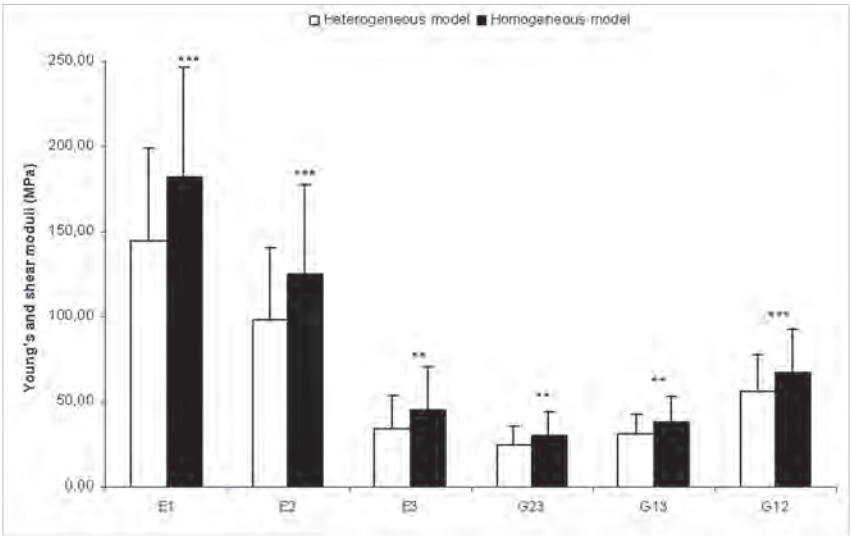

Figure 3. Influence of mineralization variations on mechanical properties of trabecular bone. On average, disregarding the TMD significantly increased the Young's (E_1, E_2, E_3) and shear moduli (G_{23}, G_{13}, G_{12}) to maximally 21% of the values from the heterogeneous FE models. *** $p < 0.001$, ** $p < 0.005$, $n = 9$ samples.

Table 3. Correlations between apparent moduli, BV/TV, and TMD in the heterogeneous FE model

	E_1	E_2	E_3	G_{23}	G_{13}	G_{12}
BV/TV	0.82***	0.92***	0.88***	0.91***	0.90***	0.92**
TMD	0.34*	0.32	0.33*	0.42***	0.38*	0.31

BV/TV: bone volume fraction; *TMD*: tissue mineral density; $E_{1\text{-}3}$: apparent Young's moduli; G_{23}, G_{13}, G_{12}: apparent shear moduli.
*$p < 0.05$, $n = 9$
***$p < 0.001$, $n = 9$.

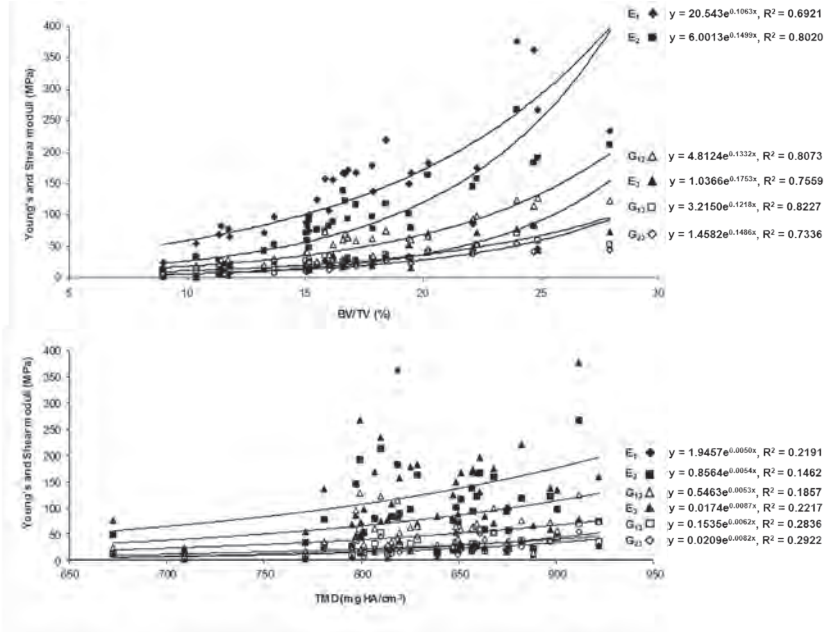

Figure 4. Relationship between Young's (E1, E2, E3) and shear moduli (G23, G13, G12), bone volume fraction, and TMD. *Top*: BV/TV versus apparent moduli; *bottom*: TMD versus apparent moduli.

Discussion

The ability of bone to function effectively under the imposed loads depends on the properties of the bone material (*e.g.*, tissue mineral density [TMD]; [143], and spatial arrangement of the bone material (*e.g.*, trabecular architecture; [137, 156]. Previously, this has been investigated with Finite Element (FE) models in which the variation of TMD was disregarded [88, 89, 150]. However, when mineral heterogeneity is incorporated in anatomically accurate FE models, refined estimations of the apparent bone moduli can be found [53, 151]. To clarify the influence of variations in mineralization, the apparent Young's and shear moduli in identical FE models incorporating or disregarding variation in mineralization were analyzed.

When the variations in bone mineralization were neglected, the apparent Young's and shear moduli decreased with maximally 21%, in comparison to homogeneous values. Our findings are in line with earlier results of decreasing mechanical moduli (20-24%) when mineral distribution was incorporated in FE models [146, 157]. However, it should be noted that these last studies used hypothetical mineral distributions in their heterogeneous models. In the present study, actual mineral distributions as measured with μCT were employed [80, 115]. Therefore, one should be cautious to compare the absolute moduli values of these studies. The suggested role of spatial mineral distribution in tissue moduli [157] influencing the biomechanics of trabecular bone was also found in the current study. The results are also in agreement with observed overestimations of apparent moduli (up to 24%) by Chevalier *et al.* [158] in their homogeneous FE models. The results of overall morphological parameters were within the same range as earlier findings in human condylar trabecular bone [152]. Furthermore, the average TMD and gradient of mineralization were in agreement with results of other recent studies [80, 115]. Within the trabecular bone, the highly mineralized older and more brittle bone is located in the core and is surrounded by layers with a, towards the trabecular surface, decreasing tissue mineral density. Other findings, such as the positive correlations between apparent moduli, bone volume fraction, and TMD, respectively, are in line with relationships found by Liu *et al.* [159]. The R^2 values of these correlations indicate more influence of bone volume fraction on the apparent moduli variation than TMD. However, TMD still accounts for up to 29% of the variation in apparent moduli, emphasizing the importance of this variable for the outcome of FE models.

The question arises how all these findings can be translated in biomechanical terms. According to Martin [160], bone needs to have a considerable resistance to deformation under loading, and within bone tissue, hydroxyapatite serves as the stiffening mineral to reach this resistance. Hydroxyapatite (HA) is an essential determinant for mechanical properties. Therefore, the relatively low TMD (*i.e.*, less HA) at the trabecular

surfaces might demonstrate a greater ability of bone to withstand strain without breaking [79, 161, 162] and the trabeculae are less prone to fracture when loaded in bending. From this perspective, heterogeneity in bone mineralization has a considerable influence on the prevention of crack initiation and propagation and will therefore be essential for research on bone toughness [163] and bone fatigue [164, 165].

Furthermore, bone has the advantage that it is a dynamic tissue capable of adapting its structure to local mechanical stimuli by changing factors like its TMD and architecture [166-170]. A change in mineralization is a product of bone remodeling, and because remodeling is dependent on the bone's loading history, this results in a bone structure capable of functional load bearing [160]. In addition, larger bending of trabeculae results in larger strain and thicker trabeculae, while less trabecular bending results in less strain en thinner trabeculae. Thus, it can be stated that trabecular bone is equipped with several tools that provide biomechanical advantages for the whole structure [162, 171]. It must be emphasized that the present study concerns the apparent moduli of gross volumes of trabeculae and does not consider the mechanics of individual trabeculae. Further research has to be performed to reveal these intratrabecular mechanical properties.

Some remarks have to be made with respect to the methods used in the present study. To avoid the influence of partial volume effects (superficial bone layers) and resolving power (effect of neighboring background voxels), the two most superficial bone layers were disregarded in the calculation of the average TMD values and in the statistical analyses. Furthermore, whereas *in vivo* bone exhibits viscoelastic behavior, the applied bone material characteristics within the FE models in this study were linear elastic and isotropic. For a more extensive description of the influence of these phenomena on the FE outcome see Renders *et al.* [115].

As hypothesized, incorporation of mineral heterogeneity did indeed considerably influence the predicted outcome of FE models. We conclude (1) that disregarding mineral heterogeneity led to a maximum increase of 21% in the apparent Young's and shear moduli measured with FE models. In addition, (2) mineralization variations of trabecular condylar bone possibly provide mechanical biological advantages to optimally withstand various loadings. Overall, the outcome of this study provides a possibility to use refined FE methods for estimations of apparent mechanical behavior. These models may in the future be used to analyze, for example, the impact of bone morphology and stiffness in bone tissue when affected by a disease as osteoarthritis [172-174].

Acknowledgements

We are grateful to Peter Brugman for technical assistance and to Jan Harm Koolstra for his critical suggestions. This work was funded by the Netherlands Organization for Scientific Research (NWO, grant number 021.001.050) and sponsored by the National Computing Facilities Foundation (NCF). The Inter-University Research School of Dentistry, through the Academic Center for Dentistry Amsterdam, institutionally supported this research.

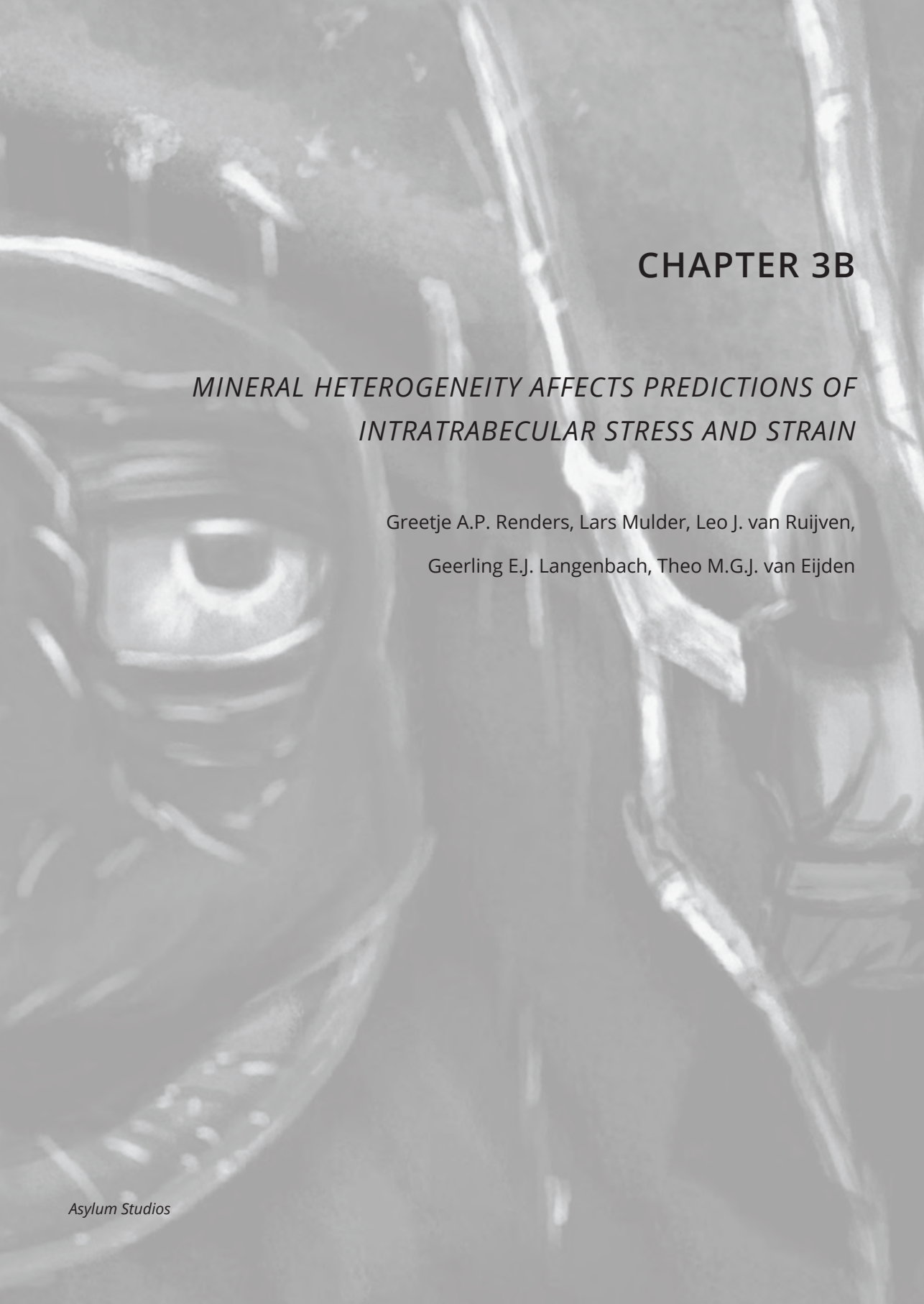

CHAPTER 3B

MINERAL HETEROGENEITY AFFECTS PREDICTIONS OF INTRATRABECULAR STRESS AND STRAIN

Greetje A.P. Renders, Lars Mulder, Leo J. van Ruijven,

Geerling E.J. Langenbach, Theo M.G.J. van Eijden

Asylum Studios

Introduction

The biomechanical behavior of bone depends not only on its microarchitecture but also on its mineral content [74, 96, 143]. In trabecular bone, *e.g.*, the microarchitecture is correlated to the apparent stiffness, *i.e.*, Young's modulus of bone tissue [159]. However, we recently have shown that variations in tissue mineral density of bone (TMD) explained up to 29% of the variance in the apparent stiffness, emphasizing the importance of this material property [175]. The knowledge of the biomechanical influence of TMD at the trabecular level is still limited and needs to be expanded.

As a result of the continuous remodeling process, trabecular bone tissue is composed of so-called bone packets, each having its own mineral content corresponding to its tissue age. A highly specific distribution of the mineral content throughout trabecular bone has been found with Fourier transform infrared microspectroscopy [81] and back-scattered electron microscopy [79, 176, 177]. At the trabecular surface, the site where remodeling predominantly occurs, relatively younger tissue with a lower TMD is found. Whereas, the relatively older and more mineralized tissue is found with increasing distance from the trabecular surfaces [177]. Although accurate, these methods are limited by their inability to measure the mineral distribution in three dimensions. This problem can be overcome with micro-computed tomography (μCT) that considers the 3-D structure and thus, the true spatial distribution of TMD [84, 178]. Indeed, several μCT studies have confirmed that mineral heterogeneity exists at the trabecular tissue level in both developing bone [75] and adult bone [53, 115, 146, 151, 157, 171].

The intratrabecular mineral distribution in bone tissue is nearly constant in healthy adult individuals and is independent of age, gender, ethnic origin, and skeletal site [171, 179]. Roschger *et al.* stated that the remarkable small biological variance in mineral distribution could suggest the existence of an evolutionary optimum with respect to the biomechanical performance of bone trabeculae [82]. Any deviations from a normal mineral distribution due to either disease and/or treatment might therefore be of significant biological and clinical relevance [180]. Nano-indentation studies have determined a close relationship between variations in tissue stiffness and the corresponding local mineralization [96, 97, 101, 142, 181]. Consequently, a change in mineral heterogeneity caused by unusually high or low levels of bone remodeling may be expected to have considerable effects on trabecular bone biomechanics due to this close relationship [98, 143, 182, 183].

MicroCT-based Finite Element (micro-FE) analysis enables predictions and visualization of the biomechanical consequences of variations in bone structure and mineralization [50, 53, 142, 175]. Micro-FE analysis has become a standard tool to examine trabecular bone's mechanical properties [184]. It allows for simulations of a

variety of load cases and can predict local stress and strain patterns at the trabecular level. The neglect of a material property, such as mineral heterogeneity, in biomechanical simulations could have significant influence on the predicted outcome. For example, in newborn porcine trabecular bone the incorporation of mineral heterogeneity in FE analysis tends to decrease the predicted average von Mises equivalent stress and to raise the average equivalent strain [185]. Moreover, predicted intratrabecular stress and strain patterns were affected. Whether such an influence is similar in adult human bone is yet to be determined. Compared to newborn bone, adult bone has had time to develop into a more defined structure due to an overall habitual loading pattern, which results in differences in structure (*e.g.*, trabecular thickness: [75, 80, 175]). These structural differences might influence the outcome of our FE study compared to previous work.

The aim of our study was to investigate how specimen-specific mineral distribution can affect predicted intratrabecular distribution of stress and strain in human adult trabecular bone. This was achieved by comparing two sets of FE simulations in which mineral heterogeneity was either included or neglected. In the latter, a homogeneous tissue stiffness was used assuming a homogeneous mineral distribution. This means that the mineral content near the trabecular core will be relatively underestimated, whereas, in the most superficial region overestimated. According to Currey [143], a relative higher mineral content leads to higher stress and lower strain values. Hence, we hypothesized that in human trabecular bone the predicted outcome of average stress and strain values and also their intratrabecular patterns will be affected when the mineral heterogeneity in FE analysis is neglected.

Materials and methods

Bone samples

This study was performed on nine right condyles of dentate mandibles obtained from nine embalmed human cadavers (mean age: 68 ± 14 yr). All cadavers were stored in a mixture of glycerol, alcohol, and phenol. Only male specimens were used to rule out any influence of postmenopausal osteoporosis. The use of these human specimens conforms to a written protocol that was reviewed and approved by the Department of Anatomy and Embryology of the Academic Medical Center of the University of Amsterdam.

μCT

A μCT 40 system (Scanco Medical AG, Brüttisellen, Switzerland) was used to obtain 3D

reconstructions from the trabecular bone of the condylar specimens. The μCT was equipped with an aluminum filter and a correction algorithm that compensates the effects of beam hardening reducing the estimated error of the measured linear attenuation to 10% or less [84]. Within all nine condyles, four cubic volumes of interest (3 x 3 x 3 mm^3) were selected giving a total of 36 trabecular samples [175]. Information on the scan and reconstruction procedures is specified in a previous paper [115].

Finite element analysis

All 36 trabecular samples (nine condyles; four regions per condyle) were transformed into FE models conform our previous FE study [175], using the 3D μCT reconstructions for which the voxels were directly converted into 8-node brick elements. Two sets of FE models of each trabecular sample were created by including or neglecting the mineral heterogeneity (*i.e.*, TMD; **Figure 1a and 1b**). The two sets were defined as heterogeneous and homogeneous. In the heterogeneous FE model the tissue stiffness (E_t^{He}; expressed in GPa) for each element was approximated from the TMD value of the corresponding μCT voxel according to $^{10}\log E_t = -8.58 + 4.05 * \log [Ca]$ [134], where [Ca] = (0.4 * [hydroxyapatite])/2.0 mg g^{-1} as approximately 40% of hydroxyapatite (HA) consists of calcium [98] and the specific density of mandibular trabecular bone tissue is 2.0 g cm^{-3} [186, 187]. This resulted in average E_t^{He} = 11.4 ± 2.6 GPa and range = 4.7 – 16.7 GPa. In the homogeneous FE model an artificially standardized E_t^{Ho} (9.0 GPa) was empirically chosen (irrespective of the corresponding μCT attenuation), so that the average E_t of both models approximately coincided [175]. By back-calculation of Currey's equation [134], E_t^{Ho} corresponded to an artificially TMD value of 791 mg HA cm^{-3}.

The models were solved using a linear elastic material model and the elements were considered isotropic with a Poisson's ratio of 0.3 [87, 188]. Uniaxial compression in superoinferior direction was simulated by applying a uniform strain (1%) on the superior surface of the specimen cubes. Displacement of nodes at the inferior surface was suppressed (**Figure 1c**). The superoinferior compressions were assumed to correspond most closely to the average joint loading direction [189]. From the stress and strain tensors, the average von Mises equivalent stress and equivalent microstrain were calculated. The intratrabecular 3D distribution of the von Mises equivalent stress and equivalent microstrain were studied by applying a peeling algorithm written in Matlab 7.0.4. [80, 115] (**Figure 1d**).

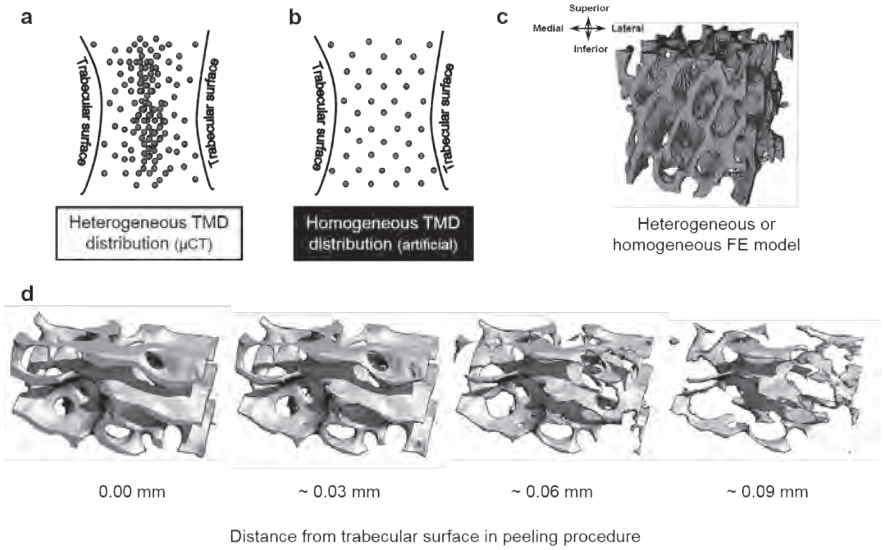

Figure 1. Graphic representation of material property implementation, FE model boundary conditions, and peeling procedure. A microCT-based heterogeneous mineral distribution (A) or an artificially homogeneous mineral distribution (B) was used to implement tissue stiffness in two different sets of FE models. C) The FE models were based on the 3D microCT reconstructions, ensuring the correct incorporation of the microarchitecture. The boundary conditions for all FE models (3 x 3 x 3 mm, n = 36) were according to our previous study [175]. The direction of loading was supero-inferior. D) A peeling procedure was used to determine intratrabecular stress, and strain distributions [80, 115]. Layers of bone-containing voxels were consecutively peeled off from trabecular surface to core (average layer thickness 7-8mm). In a small section of trabecular bone several steps of the peeling procedure are depicted with 0 to 0.09 mm distance from the trabecular surface.

Statistics

Since no significant differences were found between the four trabecular subregions, all parameters were averaged per condyle for further analysis (n = 9). A paired-samples t-test was applied for analysis of average stress and strain values *between* both models. Furthermore, a general linear model for repeated measures was used to analyze the peeling algorithm data: per layer *between* both models and the intratrabecular differences *within* both models (including all 36 trabecular specimens). In addition, the Bonferroni correction was applied to adjust for multiple comparisons. From frequency distributions the average von Mises equivalent stress, average equivalent strain and their standard deviation were determined. SPSS 16.0.2 software (SPSS Inc.) was used to perform all statistical analyses. A p-value of less than 0.05 was considered statistically significant. To avoid the influence of partial volume effects and resolving power, we did not include the two most superficial bone layers in the calculation of average values and in any statistical analysis.

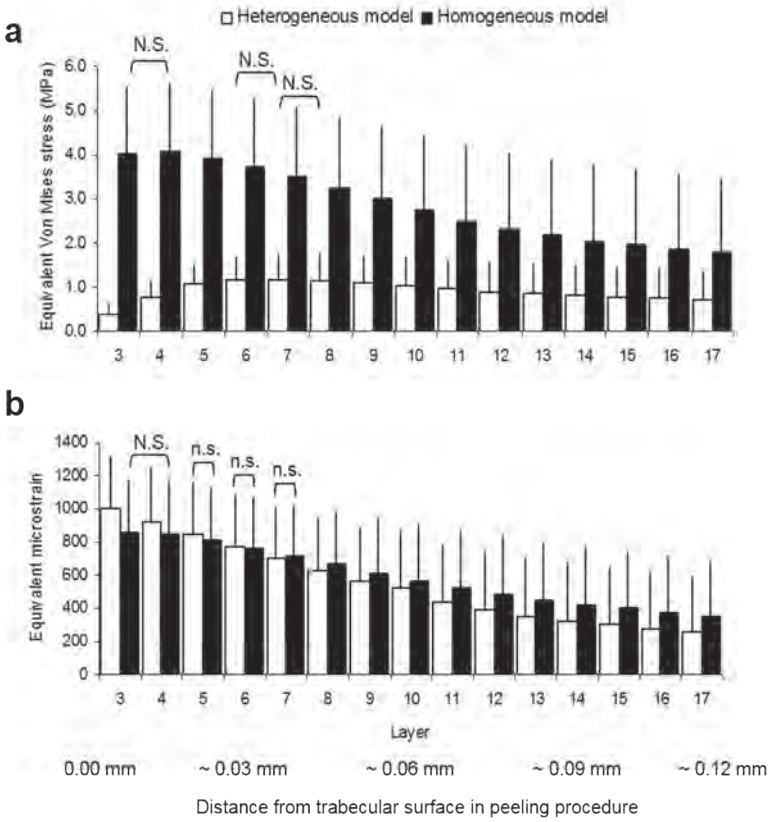

Figure 2. Intratrabecular distributions of average stress and strain estimations. These distributions were determined by the stepwise peeling procedure. On the *x-axis* the approximate distance of subsequent layers from the trabecular surface. **A** Intratrabecular distribution of the Von Mises equivalent stress in both FE models. Note the difference between the patterns. **B** Intratrabecular distribution of the equivalent microstrain in both FE models. Standard deviations are a measure for interindividual variation (n = 9). *N.S.*: No significant difference *within* FE model. *n.s.*: No significant difference *between* FE models.

Results

When mineral heterogeneity was disregarded, the average von Mises equivalent stress was approximately 3.2 times higher ($stress_{Ho}$: 3.80 ± 0.71 MPa; $stress_{He}$: 1.20 ± 0.37 MPa; $p < 0.001$). Thus, in the homogeneous model a higher stress was needed to obtain a similar strain. In both FE models, an interesting effect was seen regarding the intratrabecular stress distribution. In the homogeneous model, the highest stress was found at the surface with a significant decrease towards the core ($p < 0.001$). In the heterogeneous model this pattern was different. Between 0.008 to 0.032 mm from the trabecular surface the predicted stress value increased significantly ($p < 0.001$). A maximum was reached

at 0.040 mm from the surface. Deeper towards the trabecular core the predicted stress significantly decreased ($p < 0.005$; **Figure 2a**). When both FE models were compared, the overall predicted intratrabecular stresses were higher when the mineral distribution was

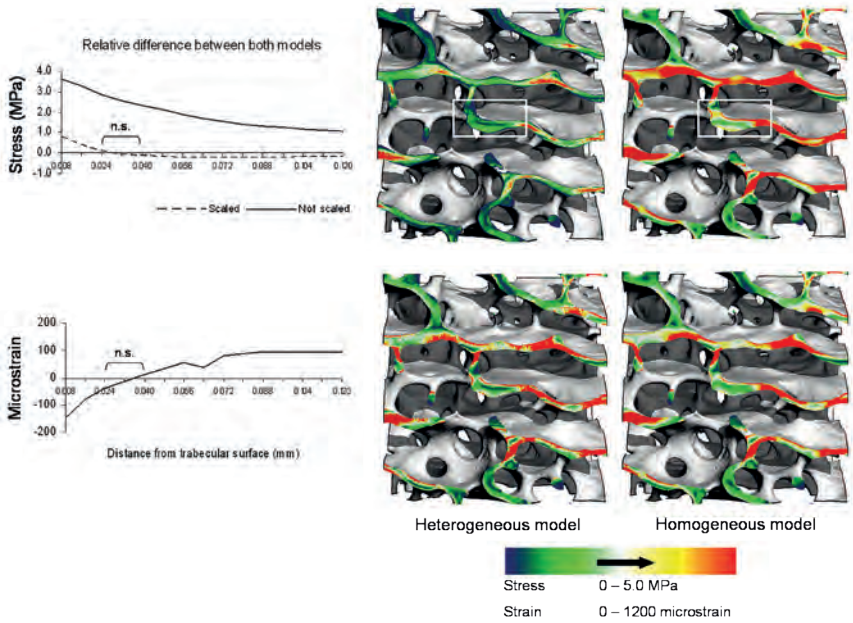

Figure 3. *Left panel*: Plots of the relative difference of intratrabecular stress/strain patterns between both models (*i.e.*, homogeneous minus heterogeneous). Dotted line in the upper plot is the stress pattern after a scaling procedure was applied (scaling factor = E_t^{He}/E_t^{Ho}). n.s.: No significant difference *between* FE models. *Middle and right panel*: Visualization of intratrabecular stress and strain distributions estimated with FE analysis (color scale increasing stress/strain from blue to red, and only visible at the cut plane). Predictions of stress and strain with the heterogeneous FE model in a trabecular cube can be seen in the middle panel. The right panel represents predictions of stress and strain patterns in the same trabecular cube but in the homogeneous FE model *(i.e.*, mineral heterogeneity neglected).

neglected (**Figure 3**: upper plot, solid line; $p < 0.001$). However, when a scaling procedure was applied to the homogeneous model (that resulted in the same apparent stiffness as that of the matching heterogeneous model; [175]) it resulted in an overall decrease in intratrabecular stress values. Nevertheless, the pattern remained the same with the highest stress at the trabecular core and a significant decrease towards the core (**Figure 3**: upper plot, dotted line). Compared to the heterogeneous model, significant higher stress values were found at the surface ($p < 0.005$) and significant lower stress towards the core ($p < 0.001$).

In retrospect, the validity of our choice for E_t^{Ho} expressed itself in the fact that the average equivalent strain in both models was not significant different (microstrain^{Ho}: 768

± 113; microstrain^{He}: 749 ± 142). Logically this should be the case because a set strain (1%) in both models was applied. At the trabecular level, in both models a significant decrease in strain values with distance from the trabecular surface was observed (**Figure 2b**: $p < 0.001$). However, statistical analysis (general linear model for repeated measures) of the difference in predicted strain per layer *between* the models showed a significant difference between both patterns, except between 0.024 and 0.040 mm (**Figure 2b**; **Figure 3**: lower plot, $p < 0.001$). The effect of incorporating mineral heterogeneity as material property in FE analysis was also visualized (**Figure 3**: middle and right panel). For instance, regions of lower stress predictions are found in the heterogeneous model compared to the corresponding regions in the homogeneous model (**Figure 3**: white bordered selections).

Discussion

The aim of this study was to investigate the effect of the bone's mineral heterogeneity on predicted intratrabecular stress and strain distributions. This was determined by μCT-based finite element (FE) analysis. We hypothesized that disregarding mineral heterogeneity in FE analysis would affect the predicted average values and patterns of intratrabecular stress and strain. This is likely due to the relative overestimation of the tissue mineral density of bone (TMD) at the trabecular surface compared to the relative underestimation of this parameter at the core in a homogeneous FE model.

When mineral heterogeneity was neglected, a 3.2 times higher average stress value was found in trabecular bone under uniaxial compression. In addition, significant higher intratrabecular stress values were predicted. These results, however, crucially depend on the choice of E_t^{ho} in our study setup. When the predicted stresses calculated with the homogeneous model were scaled, so E_t^{ho} matched the averages measured in the heterogeneous model, no significant difference was found. Nevertheless, the explicit difference in intratrabecular stress pattern between both models remained unchanged. The trabecular stress pattern in the heterogeneous model, with the lowest stress at the trabecular surface, corresponds to the profile described by Mulder *et al.* [185]. The highest stress values were found at a small distance from the trabecular surface, suggesting that the trabecular elements are bent during compression. Without scaling, an overestimation of overall intratrabecular stress was predicted using the homogeneous model, whereas Mulder *et al.* noted an underestimation. Concerning the predicted average strain, the trabecular elements showed the same tendency as the intratrabecular profile in newborn porcine trabecular bone [185]. The larger strains found at the trabecular surface indicate

that numerous trabeculae undergo bending deformation. Thus, only a small discrepancy in predicted stress between both studies exists. This indicates that the influence of mineral heterogeneity in newborn porcine trabecular bone is approximately similar to that in adult human trabecular bone.

Before elaborating more on the results of our study, a remark has to be made with respect to our method. Despite the excellent reputation of morphological analysis by μCT, a question remains of its ability to accurately measure mineral distribution. One of the causal factors for this discussion is the beam hardening effect, which is the process of increasing the average energy level of an X-ray beam by filtering out the low-energy photons. To overcome this problem a beam hardening correction algorithm is used leaving only some artefacts in the trabeculae on the outside of a sample [84]. In theory the tissue mineral density on the outside of the sample is somewhat higher than actual mineral values. As a consequence, the intratrabecular mineral distribution we found would be more distinct. Additionally, stress and strain patterns should also be clearer and more significant.

Mineral heterogeneity plays an important role in biological bone behavior [143]. The presence of minerals (*i.e.*, hydroxyapatite) gives bone tissue the ability to produce considerable resistance to deformation under loading [160]. Thus, the relatively high amount of minerals found in the trabecular core is important when the trabeculae are loaded in compression or subjected to bending. Therefore it contributes to the rigidity of the bone (*i.e.*, low strains, high stress [143]). On the other hand, relatively less mineralized bone tissue - as observed at the trabecular surface - is more compliant (low stress) and demonstrates a greater ability to undergo larger strains [79, 161, 162]. This bone behavior is consistent with the predicted behavior of the trabeculae in our heterogeneous FE model and thus confirms our findings. Although, we are obliged to mention that there is a lack of experimental validation in this study. Care should be taken when interpreting the results presented and therefore, only suggestions of possible biomechanical consequences and significance are made.

Of interest is how this work might be applied more broadly and, particularly, how these results can be applied to, for example, bisphosphonate-treated bone. FE analysis can provide the assessment of biomechanical effects of anti-resorptive treatments when mineral heterogeneity is included. Bisphosphonate treatment down-regulates bone turnover, which increases the homogeneity of bone mineral distribution and also the average mineralization [190]. This increase has been suggested as an important contributor to increased brittleness of bone tissue [191-195]. For example, due to increasing mineral homogeneity during treatment, trabecular stress patterns might shift from those found in our heterogeneous model to those predicted with the homogeneous model. The increased stress values at the trabecular surface could then indicate a

significantly higher fracture risk. Therefore, in the future, it is important to consider the bone mineral homogeneity caused by bisphosphonate treatment more carefully [196, 197], especially, as a new relevant bone quality factor when analyzing and predicting the effects of therapy duration or dose on bone properties in relation to changes in mineral heterogeneity [177].

As hypothesized, in adult human trabecular bone the mineral heterogeneity affects the predicted outcome of intratrabecular stress and strain patterns as determined with FE analysis. The stress and strain values predicted with FE analysis in this study may not reflect actual measured mechanical properties. Still, our findings do indicate that mineral heterogeneity should not be neglected in biomechanical studies on interesting topics such as the (long-term or dose dependent) effects of anti-resorptive treatments. Disregarding this parameter could have a major impact on the outcome of future fracture-risk FE studies.

Acknowledgements

Appreciation goes to Peter Brugman for technical assistance and Irene Aartman for statistical advice. We thank Jan Harm Koolstra, Vincent Everts, Nina Scheres, and Wilco de Jong for their comments on the manuscript. This work was funded by the Netherlands Organization for Scientific Research (NWO, grant number 021.001.050) and sponsored by the National Computing Facilities Foundation (NCF).

CHAPTER 3C

LETTER TO THE EDITOR

David W. Wagner, Gary S. Beaupré

&

RESPONSE TO "LETTER TO THE EDITOR"

Greetje A.P. Renders, Lars Mulder,

Leo J. van Ruijven, Geerling E.J. Langenbach

Bilou

Letter to the editor

We read with interest the recent article "Mineral heterogeneity affects predictions of intratrabecular stress and strain" by Renders *et al.* [198]. Several recent studies have identified the importance of incorporating mineral heterogeneity in tissue level analysis and the paper by Renders *et al.* adds to this literature. The authors present a method for assigning an elastic modulus to each micro-FE voxel based on the attenuation value of the corresponding voxel from a μCT scan. The implementation of the method proposed by Renders *et al.* addresses a critical need many researchers face when modeling tissue level structures; that of how to appropriately assign material properties to micro-FE models. Such a method could help improve the understanding of the complex relationship between microstructure and material heterogeneity as related to the overall macroscopic level bone strength. Because of the important need and potential widespread adoption of the method proposed by Renders *et al.* for deriving elastic modulus from μCT scan data, we feel it is necessary to highlight several assumptions that are inherent with this method, which are not explicitly stated in the text. We hope to clearly identify and discuss these assumptions such that other researchers are aware of the potential limitations when implementing a similar procedure.

In the article by Renders *et al.*, the authors relate the elastic modulus of bone tissue to the calcium content. The authors state "... the tissue stiffness (E_t^{He}; expressed in GPa) for each element was approximated from the TMD value of the corresponding μCT voxel according to $^{10}\log E^t = -8.58 + 4.05 \log [Ca]$ [134, 142], where [Ca] = (0.4 [hydroxyapatite])/2.0 mg g^{-1} as approximately 40% of hydroxyapatite (HA) consists of calcium [98] and the specific density of mandibular trabecular bone tissue is 2.0 g/cm^3 [186]."

In the equation used to determine [Ca] (calcium content weight fraction), the authors use the value of the hydroxyapatite density, [HA], obtained from the μCT scan data for each voxel within a given specimen. The authors use a constant relationship of 40% to scale the μCT derived [HA] density to an equivalent calcium density. The equation also requires a value for the bone tissue density, which the authors give as a 2.0 g cm^{-3}, to convert the μCT derived equivalent calcium density into [Ca] (mg Ca/g-dry defatted bone). In the study by Renders *et al.*, the value of bone tissue density is considered a constant and was taken from the literature.

The implementation utilized by Renders *et al.* to convert the μCT derived HA density to calcium content weight fraction has several issues related to the following inherent assumptions: (1) Bone tissue density of dry defatted marrow-free bone is constant and has a value of 2.0 g cm^{-3}; (2) The values of [HA] density and bone tissue density used in the equation to determine the Ca content weight fraction are independent.

The validity of the first assumption is evaluated with a view of the literature values for bone tissue density, which have been shown to vary substantially. For example, Giesen *et al.* [186] report a mean tissue density of 2.146 ± 0.054 g cm^{-3} for human mandibular cancellous bone in the axial direction. The range based on two standard deviations on either side of the mean value is 2.038–2.254 g cm^{-3}. For human cancellous bone taken from the proximal tibia, Ding *et al.* [199] report a mean tissue density of 2.20 g cm^{-3}, with a range based on two standard deviations of 2.06 – 2.34. Hernandez *et al.* [200, 201] calculated the tissue density of vertebral (cancellous) and femoral (cortical) bone samples using ash fraction and found results ranging from 1.634 to 2.26 g cm^{-3}. Finally, Day [201] measured the bone tissue density of dried, defatted specimens from cadaveric proximal tibiae taken from 35 donors ranging in age from 38 to 85 years. The lowest mean tissue density value was 2.11; the highest mean tissue density was 2.33. This uncertainty in bone tissue density is magnified when using the equations from Currey and Renders *et al.* to calculate an elastic modulus, due to the markedly nonlinear relationship. In the example presented by Renders *et al.*, a tissue density of 2.0 g cm^{-3} yields and elastic modulus of 9.0 GPa for an [HA] value of 1130 mg cm^{-3} (the [HA] value of 791 in Renders *et al.* is apparently a typographical error). Assuming a 15% greater tissue density (2.3 g cm^{-3}) yields and elastic modulus of 5.1 GPa. Assuming a 15% smaller tissue density (1.7 g cm^{-3}) yields and elastic modulus of 17.4 GPa. The value of the bone tissue density used in the equation to covert [HA] density to elastic modulus is obviously very important.

An additional point related to the first assumption is in regard to the appropriateness of using a dry defatted bone tissue density to calculate the calcium content weight fraction. We acknowledge that for a μCT scan voxel of a dry defatted bone specimen, the simple division of HA density (mg HA cm^{-3}) by the dry defatted bone tissue density (g cm^{-3}), and then multiplied by the constant 0.4 factor, will yield the appropriate measure of calcium content per gram soft dry defatted bone (mg Ca/g-dry defatted bone). However, if the specimens are not dry and defatted, additional calculations (not introduced by Renders *et al.*) must be performed. For example, if the specimen being analyzed is that of wet marrow free bone, the voxel of analyzed bone consists of ash, organics, and water (where previously the dry defatted bone only consisted of ash and organics). As such, the appropriate tissue density should be that calculated from a wet defatted bone to obtain the calcium content per wet defatted bone (mg Ca/g-wet defatted bone). Using a constant weight fraction of 0.828 g-dry defatted bone per g-wet defatted bone [202], an appropriate value for the equation relating Ca content weight fraction to elastic modulus can be attained.

The second assumption that [HA] (mineral density) and bone tissue density are independent is contradictory to what one would expect. The following derivation demonstrates that for a specimen of dry defatted bone, mineral density and tissue

density are related through the ratio of ash to organic weight.

Using the following definitions: [HA] is the mineral density of a bone voxel (hypothetically with no pores) from a μCT scan, rho_*t* the tissue density for the same voxel, and *V* the volume of the bone voxel. From the previous definitions, the mineral and tissue weights for the volume *V* are: [HA] x *V* = mineral weight of the bone voxel and; rho_*t* x *V* = tissue weight of the bone voxel.

Using the underlying constituents of dry defatted bone as being comprised of ash and organic components, the mineral and tissue weights can be redefined as: [HA] x *V* = mineral weight = ash weight; rho_*t* x *V* = tissue weight = ash + organic weight.
Ash weight appears as a contributor to both [HA] and rho_*t*. Therefore, only for the case where ash weight = 0 (*i.e.,* osteoid) does the original assumption that [HA] and rho_*t* are independent remains true. In all other situations, [HA] and rho_*t* will be related through the ratio of ash to organic weight.

In determining the elastic modulus using the approach given by Renders *et al.*, the ratio of hydroxyapatite density to tissue density is critical. Unfortunately, the primary output from a μCT scan is a voxel-based gray scale or attenuation value that is typically converted to HA density, based on the use of a manufacturer-specific calibration curve. The bone tissue density, however, is not directly measured during a μCT scan.

The approach proposed by Renders *et al.* addresses a critical need for voxel based material property assignment for heterogeneous models. However, the question remains of how appropriate is it to use a constant value of tissue density when the measured [HA] density on a voxel by voxel varies substantially. At this point in time it seems reasonable to conclude that if a constant value of tissue density is used for all voxels, regardless of the local [HA] density, and then there is the potential for substantial error in the estimated value of the elastic modulus for some voxels.

Response to “Letter to the editor”

We thank Drs David Wagner and Gary Beaupré for their interest in our work and their constructive comments. Generally, we agree completely with their analysis. We realize that, apart from regional variations in HA concentration, more factors determine the elastic modulus of bone tissue. The presented study can be regarded as a qualitative analysis on how local differences in HA concentration translate into mechanical behavior of whole trabecular elements. To that end we only included local differences in HA concentration, and already these differences demonstrated to have a considerable influence on trabecular, and herewith global mechanical behavior of bone. Wagner and Beaupré emphasize two additional factors that should be taken into account when

using μCT-based local HA concentrations to study its quantitative influence on trabecular bone mechanical behavior in finite element analyses. They rightly point out that these should have been discussed. Below are our two additional comments about these factors relating to the presented study.

The first deals with the fact that bone tissue density may differ from 2.0 g cm^{-3} (this value suggests constancy while ranges between 1.6 and 2.3 g cm^{-3} have been reported). However, the aim of our study was not to determine accurately the magnitudes of stress and strain, but to look at their changing patterns within the trabecular elements. We do not think that the assumption of a tissue density of 2.0 g cm^{-3} has affected these qualitative results. Furthermore, our study concerns only trabecular bone of human mandibles. Giesen *et al.* [186] found for this type of bone a standard deviation of 2.5 % in tissue density. Therefore, contrary to the example in the letter, the effect on tissue stiffness is much less. However, it still causes an uncertainty in the tissue modulus, but only of ± 1 GPa (the range is from 8.21 to 9.94 GPa). From earlier studies we know that the variation in tissue modulus due to the differences in mineral density is approximately 5 times larger. That means that the error introduced by neglecting the variations in the density is an order of magnitude smaller than the variations in HA concentration, for which we are introducing a correction.

Regarding our second additional comment, we agree with the authors that for future quantitative analysis it is also important that the equations, which, in the presented study are used for wet specimens should actually only be applied for dry defatted specimens. And that for wet specimens the equations have to be adjusted for instance in the way suggested by Wagner and Beaupré.

To conclude, we also assume that the mineral density and tissue density are correlated. But since the tissue density varies little in condylar trabecular bone from the mandible we are of the opinion that ignoring this correlation had little effect on the intratrabecular stress and strain patterns. However, it is not difficult to find bone specimens with a much larger variation in mineral densities. For these specimens we also think that this correlation can no longer be neglected to answer certain research questions. The line of thoughts of Wagner and Beaupré as expressed in their letter is an excellent guide on the additional contributors to tissue modulus for finite element analysis.

CHAPTER 4

IMPLICATIONS OF HIGH-DOSAGE BISPHOSPHONATE-TREATMENT ON BONE MEASURED WITH µCT

This chapter is based on publications in

Calcified Tissue International

Renders et al, 2014: 95; 436-445

Oral Diseases

Vermeer, Renders et al, 2017: 23; 126-133

Ourlak

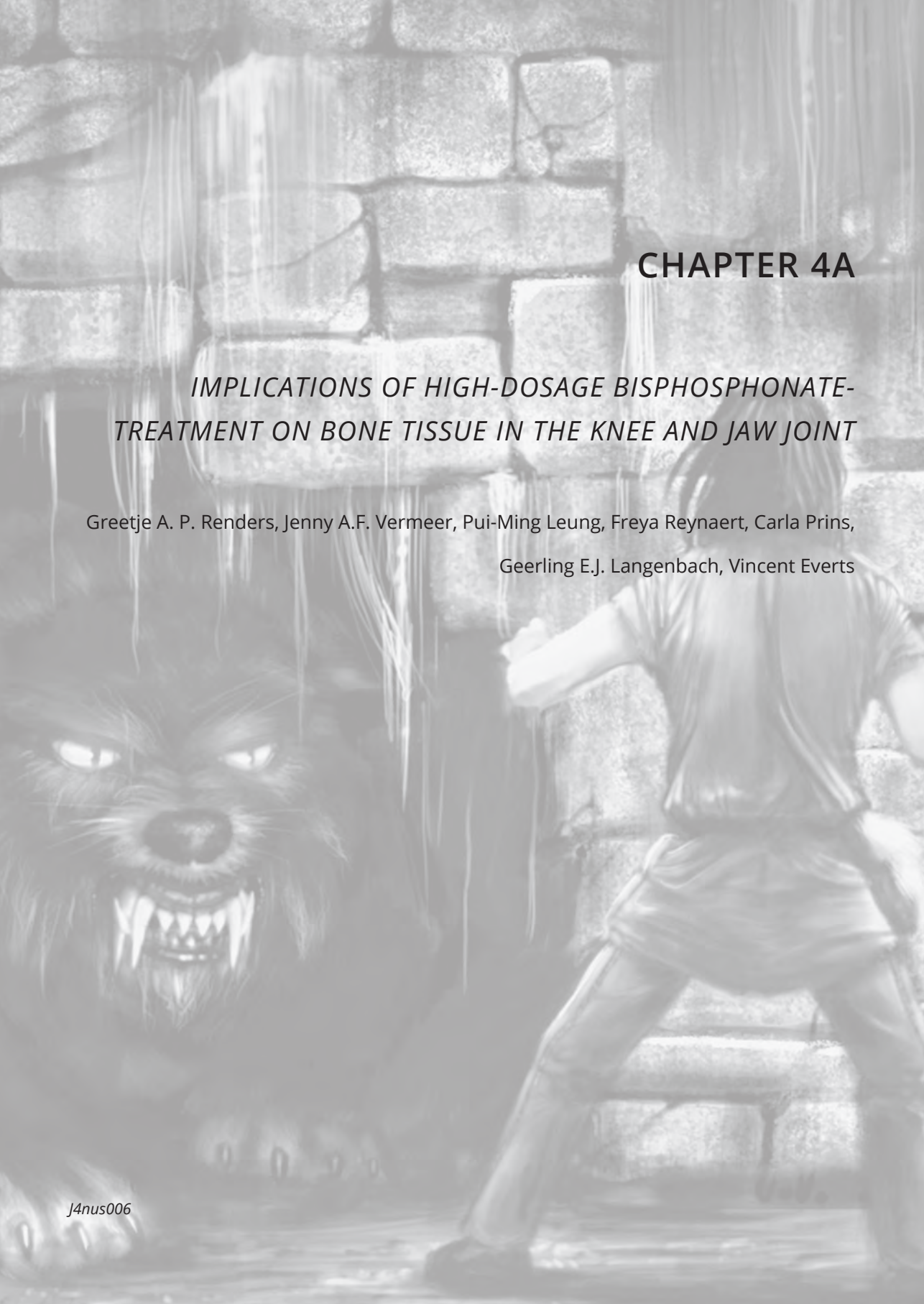

CHAPTER 4A

IMPLICATIONS OF HIGH-DOSAGE BISPHOSPHONATE-TREATMENT ON BONE TISSUE IN THE KNEE AND JAW JOINT

Greetje A. P. Renders, Jenny A.F. Vermeer, Pui-Ming Leung, Freya Reynaert, Carla Prins, Geerling E.J. Langenbach, Vincent Everts

J4nus006

Introduction

Normal bone homeostasis comprises the resorption of bone by osteoclasts and deposition of new bone by osteoblasts. In general, bone volume and tissue mineralization increase when the resorption rate decreases [58, 203-205]. This effect may also hamper subchondral bone remodeling, considered important in osteoarthritic bone alterations such as osteophyte formation and subchondral sclerosis [206]. Bisphosphonates (BPs) are bone antiresorptive agents traditionally used on a relatively large scale for treatment of bone metabolic diseases and on a smaller scale for bone metastasis treatment [58]. Nevertheless, since the early 2000s there is an increased attention in the field for the possible bone modifying effect of these agents for osteoarthritis treatment [59]. BP have an effect on areas of high bone turnover such as the subchondral bone in the osteoarthritis process [207]. For this reason, BP treatment for osteoarthritis is appealing because they enter osteoclasts, where they have a pharmacological effect on bone remodeling through a direct inhibitory effect on osteoclast activity itself and via apoptosis induction of these cells [208].

Most BP studies involve animal disease models [205]. While this is a good way to test clinical efficacy of BPs, the fundamental effects of BP treatment on other bone sites are difficult to measure reliably due to the interfering influence of the underlying disease. A study on the effects of BP treatment on healthy specimens will give more insight into the basic mechanisms of BPs and their effects on different bone sites. This becomes relevant, for instance, when BP-treated patients also have to undergo chirurgical dental treatment [209]. BP treatment has the well-known positive treatment effect of BPs on long bones in contrast to the reported worrying negative osteonecrotic effect of BP treatment on the jaw which causes further treatment difficulties for the dental specialists [210]. When BPs will be used more frequently in the clinic as a standard effective disease modifying osteoarthritis agent in the synovial joint of long bones. What can the dental specialists expect as a possible positive treatment effect or a negative side effect on the synovial joint of the jaw? To our knowledge, there is just one published study in which the effect of the second-generation BP alendronate on the jaw joint of growing rats was assessed [211]. In that study, alendronate treatment of young rats was shown to significantly alter the endochondral growth of the mandibular condyle due to an inactivation of osteoclasts. In the present study, we aimed to assess the effect of bisphosphonate on the mouse knee and jaw joint. For the treatment, zoledronic acid (ZA) was used, a third-generation BP that proved a potent osteoclast inhibitor and initiator of BP-related osteonecrosis of the jaw [212]. For bone assessment, μCT was used to make detailed analyses of the 3D bone microstructure and mineralization. We hypothesized that in the knee joint BP treatment would lead to an overall increased bone mineralization due to the influence

on bone remodeling. In addition, denser trabecular and cortical bone was expected. We furthermore hypothesized that BP treatment affects the bone in the jaw joint in a possible detrimental manner for instance comparable to BP-related osteonecrosis of the jaw. The differences between the effects of BP treatment on bone tissue in the knee and jaw joint was studied.

Materials and Methods

Animals

Healthy female C57BL/6JOlaHsd mice (age: three month at baseline) were obtained from Harlan Laboratories (Horst, The Netherlands) and maintained with a cycle of twelve hours light and twelve hours darkness in the conventional animal facility at the Center for Animal Facilities VU Medical Center (Amsterdam, The Netherlands). The animals ate commercial mice pellets and water *ad libitum*. After one week of acclimatization, we randomly allocated the animals to four groups. Two groups were ovariectomized and two groups were sham operated. The ovariectomized mice were used for other experiments, not mentioned in this study. Daily, the behavior and condition of the animals were checked visually. Weekly, the bodyweight of the animals was determined.

The experimental group or ZA treated group contained three subgroups with six animals per time-point (one, three and six months; total of eighteen animals). The animals received a weekly dosage by an intraperitoneal injection of 200 µL 0.5 mg kg^{-1} zoledronic acid (ZA; Novartis, Basel, Switzerland). This is comparable to dosage used in bone metastatic patients [205] and considered a high dosage. The control group contained six animals per time-point (baseline, one, three and six months; total of twenty-four animals). The animals in the control group received a weekly placebo treatment by an intraperitoneal injection of 200 µL sterile saline.

At baseline, and after one, three and six months the animals were euthanized by an intraperitoneal injection with a lethal dose of sodium pentobarbital (0.1 mL Euthestate, Ceva Sante Animale, Naaldwijk, The Netherlands). Both right and left knee and jaw joints were harvested. The samples were stored in a 4% phosphate-buffered formalin solution (pH 7.2, 4°C) until µCT analysis or until processing for histology. All animal experiments were approved by the Animal Welfare Committee of the VU University (Amsterdam, The Netherlands, permit number: ACTA2010-03).

µCT scanning

We used a micro-computed tomography system (µCT 40; Scanco Medical AG, Brüttisellen, Switzerland) to obtain and analyze 3D reconstructions of segmented volumes of bone. The mouse right and left knee and jaw joint samples were scanned in air. To maintain humidity, a reservoir on the bottom of the sealed specimen holder (inner diameter: 13 mm) contained a standardized amount of 2 mL phosphate-buffered saline (PBS). The samples were imaged using 8 µm isotropic voxels at 55 kVp, 145 µA, and 250 ms integration time. A complete scan required 116 minutes (397 slices) and 3.9 hours (635 slices) for the jaw and knee joints, respectively. For the study design we implemented the recent guidelines for adequate µCT research in rodent [213].

The polychromatic source and cone-shaped beam of the scanner was filtered with a 0.5 mm aluminum filter to eliminate the lowest energies from the beam. In addition, the beam hardening effect was further reduced by applying a correction algorithm developed by the manufacturer. Furthermore, the system was calibrated with phantom reference measures (QRM GmbH, Möhrendorf, Germany). Gray values were considered proportional to the local tissue mineral density (TMD). This is equivalent to the concentration of hydroxyapatite (HA) [84, 85].

µCT parameters

Imaging processing included Gaussian filtering and segmentation: sigma 0.8, support 1, threshold unit 170 (= 618 mg HA cm^{-3}). In order to enable comparisons between the knee and jaw joint, a uniform threshold was used for every measurement of each animal in both groups. Note: In this study the region of interest for jaw joint were the mandibular condyle defined as bone tissue of the mandibular head excluding the condylar process; additionally, the temporal bone defined as glenoid fossa bone tissue of the temporal bone. The regions of interest for knee joint were the femur and tibia both defined as bone tissue of both medial and lateral condyles or plateaus, respectively, including the intercondylar fossa [214]. For the knee joint, separate analyses were performed on both the tibia and femur. Trabecular and cortical bone were also analyzed separately. The region nearest to the epiphyseal growth plate was discarded, because this would most likely be newly formed bone. For the jaw joint, separate analyses were performed on both the mandibular condyle and temporal bone. The mouse jaw joint displays no specific recognizable differentiation in trabecular or cortical bone.

For the jaw joint, bone parameters such as the tissue mineral density (TMD; mg HA cm^{-3}) and bone volume (BV; mm^3) were determined. For the knee joint, additional bone parameters such as bone volume fraction (BV/TV; %), trabecular thickness (Tb.Th; mm),

and cortical thickness (Ct.Th; mm) were determined. The manufacture's morphometric software (Scanco Medical AG, software revision 3.2) was used.

Histological imaging

Following fixation and μCT scanning, one sample of each time-point within both groups was decalcified in 2.5% EDTA (pH 4.2, 21 days) at room temperature and embedded in paraffin. Frontal sections were cut (7 μm thickness) and attached to silane coated microscope slides. Paraffin was removed with xylene, sections were rehydrated and Haematoxyline-eosine (HE) staining was performed. Digital images were captured using a Leica DMRA microscope (10x magnification; fluorescence filter Green y3/cy3) equipped with a Leica DFC 420 C camera. Images were processed using Adobe Photoshop CS4.

Statistical analysis

All data sets were tested for normality using the Kolmogorov-Smirnov normality test (outcome: data normally distributed). One-way ANOVAs followed by Tukey's posthoc tests were performed to test the differences over time within a group. One-sample t-tests were used to compare the mean of the parameters against the hypothetical value 1.0 (no difference in parameter between two groups; *e.g.,* ZA/control or two regions cortical/trabecular). Tables and graphs represent means and standard deviations of six samples in which data from the right and left joints were averaged before further analysis. A *p*-value of less than 0.05 was considered statistically significant.

Results

Higher mineral density after ZA treatment in the knee joint

In the femoral trabecular and cortical bone (**Figure 1a**), TMD increased significantly over time in both groups. Only in the period between three and six months in the ZA group no significant increase was evident. The increase in tissue mineralization was significantly higher in the ZA group compared to the control group (trabecular bone up to three months; cortical bone up to one month). Comparable results were found for the trabecular and cortical bone of the tibiae (**Figure 1b**). Surprisingly, in both groups the femoral and tibial cortical TMD was significantly lower than the trabecular TMD at each time point.

ZA treatment has a profound effect on bone volume of femoral trabecular bone

In the femoral trabecular bone, a somewhat lower BV was found in the control group compared to the ZA group (not significant). A significant increase was seen in the ZA group with a significantly higher trabecular BV after six months (**Figure 1c**). In the tibial trabecular bone, a significantly decreasing pattern was found in the ZA group. There was no significant difference between the ZA group and control (**Figure 1d**). In both groups femoral and tibial cortical BV significantly increased with no differences between the groups (**Figure 1e, f**).

ZA treatment increased bone volume fraction over time in the knee joint

ZA treatment increased BV/TV significantly over time in both femur and tibia trabecular bone. In the control group BV/TV values dropped between three and six months. The BV/TV values in the ZA group were significantly higher compared to the control group in femur and tibia. There were no significant differences between femur and tibia (**Figure 2a, b**).

ZA treatment increased femoral trabecular thickness but did not affect cortical thickness

Over time, trabecular thickness increased in both groups with the most significant effects found in the femoral trabecular bone. The increase was more profound in the ZA group

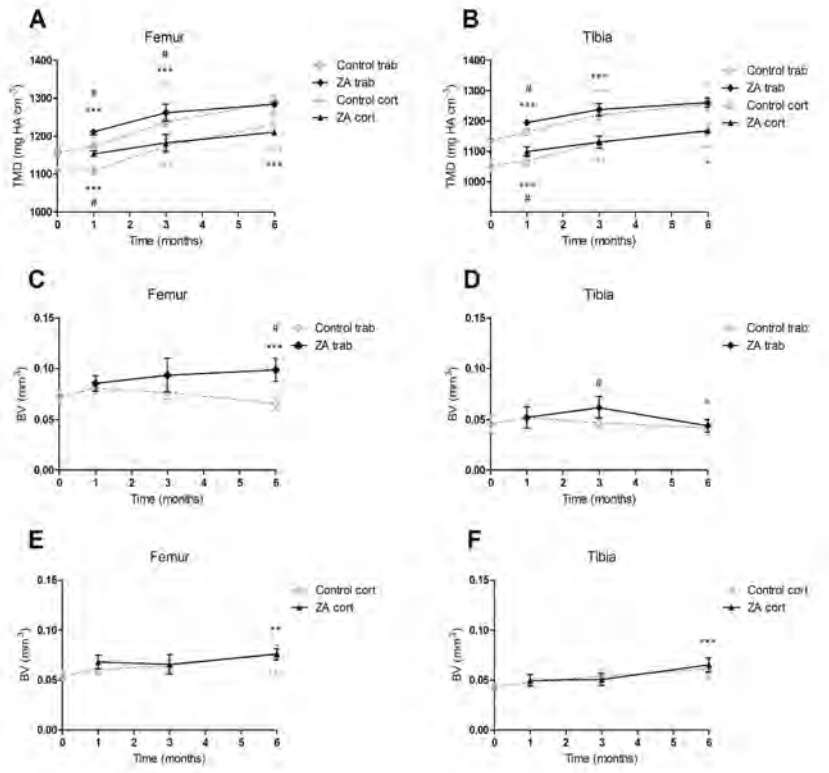

Figure 1. MicroCT analysis of femoral and tibial bone TMD and BV after ZA treatment.
A, B In both femur and tibia, tissue mineral density (TMD) was significant increased in trabecular and cortical bone in the control group and trabecular and cortical bone in the ZA group. **C** Femoral trabecular bone volume (BV) increased over time after ZA treatment and was significant higher compared to the control group. **D** Tibial trabecular BV decreased after ZA treatment. **E, F** In femur and tibia, a significantly increasing pattern was seen in the cortical bone in both control and ZA group.
The *x-axes* show the time after the start of treatment at the age of three months. Graphs show the means and standard deviations of six animals. *Filled diamonds* and *symbols* represent trabecular and cortical parameters in the control group (*gray patterns*) and ZA group (*black patterns*). *** $p < 0.001$ represent significant differences between time points within each group (*gray control*; *black* ZA significant levels). # represent significant differences between control and ZA group.

compared to the control group **Figure 2c, d**). Only trends were seen for increasing femoral and tibial cortical thickness with no significant differences between the groups. Overall, cortical thickness in both groups was significantly higher in the femur compared to the tibia in both groups (**Figure 2e, f**).

ZA treatment did not result in higher mineral density in jaw joint

A significant increase in TMD over time was found in the control group in both condylar and temporal bone. In the condylar bone of the ZA group only a significant increase was seen between baseline and one month after which TMD became stable. Condylar TMD values were significantly lower in the ZA group (**Figure 3 a**). After ZA treatment, increasing TMD was seen in the temporal bone with a sudden drop after six months (**Figure 3b**). The temporal TMD was significantly higher than the condylar bone.

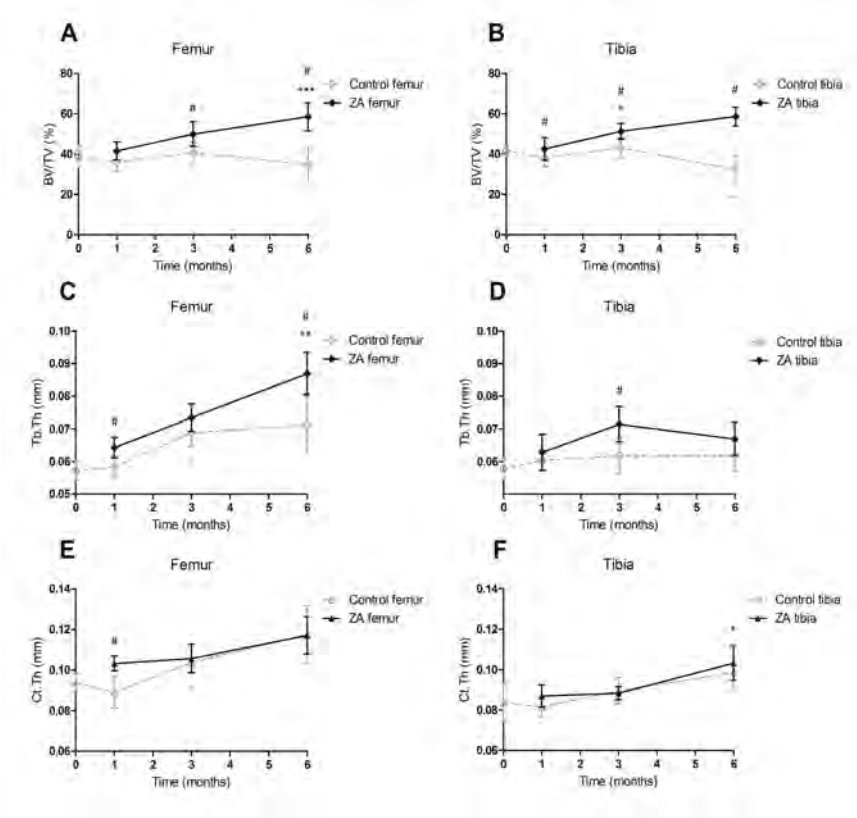

Figure 2. MicroCT analysis of femoral and tibial bone volume fraction, trabecular and cortical thickness after ZA treatment. **A, B** ZA treatment significantly increased bone volume fraction (BV/TV) in both femur and tibia compared to the results seen in the control group. **C** Trabecular thickness (Tb.Th) was significantly increased in the femur after ZA treatment but **D** unaffected in the tibia. **E, F** In both femur and tibia, a significant increased pattern was seen in cortical thickness (Ct.Th) in both groups. The *x*-axes show the time after the start of treatment at the age of three months. Graphs show the means and standard deviations of six animals. Filled diamonds and symbols represent trabecular and cortical parameters in the control group (*gray patterns*) and ZA group (*black patterns*). *** $p <$ 0.001 represent significant differences between time points within each group (*gray* control; *black* ZA signif-icant levels). *#* represent significant differences between control and ZA group.

Increase of bone volume in condyle after ZA treatment

Simultaneously with the change in TMD in the ZA group, a significant increase in bone volume was measured in the condyle. In the control group such changes were not found. BV values after ZA treatment were significant higher compared to the control group (**Figure 3c**). In the temporal bone, over time no significant BV changes were seen neither in the control nor in the ZA group (**Figure 3d**).

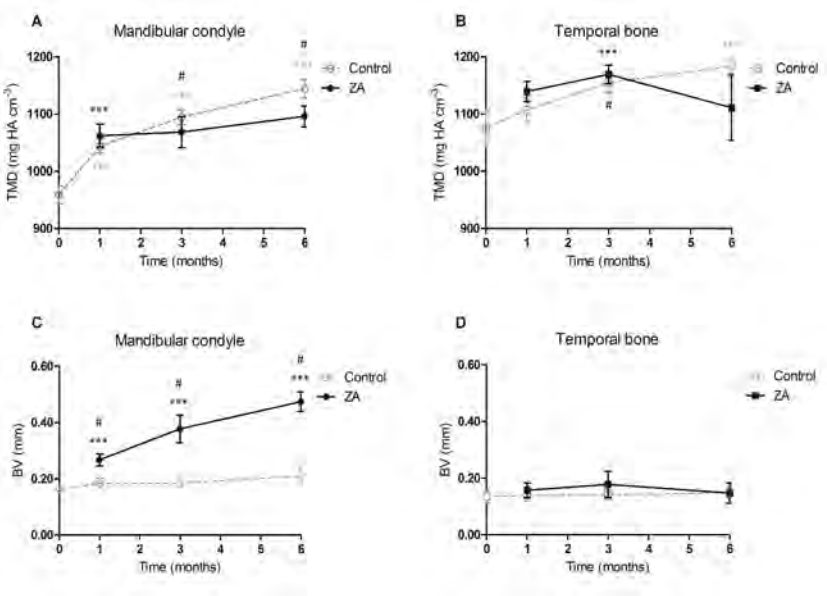

Figure 3. MicroCT analysis of mandibular condyle and temporal bone after ZA treatment. **A** Tissue mineral density (TMD) was increased in the control group and significantly higher compared to ZA group. **B** TMD was significant increased by six months in the control groups; significant increases by three months of ZA treatment but decreases by six months of ZA treatment (ns). **C** Bone volume (BV) of mandibular condyle in ZA group significantly increased over time and was higher compared to control. **D** BV in the temporal bone did not change with time in both groups. The x-axes show the time after the start of treatment at the age of three months. Graphs show the means and standard deviations of six animals. Filled circles and symbols represent condylar and temporal parameters in the control group (gray patterns) and ZA group (black patterns). *** $p < 0.001$ represent significant differences between time points within each group (gray control; black ZA significant levels). # represent significant differences between control and ZA group.

Regional differences in TMD in mandibular bone induced by ZA

The µCT images of bones of ZA treated mice showed an intriguing phenomenon (**Figure 4a**): the subchondral bone had a significantly lower TMD, whereas the "condylar core" had

a significantly higher TMD. This regional effect became more pronounced with increasing time (**Figure 4b**). Visualization of this phenomenon was possible after 3D reconstructions (**Figure 4c**). In the control's condylar bone and in the temporal bone of both groups this phenomenon was absent. The µCT images were compared with histology. If H&E histological sections are visualized with a fluorescence filter calcified tissues illuminate most bright [215]. In the histological images, the bone tissue can clearly be seen but also the different cartilaginous regions such as the hypertrophic (low mineralization) and proliferative (no mineralization) layers. After ZA treatment the hypertrophic layer thickens over time (**Figure 5**). For reference, the average thickness of proliferative and hypertrophic zone in three-month old C57BL mice is 113 µm [216].

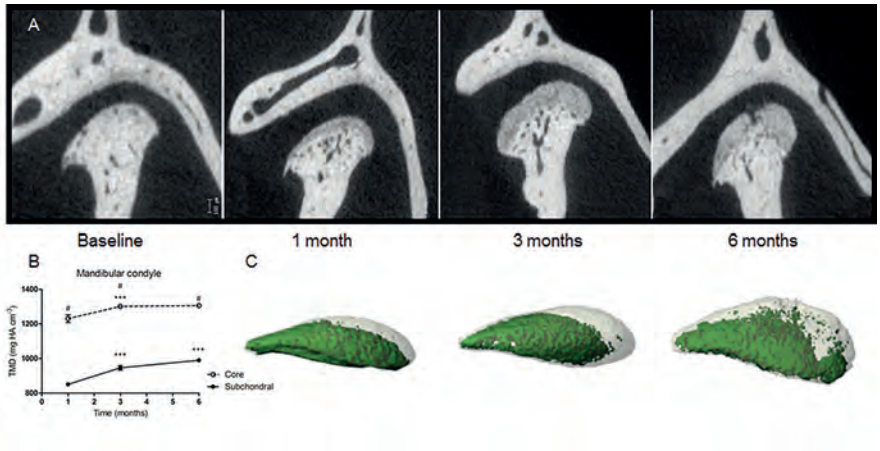

Figure 4. MicroCT images and 3D reconstructions of mandibular condyle after ZA treatment. **A** Transversal plane cross-sections of right jaw joint shows an increased subchondral region of lower tissue mineral density. **B** Tissue mineral density (TMD) was significant increased by six months in both core and subchondral region. The subchondral TMD was significantly lower compared to the core TMD. **C** MicroCT 3D reconstructions allowed visualization of the regional TMD after ZA treatment (green is core region). The *x-axes* show the time after the start of treatment at the age of three months. Graph show the means and standard deviations of six animals. *** $p < 0.001$ represent significant differences between time points within each region. # represent significant differences between subchondral and core region.

Discussion

The goal of our study was to assess and compare the effects of bisphosphonate treatment on bone tissue of the knee and jaw joint in healthy mice. We foresaw that treatment with the third-generation bisphosphonate zoledronic acid (ZA) elevates tissue mineral density, bone mass, trabecular, and cortical thickness in the knee joint in line with the literature. We hypothesized that a different, and possible detrimental, effect on bone tissue in the

jaw joint would occur.

Our results confirmed that ZA treatment indeed increased tissue mineral density (TMD) in the knee joint. Although, this was only evident at short term (three months). Regional differences in mineralization were detected between cortical and trabecular bone in both femur and tibia. We found a higher trabecular TMD compared to cortical bone in both groups over time (**Figure 1a, b**). The effect was accompanied by a long-term effect on microarchitecture such as bone volume (BV; **Figure 1c-f**), bone volume fraction (BV/TV; **Figure 2a, b**), and trabecular thickness (Tb.Th; **Figure 2c, d**). The most profound effect of ZA treatment on these parameters was seen in the femur. Further, ZA had no evident long-term effects on cortical bone (**Figure 2e, f**). The observed TMD values the paradigm of overall lower trabecular TMD due to the higher remodeling rate expected in trabecular bone [73, 74]. Bone mineralization occurs in two phases, the first one being primary mineralization: the initial mineralization of newly deposited matrix. The second phase is secondary mineralization in which the recently mineralized bone slowly matures, including small increase in mineral density and crystal size/perfection toward their maxima [217, 218]. This means that younger bone is less mineralized than older bone, simply due to having had less time for secondary mineralization. Trabecular bone has a larger surface area than cortical bone, meaning that at one point in time, more bone should remodel. This would in turn hinder the secondary mineralization resulting in a lower TMD when compared to cortical bone, where secondary mineralization lasts longer. An explanation for the "unusual" higher trabecular TMD can be found in the same paradigm of bone remodeling. If the remodeling rate is locally inhibited leading to thicker trabeculae and co-occurring increased bone volume and bone volume fraction, the number of highly mineralized bone modeling regions can increase, and subsequently TMD increases [219]. It is possible that the higher trabecular mineralization is not present within the entire femoral and/or tibial structure. Our data, however, did not indicate a difference between medial and lateral part of the joint (data not shown). To further elucidate these findings, additional studies that investigate the differences between trabecular and cortical bone mineralization in different parts of the femur and tibia are required. It should be noted that proposed explanation has to be completed with the footnote that data provided by Gamsjaeger *et al* [220] suggests that ZA can influence bone matrix formation and mineralization alterations in addition to its antiresorptive effects.

For the bone volume fraction of the femoral and tibial trabecular bone, a significant difference was detected between the ZA group and the control group at six months. With regard to the antiresorptive effects of BP, we expected bone volume fraction to increase. However, this did not seem to be the case for cortical thickness. An increase in the ZA group compared to the control group was seen in the femur at one month, while at six

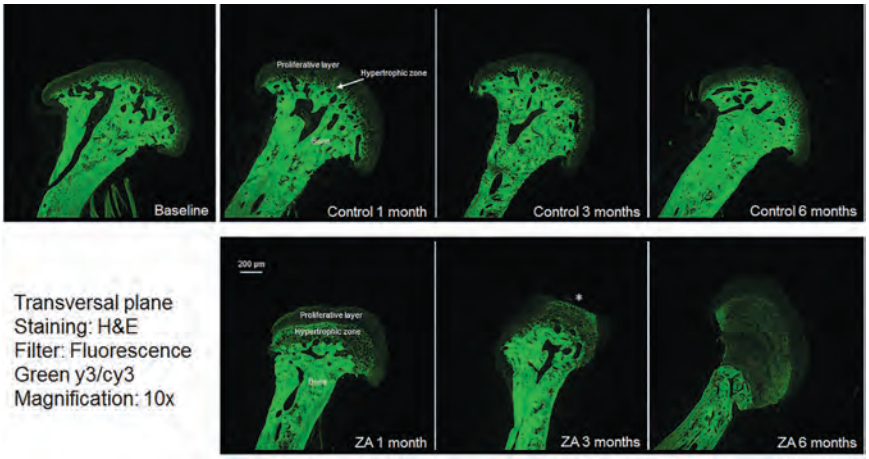

Figure 5. Representative H&E histological images captured with a fluorescence filter. Clear illumination of the bone tissue in the baseline and control samples is evident. In the control sample the hypertrophic and proliferative layers are visible. In the ZA samples the hypertrophic layers become more evident and dominantly present layer and can be seen on the µCT images. *Asterisk* is a cutting artifact, a small section of the cartilage is missing.

months this effect was gone. In the tibia there were even no significant differences at one month, although an overall increase over the course of months was present. In contrast to our expectations, no significant differences were found in cortical thickness between the groups at six months. This is in line with results from another study by our group (unpublished results) in which the diaphyseal region of the humeri in the same animal batch showed reduced bone turnover. For the current results, this could indicate a similar effect in the epiphyseal region of the femurs and tibiae, where both bone resorption and bone formation may be inhibited.

In the past different treatment effects of BPs on long and jaw bone were found [221-223]. Therefore, we hypothesized that BP treatment affects the bone tissue in the jaw joint in a possible detrimental manner since it is part of the mandible. Based on the literature we also hypothesized that there is likely a difference in how ZA affects bone tissue in the jaw joint compared to the knee joint [222, 224, 225]. In our study, ZA treatment resulted in bone-site specific changes in mineralization; a significant time-dependent higher TMD was evident in the subchondral bone compared to the most distal region of the condyle (**Figure 4**). Our µCT images revealed the presence of mineral in this region. Histological sections showed that this region does not contain mature bone tissue but a cartilaginous region with a low level of mineralization depicting the hypertrophic (low mineralization) and proliferative (no mineralization) layers. After ZA treatment, the hypertrophic layer clearly thickens over time (**Figure 5**). This region is where endochondral ossification normally occurs involving mineralization of the cartilage, vascular invasion, loss of chondrocytes, and differentiation of osteoblasts to deposit

bone on the mineralized cartilaginous framework [226] similar to the zone of provisional calcification in the knee joint [227]. Bradaschia-Correa and co-workers [211] reported significant alterations of the endochondral ossification in the mandibular condyle after alendronate treatment in growing rats. In the latter study, the recruitment and fusion of osteoclasts at the ossification zone during growth were not the impedimental factors for remodeling but a latent osteoclast phenotype (*i.e.*, inactivated) was. The regional ZA effect we found can explain the excessive increase in bone volume combined with the lack of increase in mineralization compared to the control group. This could mean that BP has an impairing effect on mineralization of bone and cartilage in the mandibular condyle as seen in the tibial epiphyses of rats [228] not only due to bone-specific differences [224] but also to cartilage-related differences [229] between these two synovial joints.

Before summarizing our study, a remark has to be made with respect to our method. Despite the excellent reputation of morphological analysis by µCT, a question of its ability to accurate measure TMD values remains. One of the causal factors for this discussion in the beam hardening effect, which is the process of increasing the average energy level of an X-ray beam by filtering out low-level photons [230]. To overcome this problem, the µCT system is equipped with a 0.5 mm aluminum filter to eliminate the lowest energies from the beam. Additionally, improved beam hardening algorithms are applied to make TMD measurements by µCT more accurate, however, residual artifacts must still be contented with [84, 231-233]. These residual artifacts maybe can partially explain the TMD differences we have observed between cortical and trabecular bone in femur and tibia. Although we think that it cannot explain the total difference.

In summary, some unexpected observations were made in this study. In the femoral and tibial epiphysis a higher trabecular tissue mineral density compared to the cortical tissue mineral density was found. In our research set-up, treatment with zoledronic acid had mainly influenced the other trabecular bone parameters in the knee joint. Unseen in the knee joint, an intriguing phenomenon was detected in the jaw joint that consisted of increased bone volume of the mandibular condyle probably due to impaired ossification in the zone of provisional calcification causing a thickened layer of lowly mineralized tissue. Additional studies are needed to further elucidate these findings. Bisphosphonate usage will not only increase due to its usefulness for osteoarthritis treatment, it is also frequently recommended for treatment of bone disorders such as osteogenesis imperfecta, juvenile Paget's disease and secondary osteoporosis [234]. Our data could indicate the possibility of negative side effects, *i.e.* disturbing normal mandibular development in the group of young adults that undergo bisphosphonate therapy.

Acknowledgements

This project was funded by the Dutch Organization for Scientific Research (NWO; grant number: 021.001.050). The authors thank Rika van der Laan (Center for Animal Facilities VU Medical Center, Amsterdam); Jolanda Hogervorst, Marion van Duin, Hans Korfage (Oral Cell Biology and Functional Anatomy, ACTA, Amsterdam), and Jan Stap (LCAM-AMC, Amsterdam) for their technical assistance. Appreciation goes to Lars Mulder for editorial advice.

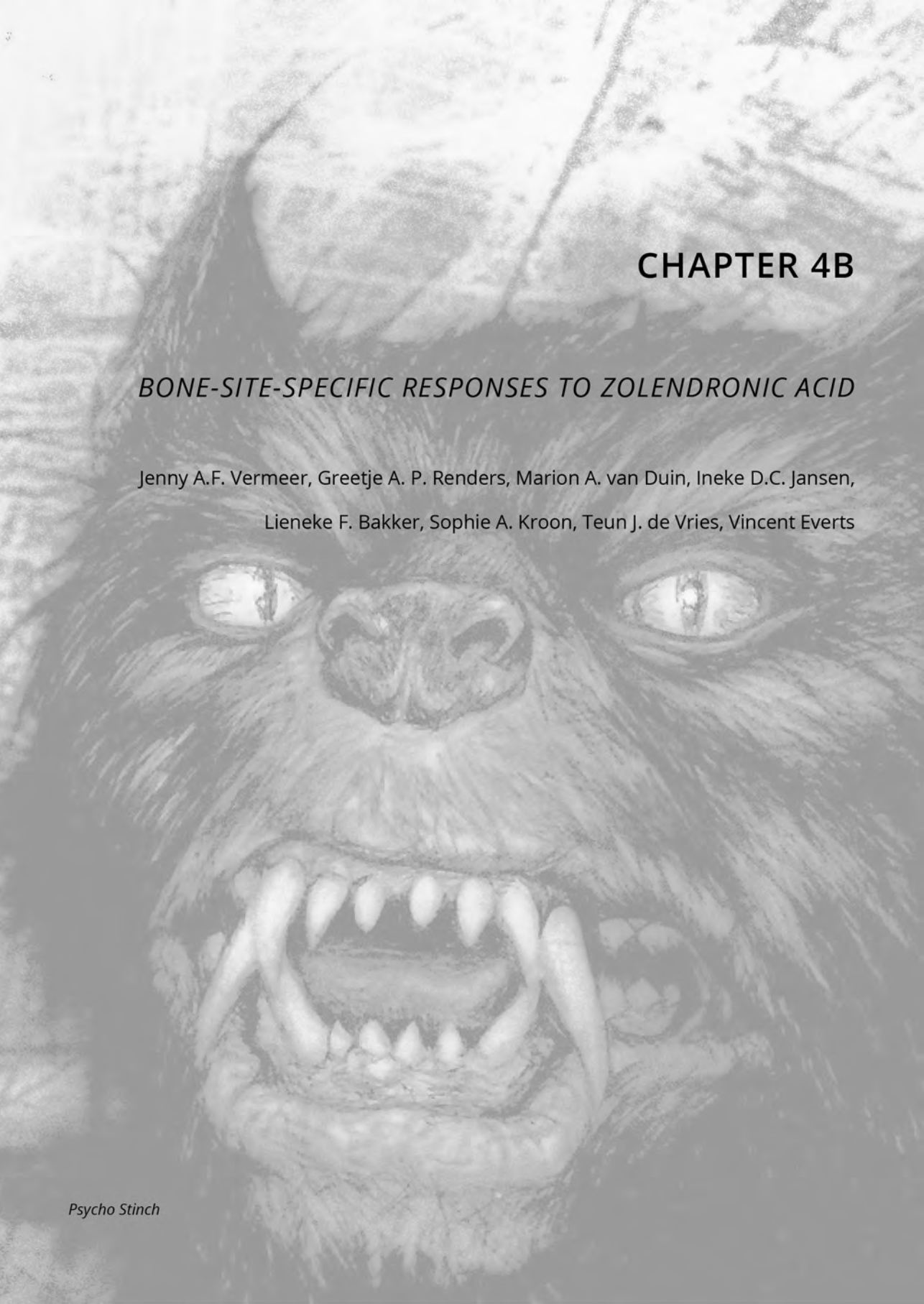

CHAPTER 4B

BONE-SITE-SPECIFIC RESPONSES TO ZOLENDRONIC ACID

Jenny A.F. Vermeer, Greetje A. P. Renders, Marion A. van Duin, Ineke D.C. Jansen, Lieneke F. Bakker, Sophie A. Kroon, Teun J. de Vries, Vincent Everts

Psycho Stinch

Introduction

Bisphosphonates (BPs) such as zoledronic acid (ZA) are used to treat diseases characterized by excessive bone resorption. By inhibiting osteoclastic bone resorption, BPs improve bone quality and reduce fracture risk. A side effect of high-dose BPs containing nitrogen is bisphosphonate-related osteonecrosis of the jaw (BRONJ) [235]. Its prevalence is low (<0.001%) in the general population and in patients receiving low doses; however the incidence increases to around 5% in patients receiving high intravenous doses [236]. In the majority of the cases (67%), BRONJ was preceded by a dental extraction or other oral trauma [209] and BRONJ was often (84%) accompanied by periodontitis [237].

Although several *in vivo* models have shown that BP treatment induces necrotic jaw bone, these signs of BRONJ have not been consistent. ZA treatment did not lead to mandible necrosis in beagle dogs when used up to six months [222] or when combined with dexamethasone after tooth extraction for nine months [238]. In contrast to this, 3 years of oral alendronate treatment caused mandible necrosis in 25-33% of the treated dogs [221], indicating that long-term treatment may be necessary to cause signs of jaw necrosis in dogs [222]. In mice, BPs delayed alveolar bone healing after tooth extraction, especially in combination with an immunosuppressive agent [239, 240]. BP treatment did induce signs of BRONJ in rat models for periodontal disease [241, 242]. Despite the development of these models, previous studies generally lack a direct comparison of long bones and jaw, and it remains unclear how and why specifically the jaw is affected by BP treatment. To explain bone-site-specific effects of BPs, it is essential to gain more insight into the bone remodelling activity in the different bones in the absence of trauma.

Previously, we hypothesized that different effects of BPs on osteoclasts in the jaw and in long bone may explain the aetiology of BRONJ [224]. We showed that BPs affected long bone and jaw osteoclastogenesis similarly *in vitro*, but that osteoclast precursors from the jaw internalized more BPs than long-bone marrow precursors from mice. In the current study, we used the same animal model to investigate whether BP treatment affects osteoclasts and their precursors differently in the jaw and long bones of mice. Moreover, we studied the effect of BP treatment on markers of bone turnover in the different bones. The aim of this study is to give insight into bone-site-specific effects of enduring bisphosphonate treatment, which may provide a better understanding of the pathophysiology of osteonecrosis of the jaw.

Materials and Methods

Mice and bone marrow isolation

Animal experiments were performed according to the European Communities Council Directive of 24 November 1986 and institutional guidelines and were approved by the Animal Welfare Committee of the VU University (Amsterdam, The Netherlands, Permit Number: ACTA2010-03). Mice (Harlan, Horst, The Netherlands) were maintained and treated as described previously [216]. Female, 3-month-old C57BL/6J mice were randomly divided into four groups: two groups were ovariectomized and two groups were sham-operated. The ovariectomized mice were used for other experiments, not mentioned in this study. Sham-operated mice were injected intraperitoneally with a high dose (0.5 mg/kg, comparable to the dose used in cancer patients [243]) of zoledronic acid (ZA; Novartis, Basel, Switzerland) or with saline (control) once per week. Six animals per group per time point were sacrificed by an i.p. injection of a lethal dose of sodium pentobarbital (0.1 mL Euthestate, Ceva Sante Animale, Naaldwijk, The Netherlands) at baseline, and at one, three, and six months after the start of the experiment. After six months of treatment, BP-treated mice were smaller than control mice (25±2g. versus 29±2g.). At all other time points, mice had similar weights. Eight days before sacrifice, mice were injected i.p. with fluorescently-labelled calcein (10 mg/kg; Sigma, St. Louis, MO, USA), and two days before sacrifice, they were injected with alizarin complexone (20 mg/kg; Sigma). Left mandibles, maxillae, and left humeri were fixed with 4% formaldehyde and stored at 4°C until μCT analysis and processing for histology. Bone marrow cells were isolated from the right mandibles and long bones (tibia and femur) as described previously [224]. Briefly, soft-tissue-cleaned bones were crushed in sterile mortars containing culture medium. Bones were flushed until the medium was clear to ensure total marrow isolation, and filtered through a 70 μm pore size cell strainer (Falcon/Becton Dickinson, Franklin Lakes, NJ, USA).

Osteoclastogenesis and TRACP staining

Cells were stained with Türk's solution (Merck, Darmstadt, Germany) and counted using a haemocytometer. Freshly isolated long bone and jaw bone marrow cells were seeded in 96-well plates (Greiner Bio-One, Monroe, NC, USA; 10^5 cells per well). Osteoclastogenesis was induced with 30 ng/mL M-CSF (R&D Systems, Minneapolis, MN, USA) and with 20 ng/mL recombinant mouse RANKL (R&D Systems). After six days, cells were fixed, and a tartrate-resistant acid phosphatase (TRACP) staining was performed with the leukocyte acid phosphatase kit (Sigma). Nuclei were visualized with DAPI. The number of TRACP-positive, multinucleated (≥3 nuclei) cells was assessed using an inverted microscope.

Micro-computed tomography

Micro-computed tomography (μCT; Scanco Medical AG, Brüttisellen, Switzerland) was used to assess bone volume and tissue mineral density (TMD) of the humeri and hemi mandibles. Scanning was performed in fixation fluid with an 8 μm voxel size, a peak voltage of 55 kV, and an integration time of 250 ms. Imaging processing included Gaussian filtering and segmentation: sigma = 0.8, support = 1, threshold unit 170 (= 618 mg HA cm^{-3}) and 200 (= 727 mg HA cm^{-3}) for humeri and mandibles, respectively, for all analysed time points and groups. Total humeri were analysed by exactly outlining the bones, *i.e.* without including empty volume. The volume of interest for the jaw was selected as indicated (**Figure 2**, arrows and dashed lines). For both long bone and jaw, 20-30 slices per sample were analysed.

Histology and histomorphometry

Following fixation, tissue samples were dehydrated with ethanol and subsequently embedded in methyl methacrylate. Transverse sections of the left maxillary bone and longitudinal sections of the proximal humeri were made using a Jung K microtome (Leica Microsystems GmbH, Wetzlar, Germany). Five μm sections were attached to gelatine-coated microscope slides and dried for at least three days at 37°C. Sections were mounted in DePeX mounting medium (Gurr, VWR International, Lutterworth, UK) and stored at room temperature in the dark for the analysis of dynamic bone formation in the diaphysis of the proximal humeri and the alveolar bone surrounding two or three roots of the second molar (**Figure S 3**). The mineralizing surface was expressed as the average of the percentage of bone surface covered by calcein and alizarin red labels. Mineral apposition rate was calculated by the average distance between calcein and alizarin red labels divided by the number of days between the injections (six days). Analyses were performed using Leica QWin (Leica Microsystems Image Solutions, Rijswijk, The Netherlands) and Image Pro-Plus Software (Media Cybernetics, Silver Spring, MD, USA).

Right maxillae and distal humeri were decalcified in 4.2% EDTA containing 0.8% formaldehyde for five weeks at room temperature, dehydrated, and embedded in paraffin. Transverse sections of the maxilla and longitudinal sections of the distal humeri were cut (7 μm thickness) and attached to silane-coated microscope slides. Sections were deparaffinized using a xylene substitute, rehydrated, and stained using TRACP as described previously with minor changes [244]. Sodium-potassium tartrate was used at 2 mM and the solution was added to the sections for three hours at 37°C. Counterstaining was performed with Mayer's haematoxylin. Micrographs were taken with a Leica DMR microscope (Leica Microsystems, Wetzlar, Germany) using a 20x magnification. To get

a complete image, micrographs were merged using Adobe Photoshop CS5.1 (Adobe Systems). The number of TRACP-positive cells covering the bone in the endocortical, distal diaphysis, and the alveolar bone surrounding the roots of the second molar was determined (**Figures S 2a** and **S 2b** in supporting information). The number of osteoclasts attached to the cementum of the roots of the second molar was also counted, and the periodontal ligament (PDL) area was determined.

Statistical analyses

The Kruskal-Wallis test, followed by Dunn's multiple comparison test, were performed to test the effect of age on the number of bone marrow cells, osteoclast formation *in vitro* and *in vivo*, and bone formation. To test the effect of age on µCT parameters, we used a One-way ANOVA followed by Tukey's multiple comparison tests. Unpaired, two-tailed t-tests were used to test the effect of ZA treatment on TMD and bone volume fraction. To test the effect of ZA treatment on the number of bone marrow cells, on the osteoclastogenic potential of bone marrow cells, on mineralization parameters, and on the number of osteoclasts *in vivo,* we used the Mann-Whitney U test. GraphPad Prism 5 Software was used to perform statistical tests (GraphPad Software, Inc., La Jolla, CA, USA). Graphs represent means and SDs of n=3-6 mice. Differences were considered significant when p <0.05.

Results

Bisphosphonates reduce the number of jaw bone marrow cells

The number of bone marrow cells that could be isolated from the long bones decreased with age; a phenomenon not affected by ZA (**Figure 1a**). Interestingly, ZA significantly reduced the number of bone marrow cells that could be isolated from the jaw after six months of treatment, without affecting the number of long-bone marrow cells (**Figure 1b**). Significantly fewer long bone osteoclasts formed from control bone marrow after six months of treatment than after one and three months (**Figure 1c**). The age of the mice did not affect the number of osteoclasts that formed from control bone marrow from the jaw (**Figure 1d**). Since six months of ZA treatment reduced the number of jaw bone marrow cells (see above), we were not able to isolate enough cells from the jaw at that time point to assess their osteoclastogenic potential. Therefore, the effect of ZA treatment on jaw osteoclastogenesis was only studied after one and three months of treatment (**Figure 1d**). There was no significant effect of ZA treatment on the number of osteoclasts that formed from both long bone and jaw bone marrow precursors at any time point (**Figures 1c and 1d**).

Bisphosphonates increase bone volume and bone mineral density

ZA may reduce the number of bone marrow cells either directly by inducing bone marrow cell apoptosis, indirectly by decreasing bone marrow space due to a higher bone volume, or by a combination of both. To investigate whether a decrease in the number of jaw bone marrow cells (**Figure 1b**) was the result of an indirect effect, we assessed bone volume by μCT (**Figure 2a**). In the long bones, bone volume mainly accumulated in the area of the growth plate (**Figure 2a**). Also, more and thicker trabeculae were present in the long bones after treatment with ZA. Single trabeculae could not be distinguished in the jaw (**Figure 2a**). ZA similarly increased bone volume fraction (BV/TV) in the long bones and in the jaw after one, three, and six months of treatment (**Figure 2b**). However, the bone volume fraction in jaw increased to above 90% after ZA treatment and was higher than that of long bone. This probably resulted in a reduction of the marrow spaces, potentially explaining the lower number of marrow cells that could be isolated. ZA decreased the periodontal ligament (PDL) space of the lingual root after six months of treatment, but did not affect the PDL spaces surrounding the other roots (**Figure S 1**).

The TMD of both types of bone increased with the age of the mice and was higher in the jaw than in long bones (**Figure 2c**). After three and six months of ZA treatment, both long bone (**Figure 2c**, left panel) and jaw (right panel) TMD were significantly higher than that of the control animals.

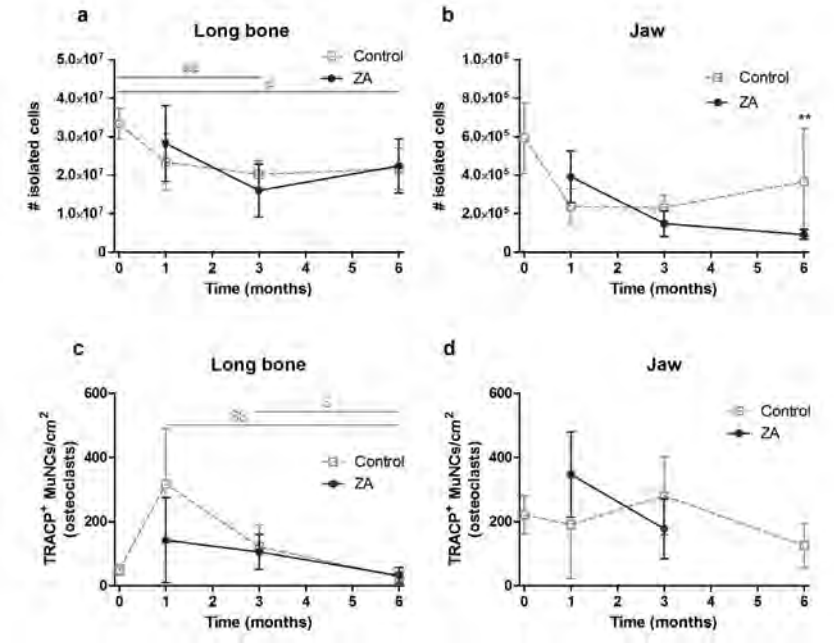

Figure 1. Bone marrow cell isolation and osteoclastogenic potential of marrow cells from long bones and jaws. **A** The number of long-bone marrow cells from tibia and femur was not affected by ZA treatment. **B** Six months of ZA treatment inhibited the number of jaw bone marrow cells in the hemi-mandible. **C, d** The osteoclastogenic potential of long bone c and jaw d bone marrow was not affected by ZA treatment. Osteoclastogenesis of jaw bone marrow cells after six months of treatment was not determined. The *x*-axes show the time after the start of treatment at the age of three months. Means of six a, b or four to six c, d mice and standard deviations are shown. ** $p = 0.01$ (Mann-Whitney U test) represents a significant difference between ZA treatment and control, # $p < 0.05$, ## $p < 0.01$ represent a significant difference of the controls at that time point versus baseline (0), $$ represents a significant difference of the control group at six months versus one month ($p < 0.01$) and three months ($, $p < 0.05$) using a Kruskal-Wallis test, followed by Dunn's multiple comparison. There was no significant difference between the number of osteoclasts at baseline and after one month of treatment c.

Osteoclast numbers in the long bones increase with age

In the long bones the number of osteoclasts increased with age (**Figure 3a**, see **Figure S 2** for example osteoclasts). In the jaw, such an effect was not seen (**Figure 3b**). After three and six months of treatment, more osteoclasts were present per long bone surface than per jaw bone surface (p <0.05, **Figure 3a** versus **3b**). ZA treatment did not significantly affect the number of osteoclasts per bone perimeter in the long bones (**Figure 3a**), or in the jaw (**Figure 3b**).

ZA differently affects mineralization in long bone and jaw

The mineralizing surface in the long bones of control mice decreased with age (**Figure 3c**, see **Figure S 3** for examples). Interestingly, mineralizing surface of the control long bones was 1.4 to 2.4 times higher than that of the jaw (**Figure 3c** vs. **3d**, p <0.01 at 3 months). The mineral apposition rate was 2.2 to 3 times higher in the control long bones than in the jaw (**Figure 3e** vs. **3f**, p <0.01 at three and six months). ZA treatment significantly reduced the bone formation parameters in the long bones after three and six months of treatment, whereas it only affected bone formation parameters in the jaw after three months (**Figure 3c-f**). This might indicate that six months of ZA treatment reduced bone turnover in the long bones, but not in the jaw. These results also indicate that the higher bone volume fraction and TMD were either the result of reduced osteoclast activity, or the result of induction at an earlier stage of treatment.

ZA induces molar root resorption

Analysis of the root surfaces of the molars revealed the presence of osteoclasts attached to the cementum layer; a phenomenon almost exclusively seen in ZA treated animals after three and six month of treatment (**Figure 4a, 4c**). The osteoclast size of 16.0 µm at this location was slightly smaller than the size of the osteoclasts attached to the alveolar bone (18.6 µm) and to the long bones (21.0 µm, not shown). The molar-root-associated osteoclasts were associated with resorption pits, resulting in loss of cementum adjacent to osteoclasts (**Figure 4b**), and the root resorbing surface increased with time (**Figure 4d**). After three months, 9.1% of the osteoclasts were active, and after six months, 15.4% of the osteoclasts were associated with a resorption pit (not shown), thus indicating resorptive activity at the molar root despite the presence of the bisphosphonate.

ZA differently affects mineralization in long bone and jaw

The mineralizing surface in the long bones of control mice decreased with age (**Figure 3c**, see **Figure S 3** for examples). Interestingly, mineralizing surface of the control long bones was 1.4 to 2.4 times higher than that of the jaw (**Figure 3c** vs. **3d**, p <0.01 at 3 months). The mineral apposition rate was 2.2 to 3 times higher in the control long bones than in the jaw (**Figure 3e** vs. **3f**, p <0.01 at three and six months). ZA treatment significan-tly reduced the bone formation parameters in the long bones after three and six months of treatment, whereas it only affected bone formation parameters in the jaw after three months (**Figure 3c-f**). This might indicate that six months of ZA treatment reduced bone turnover in the long bones, but not in the jaw. These results also indicate that the higher bone volume fraction and TMD were either the result of reduced osteoclast activity, or the result of induction at an earlier stage of treatment.

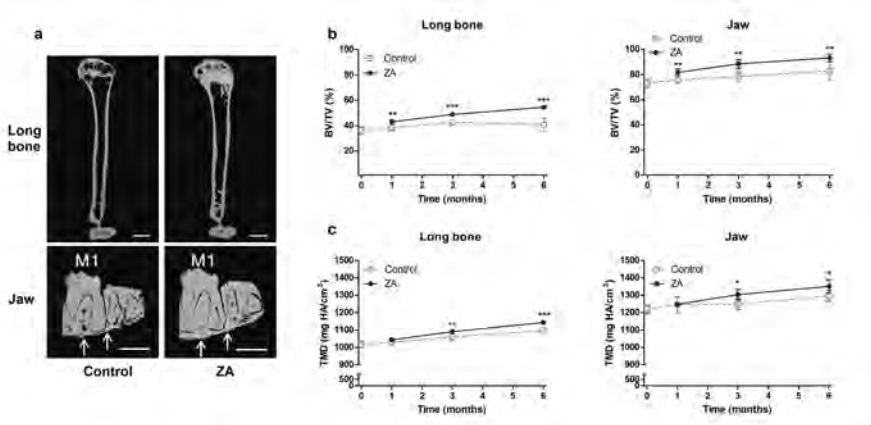

Figure 2. MicroCT analysis of long bones and jaws from mice treated with BPs. **A** 3D recon-structions and the volume of interest (VOI) of the humeri (*top*, total humerus was analysed) and the 1st and 2nd molar region of the mandible (*bottom*, VOI indicated with arrows and dashed lines) after six months of treatment. *M1* = first molar, *bar* = 1 mm. **B** Bone volume (% of total volume) of long bones (left) and jaws (right) was higher after one, three, and six months of ZA treatment. **C** Tissue mineral density (TMD) was increased by three and six months of ZA treatment. The *x*-axes show the time after the start of treatment at the age of three months. Graphs show the means and standard deviations of five to six mice. * $p < 0.05$, ** $p < 0.01$, *** $p < 0.001$ represent significant differences between ZA treatment and control, determined by an unpaired, two-tailed *t*-test.

ZA induces molar root resorption

Analysis of the root surfaces of the molars revealed the presence of osteoclasts attached to the cementum layer; a phenomenon almost exclusively seen in ZA treated animals after three and six month of treatment (**Figure 4a, 4c**). The osteoclast size of 16.0 µm at this location was slightly smaller than the size of the osteoclasts attached to the alveolar bone (18.6 µm) and to the long bones (21.0 µm, not shown). The molar-root-associated osteoclasts were associated with resorption pits, resulting in loss of cementum adjacent to osteoclasts (**Figure 4b**), and the root resorbing surface increased with time (**Figure 4d**). After three months, 9.1% of the osteoclasts were active, and after six months, 15.4% of the osteoclasts were associated with a resorption pit (not shown), thus indicating re-sorptive activity at the molar root despite the presence of the bisphosphonate.

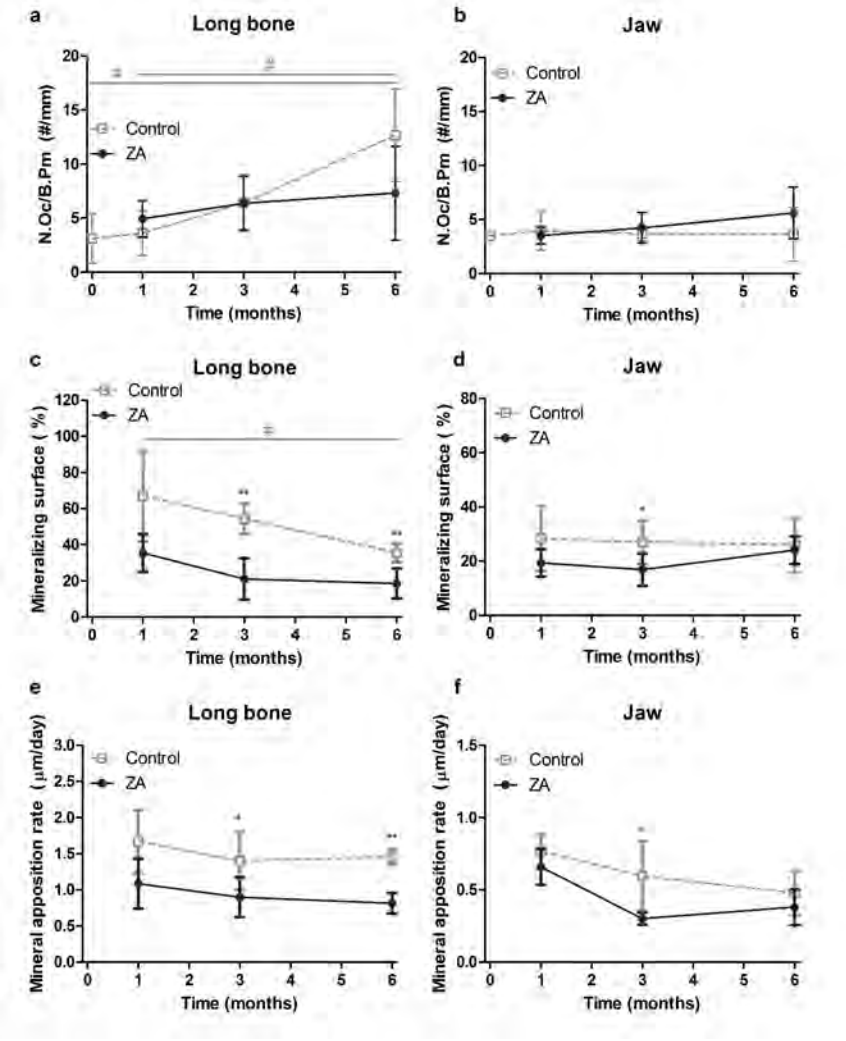

Figure 3. Osteoclast counts on decalcified sections and mineralization parameters. **A** The number of long bone and **b** jaw osteoclasts that were attached to bone were not significantly affected by ZA treatment. The *x-axes* show the time after the start of treatment at the age of three months. **C** Long bone mineralizing surface and mineral apposition rate **E** were inhibited by three and six months of ZA. **D** Jaw mineralizing surface and mineral apposition **F** rate were only affected after three months of ZA. Graphs show the means and standard deviations of four to six measurements or three to six measurements for the jaw. *# indicates p<0.05*, between six months and baseline, or between six months and one month within the control group, as determined by The Kruskal-Wallis test, followed by Dunn's multiple comparison. ** p<0.05*, *** p<0.01* using the Mann-Whitney U test between ZA and control at that time point.

Discussion

Previously, we showed in an *in vitro* study that jaw bone marrow cells internalized more BPs than long-bone marrow cells. However, this did not differentially affect osteoclastogenesis, indicating that jaw bone marrow cells might be less sensitive to BPs than long-bone marrow cells [224]. Here, we showed that the bone marrow cells in the jaw were affected by BP treatment, whereas those in the long bones were not. Six months of ZA

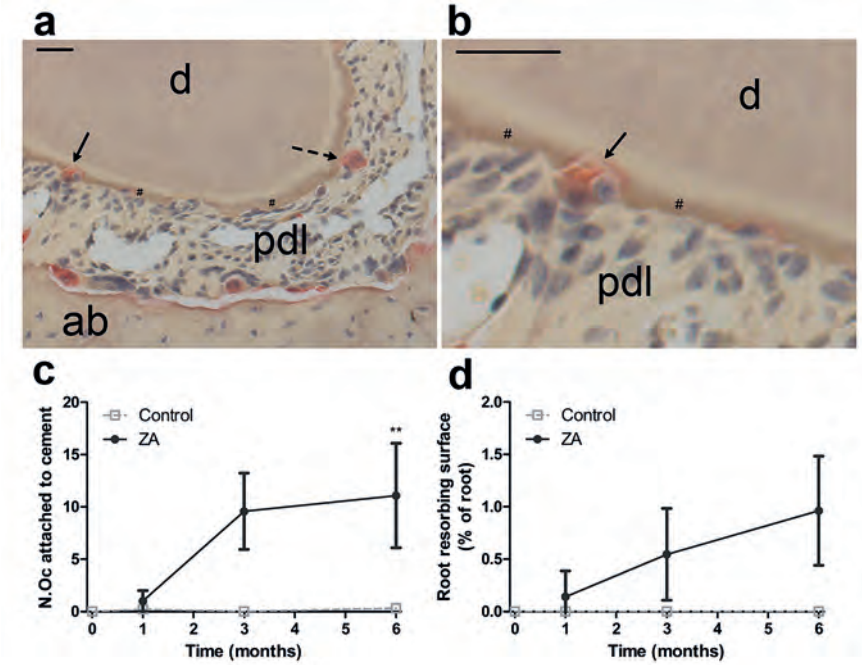

Figure 4. Osteoclast attachment to root cementum. **A** Active (*arrow*) and non-active (*dashed arrow*) osteoclast attached to the root cementum of ZA-treated mice. d: dentine, ab: alveolar bone, pdl: periodontal ligament, #cementum. **B** Higher magnification of the resorbing osteoclast, clearly showing disrupted cementum. *Bars*: 30 µm. **C** Root-associated osteoclasts are exclusive to ZA treatment; in controls, cementum-associated osteoclasts are very rare. **D** The root resorbing area after ZA treatment expressed as a percentage of the root surface. Root resorbing osteoclasts were not detected in the controls. The *x-axes* show the time after the start of treatment at the age of three months. The graphs show the means and standard deviations of five to six mice or three mice at baseline. ** *p<0.01* represents a significant differences between ZA treatment and control using the Mann-Whitney U test.

treatment reduced the number of bone marrow cells in the jaw, but not in long bones (**Figure 1b**). This might be attributed to the very limited bone marrow cavity in the jaw (**Figure 2**) or to higher BP uptake by the bone marrow cells at that site [224]. Perhaps, jaw bone marrow cells are exposed to higher BP concentrations *in vivo*. Jaw and long bones

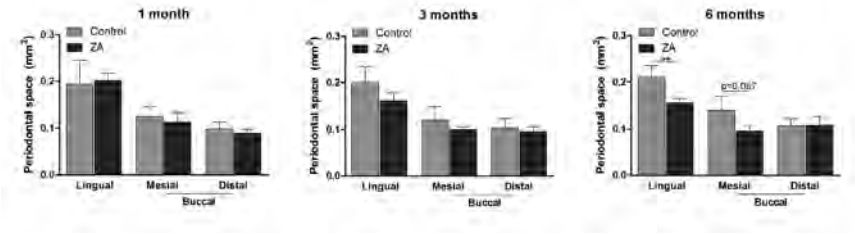

Supplementary Figure 1. Periodontal ligament area. ZA affected the periodontal ligament area surrounding the root on the lingual side, only after 6 months of treatment as tested with a Mann-Whitney U test (***p* < *0.01*). The x-axes indicate the locations of the molar roots.

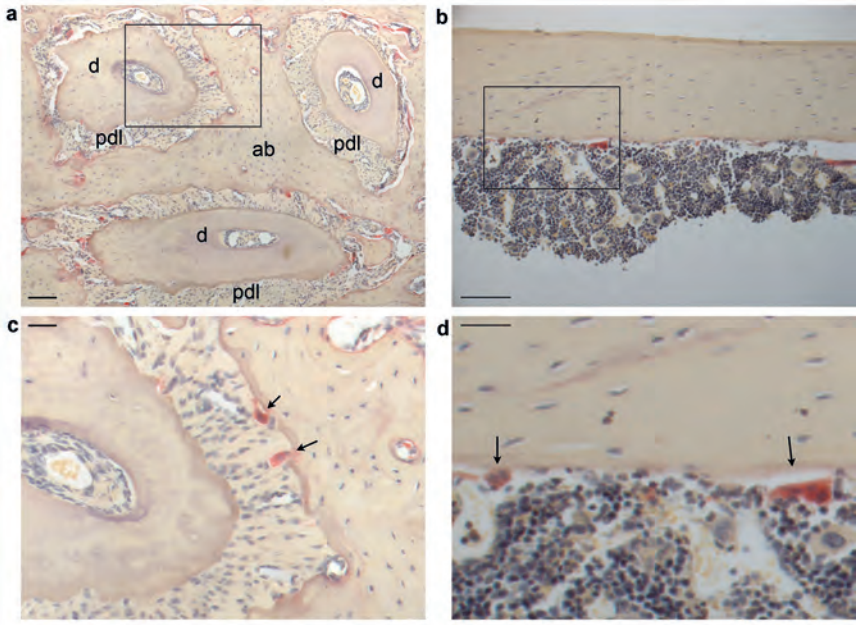

Supplementary Figure 2. TRACP staining on decalcified sections. **A** Transverse section of the maxilla from a ZA-treated mouse, showing the roots of the second molar. ab: alveolar bone, pdl: periodontal ligament, d: dentine. **B** Longitudinal section of the distal humerus from the same mouse. Squares (a-b) indicate the area that is magnified in c (maxilla) and d (humerus). Arrows indicate osteoclasts. *Bars*: 100 µm (a-b), 30 µm (c-d).

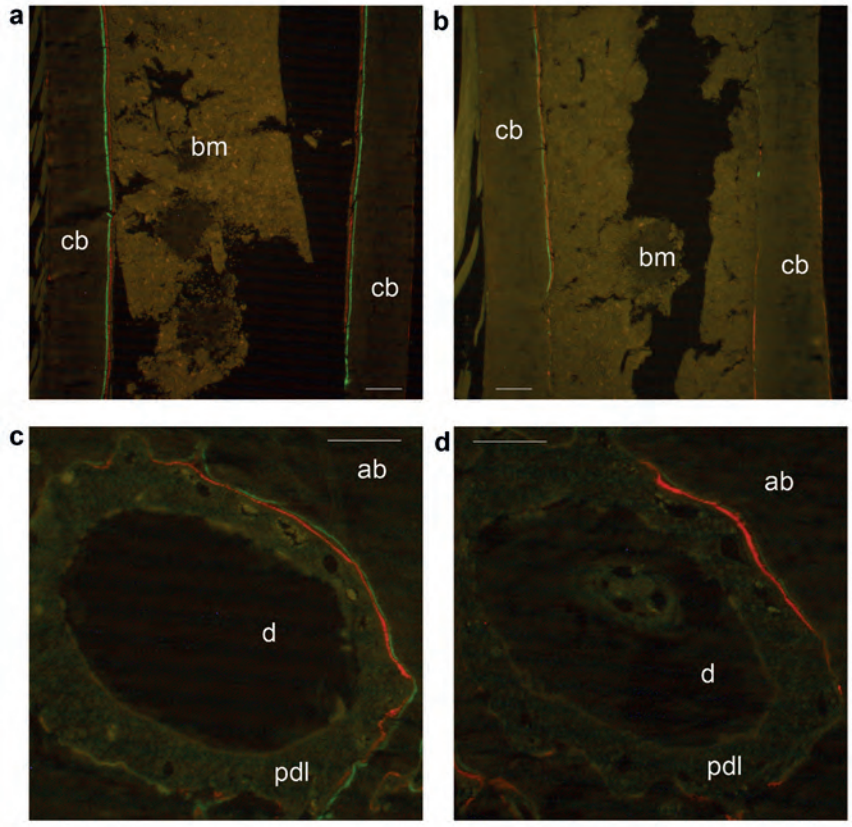

Supplementary Figure 3. Fluorescent labelling of bone formation sites. **A, b** Longitudinal section of the distal humerus. **C, d** transverse section of the maxilla, showing one root of the second molar. ab: alveolar bone, pdl: periodontal ligament, d: dentine, bm: bone marrow, cb: cortical bone. **a, c** controls; **b, d** 1 month of treatment with ZA. *Green*: calcein, *red*: alizarin complexone; the bone surface covered by labels was expressed as the average percentage of green and red labels. The distance between the two labels was measured and the mineral apposition rate was calculated from these values. *Bars*: 100 µm.

from rats were shown to contain a similar amount of BPs per unit of dry weight or calcium [245, 246]. Since the jaw contains more mineral per bone volume ([246]; **Figure 2**) than the long bones, it likely adsorbed more BPs than long bones. Together with the finding that jaw osteoclasts resorb at least as much bone [224] or dentine [247] as long bone osteoclasts *in vitro*, more BP is likely released from the jaw than from long bone, making it available for the surrounding cells in the bone marrow [248, 249]. The resulting high local BP concentration might cause apoptosis of bone marrow cells, leading to a reduced number of jaw bone marrow cells. Also, Hokugo et al. showed that newly administered BPs can replace previously adsorbed BP [250]. Since we applied ZA weekly, it is likely that the BP replaced previously administered ZA, releasing BPs into the bone microenvironment and making it available for internalization by other cell types such as macrophages. Whether cells in the jaw internalize more BPs *in vivo* requires more research.

The reduced number of jaw bone marrow cells after six months of ZA treatment was not associated with fewer osteoclasts at the alveolar bone surface (**Figures 1** and **3**). This may indicate that the osteoclasts were not formed from precursors in the bone marrow, or that the osteoclast precursors still present in the bone marrow were not affected by BPs. The latter assumption was supported by the finding that ZA treatment did not affect the osteoclastogenic potential of bone marrow cells, although it should be noted that the osteoclastogenic potential after six months could not be measured (**Figure 1d**). Yet, since ZA reduced the number of jaw bone marrow cells, our findings seem to provide support for the hypothesis that BPs may affect other cell types in the bone marrow, such as macrophages [251] and monocytes [252]. A recent study using THP-1 cells showed that BPs altered migration and the phagocytic capacity of those monocytes, implying that BPs may impair the function of those cells [253]. Also, the jaw is exposed to pathogens present in dental plaque. Thus, a negative effect of BPs on macrophages and a consequent inflammatory response may explain why the jaw is specifically vulnerable for osteonecrosis [254]. Inhibition of the inflammatory response was also shown to be involved in the induction of BRONJ [239, 240]. Therefore, it would be of interest to study BP release from the bone and its uptake by bone marrow cells in the jaw of a mouse model in which inflammation is studied in combination with bisphosphonates, such as the previously designed models for BRONJ [241, 242].

Another hypothesis regarding the aetiology of BRONJ is the oversuppression of bone turnover. Reduction in the bone remodelling capacity and in the ability to repair bone damage can lead to the accumulation of microdamage [255, 256]. Our results however, strongly support a reducing effect on bone turnover markers only in the long bones (**Figure 3**). Also, the number of osteoclasts increased with age only in long bones of controls, to levels that were up to 3.4 times higher in the long bones than in the jaw (**Figures 3a** and **3b**). Therefore, our results suggest that oversuppression of bone turnover and

the alleged microdamage would more likely cause side effects in the long bones than in the jaw.

Interestingly, under the influence of BPs, active osteoclasts were found at the molar root cementum (**Figure 4**). Previous studies on the effect of bisphosphonates during orthodontic treatment reported an inhibiting effect of BPs on root resorption during orthodontic tooth movement [257-259]. However, under our treatment regime with ZA that was applied without external force, at least 9-15% of the root osteoclasts were active. Therefore, we demonstrate that under the influence of BPs, osteoclasts are associated with tooth cementum and are actively resorbing. A stimulating effect of BPs on osteoclast activity has, as far as we know, never been reported. This was unexpected and surprising, since BPs are used as a treatment to inhibit osteoclast activity. Possibly, those molar-root-associated osteoclasts were less exposed to BPs, as little BP accumulates at the root cementum [260].

An explanation for the induction of osteoclast activity may be similar to the mechanism of osteoclast activity that is induced during orthodontic tooth movement. Mechanical loading induces bone resorption in the direction of the load [257, 261, 262]. Also, PDL fibroblasts under compressive loading were shown to induce osteoclastogenesis [263]. We speculate that through mechanical loading, osteoclasts accumulate at the root after BP treatment. The increased bone volume after BP treatment (**Figure 2**) may induce mechanical loading that is transmitted through the periodontal ligament, which may subsequently induce root resorption in order to make space for the newly formed bone. In our study, the periodontal ligament space was only mildly affected (**Figure S 1**). However, after orthodontic tooth movement, this space almost completely disappeared at the pressure site where root resorption was taking place [257]. Therefore, in the orthodontic tooth movement model, root resorbing osteoclasts may be more exposed to BPs than osteoclasts in our model due to their close proximity to the BP-containing alveolar bone. This may explain why root resorption in the orthodontic movement model was inhibited by BPs, whereas BPs stimulated root resorption in our model. It should also be noted that even though BPs could suppress tooth-movement-induced root resorption, root resorption in the presence of BPs was still higher than that measured in control mice that were not subjected to tooth movement [257]. Finally, in the tooth movement model, the periodontal ligament itself was impaired, whereas in our model without force, BPs had a minor effect on the periodontal ligament. A differentially affected periodontal ligament may differently affect root resorption, as periodontal ligament fibroblasts were shown to stimulate osteoclastogenesis [264, 265]. Taken together, these results show that BPs differentially affect molar root resorption under static versus mechanically loaded conditions.

In conclusion, we show that BPs can differently affect long bone and jaw bone

turnover *in vivo*. Furthermore, we found resorption of tooth root cementum, in spite of the presence of ZA, indicating that the drug can *stimulate* osteoclast-mediated resorption. This stimulated resorption was site-specific, again indicating the diverse effects the drug has on osteoclasts at different bone sites. Finally, the evidence that BPs, either directly or indirectly, affect specifically jaw bone marrow cells may help to improve our understanding of the pathogenesis for BRONJ.

Acknowledgments

The authors would like to thank Dr. Geerling E.J. Langenbach for his input in the design of the study and Dr. Clara M. Korstjens for the development of analysis protocols for the measurement of dynamic bone parameters. We are grateful to Carla Prins and Rika van der Laan for conducting the animal experiments. We thank Dr. Behrouz Zandieh Doulabi for development of the TRACP staining protocol on decalcified sections. Finally, we thank Dr. Pavitra Kannan for proofreading the manuscript. This project was funded by the Dutch Organization for Scientific Research (NWO grant number: 021.001.050 to GAPR).

CHAPTER 5

CONTRAST-ENHANCED μCT (EPIC-μCT) EX VIVO APPLIED TO THE MOUSE AND HUMAN JAW JOINT

Greetje A. P. Renders, Lars Mulder, Angela L. Lin, Geerling E.J. Langenbach,

Jan Harm Koolstra, Robert E. Guldberg, Vincent Everts

This chapter is published in

Dentomaxillofacial Radiology

Renders et al, 2014; 43 (2): 20130098

Azenor

Introduction

Osteoarthritis (OA) is a destructive and progressive joint disease with a large impact on joint function. One of the major characteristics of OA is the progressive damage of the articular cartilage layer. The initiating events are still not fully understood, yet the involvement of the underlying (subchondral) bone tissue in the process is gaining support. A significant role of the subchondral bone is suspected because it acts as an integrated functional unit with the cartilage layer [1, 2, 8, 9, 266]. Like all other synovial joints, the temporomandibular joint (TMJ) is susceptive to the development of OA [267, 268]. OA in the temporomandibular joint (TMJ-OA) is likely caused by a disturbed biomechanical environment due to a history of joint overload [267, 269]. The expected bone changes (*e.g.*, sclerosis, subchondral bone plate thickening) may negatively affect the biomechanical environment of the articular cartilage and cause progressive cartilage degradation and/or damage [207, 270, 271].

Presently, there is a gap in our understanding about the morphological bone-cartilage interaction in the aetiology of TMJ-OA. More detailed knowledge about TMJ-OA initiation and development is essential to improve our insight into this disease. It is thereby imperative to have a standardized, reliable, and preferably three-dimensional (3-D) imaging method that allows detailed assessment of both bone and cartilage properties in this specific joint in the healthy and diseased situation.

For TMJ-OA research, the normally used histological and biochemical evaluation techniques are incapable of describing the 3-D spatial distribution of tissue constituents [272]. Current available magnetic resonance imaging (MRI) techniques, including delayed gadolinium-enhanced MRI of cartilage, can produce 3-D, non-destructive measurements of cartilage *in vivo* in clinical applications in the human knee joint [29, 273, 274]. However, even the most recent MRI systems do not have sufficient resolution to detect local changes in the thin cartilage layers found in the TMJ of humans and small animals [32, 33].

Conventional micro-computed tomography (μCT) can provide fast high-resolution 3-D imaging of bone tissue for qualitative and quantitative assessment in the human and the small animal TMJ [25, 110, 115, 275, 276]. Bone abnormalities related to TMJ-OA, like erosion, sclerosis, and osteophytosis can thereby be detected and quantified [27, 28, 271, 276]. Until a couple of years ago, cartilage measurements with conventional μCT were not feasible due to too low X-ray attenuations of the soft tissues. However, a novel imaging technique was successfully introduced and applied to the rat knee joint that measured the Equilibrium Partitioning of an Ionic Contrast agent via micro-Computed Tomography (EPIC-μCT) [36, 37]. With this method the X-ray attenuation of cartilage is enhanced by treatment of the samples with a contrast-enhancing ionic fluid, and this

allowed for qualification and quantification of cartilage morphology and its sulfated glycosaminoglycan (sGAG) composition in small animals [37, 38, 42].

The TMJ has unique properties compared to other articular joints like the knee, because it is made of fibrocartilage and acts both as an articular joint cartilage and as a site for endochondral ossification [269]. The EPIC-μCT technique has, thus far, predominantly been applied to knee joints [37-39, 43, 44, 277-279]. The dimension of the mouse TMJ is smaller than, for instance, the rat knee joint (width: 0.5 and 4 mm, respectively). Thus with respect to sample size, a small animal knee joint protocol [37] can probably be easily applied to the mouse TMJ to obtain a reliable 3-D imaging technique for TMJ-OA research. In contrast, the dimension of the human TMJ is larger (width: 15-20 mm) which might indicate a need for adjustment of the protocol [61]. Furthermore, the TMJ predominantly contains fibrocartilage [269, 280] and the extracellular matrix is composed of less negatively-charged sGAGs and more collagen type I fibers compared to hyaline cartilage [229]. This can result in a different so-called fixed charged density (FCD) of the cartilage layer in the jaw joint compared to the knee joint. The EPIC-μCT technique is based on this FCD (as described in more detail in the Materials & Methods section) and therefore the required immersion time for the larger human TMJ is likely to be different.

We hypothesized that it is possible to use the EPIC-μCT technique to make visualization of the thin articular cartilage layer in the TMJ feasible. The aim of this study was to determine the applicability of this novel method for research in both small animal and human TMJs. We assessed the *ex vivo* ability of the EPIC-μCT technique to provide quantitative 3-D morphology of mouse and human TMJ cartilage layers.

Materials & Methods

Sample collection

From five 3-month-old healthy female C57BL/6J mice (Harlan, Horst, The Netherlands) mandibular condyles were harvested and stored in a 4% phosphate-buffered formalin solution (pH 7.2, 4°C). Permission for the use of this material was obtained from the Animal Welfare Committee of the VU University Amsterdam (The Netherlands).

A collection of human jaw joints was obtained from embalmed cadavers (fixation fluid: 2.4 % formaldehyde, 33 % ethanol, 8 % glycerol, and 0.33 % phenol during 1 hour). The mandibular condyles were harvested and stored in 4% formalin solution (pH 7.2, 4°C). These condylar samples were macroscopically examined and classified as healthy, OA-early stage or OA-late stage (three groups; n = 5 per group). The classification was adapted from the principles of Byers *et al.* [281] as follows. Healthy: no visible changes in

the cartilage of the type described below. OA-early: early or advanced fibrillation of the articular cartilage or local reduction. OA-late: total loss of the articular cartilage with bone exposure; or osteophytosis of articular cartilage. The use of human samples conformed to a written protocol that was reviewed and approved by the Department of Anatomy and Embryology of the Academic Medical Center of the University of Amsterdam (The Netherlands).

μCT scanning

A μCT 40 system (Scanco Medical AG, Brüttisellen, Switzerland) was used to obtain and analyze 3-D reconstructions of segmented volumes of bone and cartilage. The mouse samples were scanned in air with the inferior side facing downwards. After the immersion in the contrast fluid (contrast enhancement treatment) the samples were gently dabbed dry. To maintain humidity, a reservoir on the bottom of the sealed specimen holder (diameter: 16 mm) contained a standardized amount of 4 mL phosphate-buffered saline (PBS). The samples were imaged in air using 8 μm isotropic voxels at 55 kVp, 145 μm, and 250 ms integration time. A complete scan required approximately 116 minutes (397 slices). After scanning, the samples were immersed in PBS for desorption to allow histological processing.

The human samples were scanned in air with the lateral condylar facing downwards in a sealed specimen holder (diameter: 20 mm) containing 4 mL PBS. After the immersion in the contrast fluid (contrast enhancement treatment) the samples were gently dabbed dry. The samples were imaged in air using 18 μm isotropic voxels at 70 kVp, 114 μm and 250 ms integration time. A complete scan required approximately 36 minutes (150 slices).

Contrast-enhancement treatment

The EPIC-μCT technique is based on the principle that diffusion through the cartilage matrix, differs with variable proportion of the local constituents. The cartilage matrix contains collagen fibers and proteoglycans. Negatively-charged sGAGs are attached to the proteoglycan-backbone, resulting in the negative fixed charged density (FCD). A negatively charged, radio-opaque contrast agent will be preferably excluded from regions with higher negative FCD associated with higher concentrations of sGAGs [36]. Thus the distribution of the ionic contrast agent (x-ray attenuation in μCT) is inversely related to the density of the negatively charged sGAGs. The clinically available CT contrast agent Hexabrix 320 (Guerbet Nederland BV, The Netherlands) was applied, containing the negatively charged hexaiodinated dimer ioxaglate.

The contrast-enhancement protocol for the mouse samples was similar to the EPIC-μCT protocol described by Xie *et al* [38]: Immersion for 30 minutes in 40/60% Hexabrix/PBS solution (37°C). We expected differences in optimal immersion time for the human samples due to the larger dimensions of the human TMJ. Therefore, we decided to test the 30 minutes 40/60 Hexabrix/PBS protocol and adapt the immersion time if needed.

All human samples were scanned prior to immersion and then at timed intervals of immersion as described below (**Figure 1a, b**). The process was repeated for cumulative immersion times up to 20 hours to identify the time required to reach equilibrium.

Histological staining for validation purposes (mouse samples)

Following μCT scanning, the five condyles of five different mice were decalcified in 2.5% formic acid (pH 4.2, 10 days), paraffin embedded, and 7 μm frontal sections were cut and stained with alcian blue. For each condylar sample, three sections were used for cartilage thickness analysis. Digital images of each section were captured at a 1392x1040 pixel screen (10x magnification; Leica, Qwin Pro). Using Leica software, the cartilage thickness was defined as the average value of up to 20 manual thickness measurements at regular intervals perpendicular to the superficial cartilage surface. The histology sections were compared to the corresponding 3-D spatial images generated by EPIC-μCT.

Attenuation-histogram analysis (human samples)

The human samples were used for attenuation histogram analysis to determine the appropriate immersion time for reproducible cartilage contrast-enhancement. For each scan, 150 images were reconstructed. In the sagittal plane, the images were manually contoured every ten slices to isolate a region of interest (ROI) containing the subchondral bone plate (white), cartilage (gray) and the scanning-medium (air *black*; **Figure 1c**). Care was taking not to include bone marrow spaces and joint capsule or lateral pterygoid muscle remnants in the ROIs. The manufacturer's software was used to contour the intervening slices and producing a volume of interest (VOI: 150 slices ~ 2.7 mm). Histograms from the attenuation values were obtained to analyze the three peaks corresponding to bone, contrast-enhanced cartilage, and scanning-medium voxels (**Figure 1d**). Per sample, the average attenuation for the cartilage tissue (gray peak) for all three VOIs was determined and averaged. This average value was directly compared per group between all cumulative immersion times.

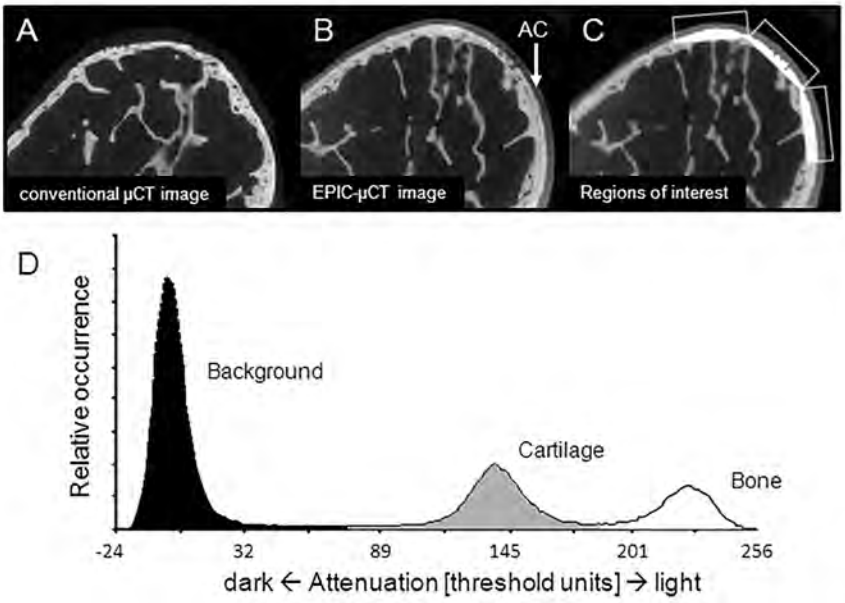

Figure 1. A, B MicroCT (µCT) sagittal cross-section of a condylar sample before and after contrast enhancement. The articular cartilage (AC) showed higher attenuation due to the immersion of the contrast medium and allowed segmentation. **C** Selection of the regions of interest (scanning-medium *black*; articular cartilage *gray*; subchondral bone plate *white*), and **D** an example of the produced attenuation-histogram with the relative occurrence of the corresponding voxels. *EPIC-µCT*, equilibrium partitioning of an ionic contrast agent *via* µCT.

Cartilage segmentation procedure

Contour lines surrounding bone, articular cartilage, and scanning-medium were manually drawn. Care was taking not to include any bone marrow space or soft tissue remnants. To measure cartilage thickness, the cartilage was segmented by choosing global upper and lower thresholds. For mouse samples these thresholds were 70 and 170 (expressed in threshold units), respectively, and for human samples 70 and 220, respectively. Thus, in segmented images every voxel with a linear attenuation within these threshold ranges (assumingly representing cartilage tissue) kept their original gray value and voxels below or above these thresholds (representing scanning-medium or bone) was made transparent. Standard gauss filter parameters of sigma = 1.2 and support = 2 were applied. The 3-D morphology of the cartilage layer was visualized and quantified in terms of average cartilage thickness (µm) using direct distance transformation algorithms [282]. The thickness measurements were obtained for the entire cartilage layer.

Statistical analysis

All data sets were tested for normality using the Kolmogorov-Smirnov normality test (outcome: data normally distributed). Mouse cartilage thickness measurements via the EPIC-μCT technique and histology were compared via paired *t*-test, and the relationship and agreement between these two methods were examined separately via linear regression analysis (Pearson) and Bland-Altman analysis. For the human samples, ANOVA for repeated measures (Tukey's multiple comparison test) was used to test for differences between the different immersion times within the groups, and one-way ANOVA to test for differences between the groups per time point (healthy, OA-early, OA-late). An unpaired *t*-test with Welch correction was used to test the differences in cartilage thickness between the three groups, and to determine if the variance within each group was significant different. All data were expressed as mean ± standard deviation. All statistical analyses were performed by SPSS 16.0.2. (SPSS Inc., Chicago, IL, USA) and GraphPad Prism 5 (GraphPad Software, San Diego, CA, USA). A *p*-value of less than 0.05 was considered statistically significant.

Results

Histological staining allowed 2-D histomorphometric measurements of the cartilage thickness in the mouse samples. Cartilage thickness determined via histology was not significantly different from measurements provided *via* EPIC-μCT (paired *t*-test: $p = 0.220$; 95% confidence interval = -2.24 to 8.84). The average thickness of the articular cartilage was 113 ± 19 μm and 110 ± 16 μm as assessed by histology and EPIC-μCT, respectively. Linear regression analysis of thickness measurements from EPIC-μCT and histology revealed a strong linear relationship ($r^2 = 0.80$, $p < 0.0001$; **Figure 2a**). Bland-Altman analysis demonstrated good agreement between these two methods for thickness measurements, with an average thickness difference of 3 ± 9 μm and 95% limits of agreement – 14 to 20 μm (**Figure 2b**). Thus, the two methods agree within

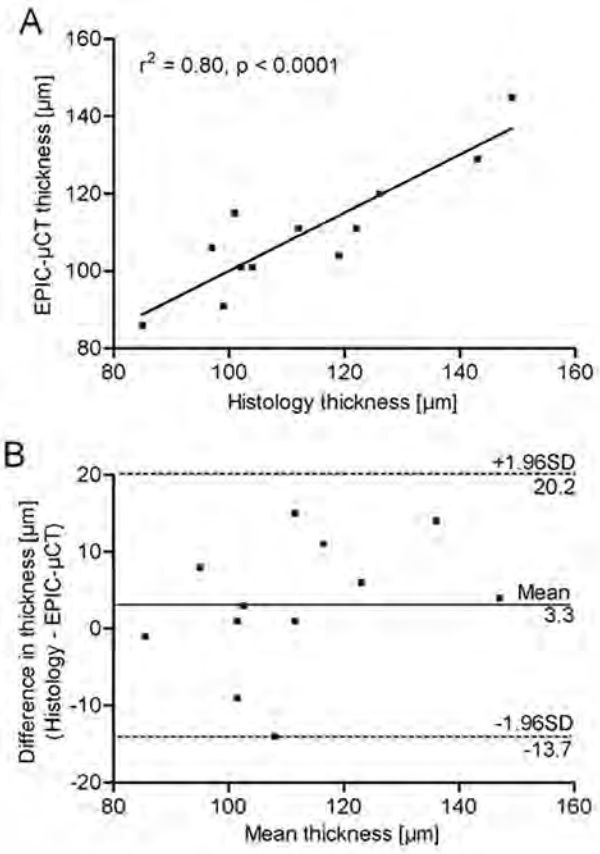

Figure 2. A A strong linear relationship between measurements of cartilage thickness obtained by EPIC-µCT and histology. **B** The differences (histology - EPIC-µCT) *vs* average cartilage thickness measured by histology and EPIC-µCT with 95% limits of agreement. *n* = 12 comparisons between histomorphometric measurement and corresponding µCT section.

approximately 15-20 µm. In the mouse jaw joint, 3-D reconstructions of the bone and cartilage components were successfully produced via a similar dual threshold procedure (**Figure 3**).

For the healthy human samples, the average cartilage attenuation increased with For the healthy samples, the average cartilage attenuation increased with immersion time from 15 minutes to one hour. The increase up to 30 minutes was found to be significant ($p < 0.001$; **Figure 4**, black bars). We determined comparable patterns with cumulative immersion times in the OA-early and OA-late groups (**Figure 4**, white and striped bars, respectively: $p < 0.001$). Thus, no significant differences were found between the three groups. For the OA-late samples, after a three-hour immersion period the attenuation values of the cartilage approached the bone attenuation. Therefore, reliable

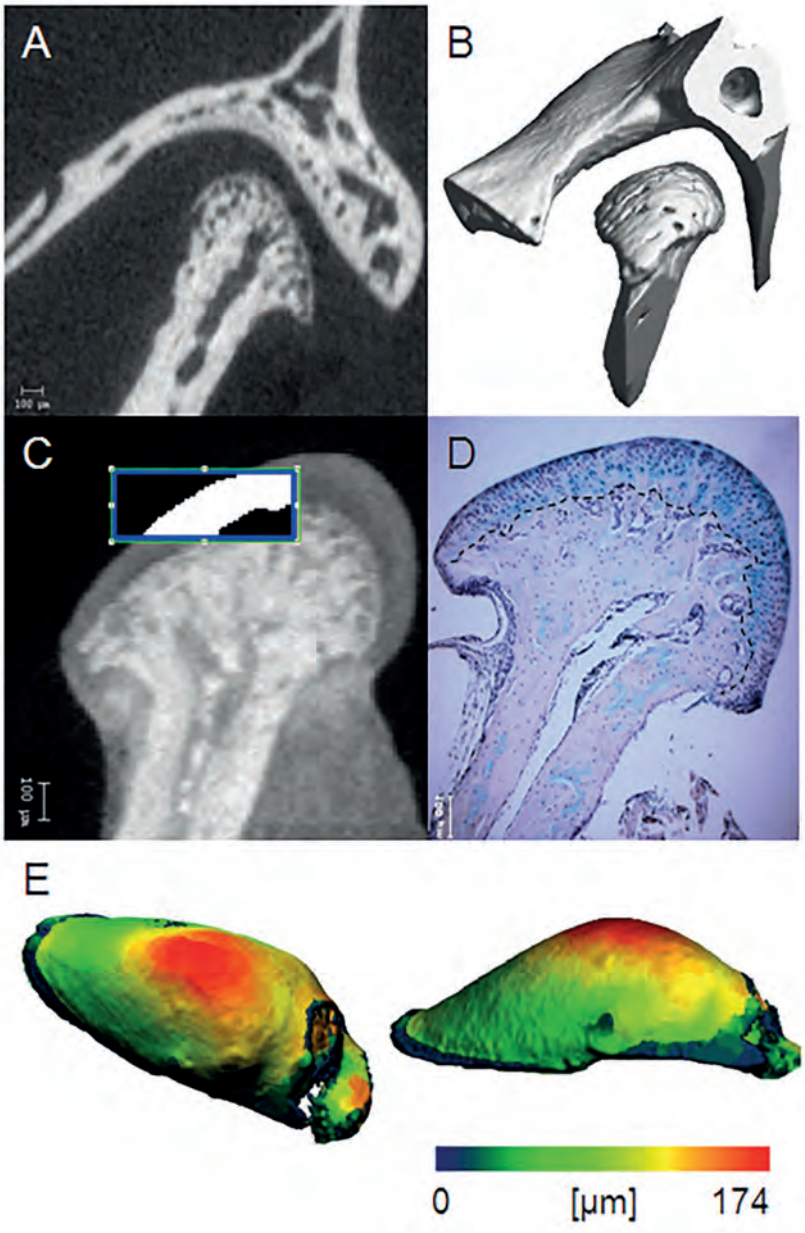

Figure 3. EPIC-µCT technique applied *ex vivo* to the mouse jaw joint. **A, B** In the µCT image a frontal cross-section of the left jaw joint is shown and its 3D-reconstruction produced with conventional µCT. **C** With the EPIC-µCT technique the visibility of the articular cartilage is enhanced. A dual-threshold procedure allowed segmentation of the cartilage. **D** The cartilage thickness measured with EPIC-µCT was compared to histological sections (alcian blue staining). **E** A thickness map of the cartilage layer (inferior and sagittal view) could be generated with a direct distance transformation algorithm and presented as a pseudo-color-scaled image (*i.e.,* blue to red; increasing cartilage thickness).

segmentation of the cartilage and bone peaks became unfeasible. For this reason, the results after three hours were omitted for the OA-late group. To evaluate the method's reproducibility, the complete procedure was repeated twice with a healthy condylar sample. Comparison of the repeated measures showed no significant differences between the average cartilage attenuations (paired t-test: p = 0.157). Based on these results, immersion for one hour in 40/60% Hexabrix/PBS (37°C) was selected as a standard protocol for human samples.

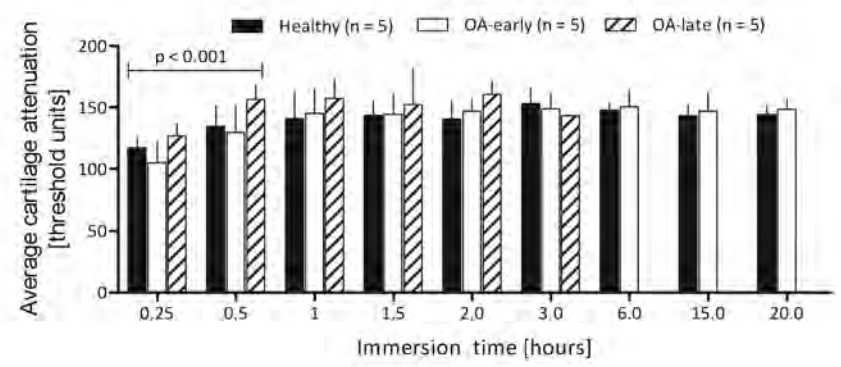

Figure 4. The average cartilage attenuation in the three groups as function of immersion time (n = 5 samples per group). A significant increase in cartilage attenuation was seen from 0 to 30 minutes. After 60 minutes, there were no significant changes seen in any of the groups. (values are mean ± standard deviation). *OA*, osteoarthritis.

Using the adapted EPIC-µCT technique, 3-D reconstruction of the bone components (**Figure 5a**) as well as the articular layer of the human jaw joint was feasible (**Figure 5b, c**). The 3-D morphology of the cartilage layer could be visualized and quantified in terms of average and local cartilage thickness (**Figure 5d**). Average cartilage thickness values determined in the human mandibular condyle were 240 ± 51 µm, 414 ± 123 µm, and 197 ± 160 µm, for healthy, OA-early, and OA-late samples respectively. There was a significant difference in cartilage thickness between healthy and OA-early samples (p = 0.032), and between OA-early and OA-late samples (p = 0.047). Furthermore, thickness variance was significantly different between healthy and OA-late samples (p = 0.047). These local thickness changes could be visualized by producing thickness maps (**Figure 6**).

Discussion

The great advantage of the EPIC-µCT technique is the 3-D measurement ability. The aim of this study was to extend the application of the EPIC-µCT technique for morphological

bone-cartilage research in the human and small animal temporomandibular joint (TMJ). We are the first to apply EPIC-µCT in this specific joint. Successful use of this technique provides the potential to further investigate the relationship between bone and cartilage changes in osteoarthritis or other cartilage-related diseases in the jaw joint.

Previously, EPIC-µCT was applied in the knee joint of a rat model [37, 38]. The cartilage thickness determined in these studies ranged from 403 ± 11 µm in 4-week-old

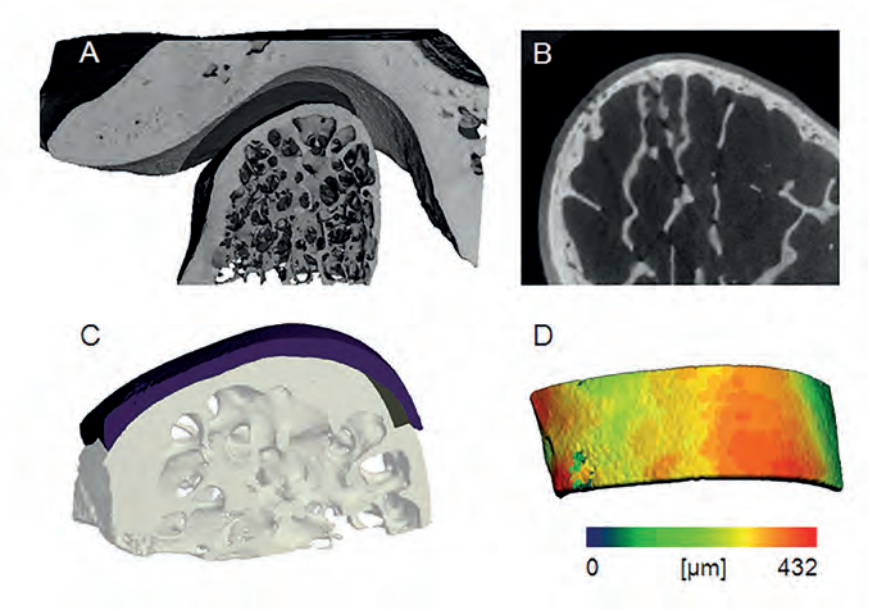

Figure 5. EPIC-µCT technique applied *ex vivo* to the human jaw joint. **A** In the µCT image a sagittal cross-section of a right human jaw joint is shown and its 3-D reconstruction produced with conventional µCT. **B** With the EPIC-µCT technique the visibility of the articular cartilage is enhanced. **C** A dual-threshold procedure allows for 3-D reconstruction of both bone tissue (transparent structure) and overlying cartilage layer (purple structure). **D** A thickness map of the cartilage layer (inferior view; 150 slices width) is presented as a pseudo-color-scaled image (*i.e.,* blue to red; increasing cartilage thickness).

rats to 111 ± 8 µm in 16-week-old rats. The accuracy for these thickness measurements was validated through precision evaluation (RMS-CV: 1.5%; RMS-SD: 7.3 µm) and by comparison to conventional needle probing (r^2 = 0.95, p < 0.010). Their power analysis indicated the possibility to detect a 1.3% thickness change with a sample size of ten animals. In the present study, the average cartilage thickness found in the mouse TMJ showed a thickness range (110 ± 16 µm) comparable to the 16-week-old rats. The reliability of our findings was confirmed by a strong correlation between histology and EPIC- µCT (r^2 = 0.80, p < 0.0001). For these results we conclude that EPIC-µCT is applicable for TMJ-OA research in a small animal model such as the mouse. There might be a crucial role for the subchondral bone tissue in the process of OA. This fascinating concept needs to be

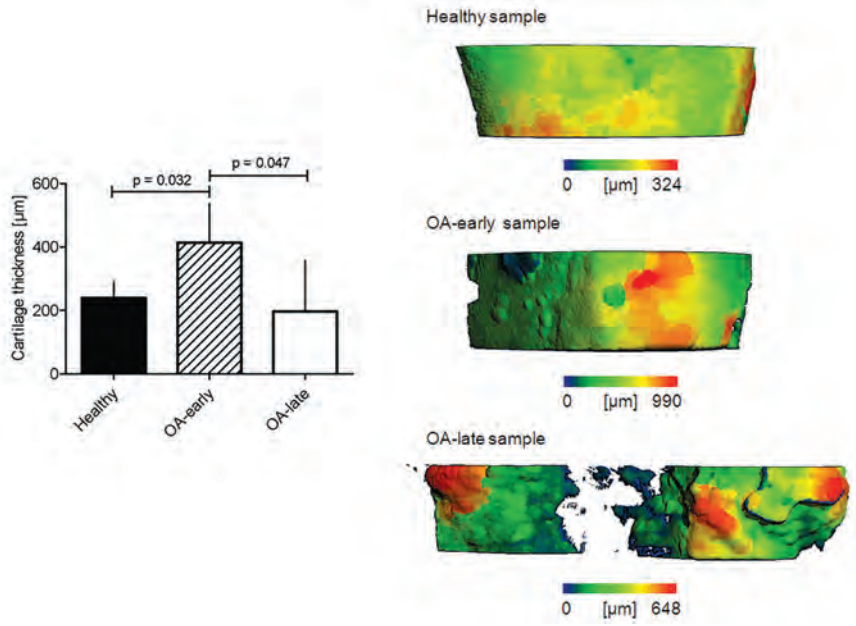

Figure 6. 3-D articular thickness measurements were performed for the three groups of human samples. Differences were found between the average thicknesses of the cartilage layers between the groups. Furthermore, local differences in cartilage thickness were evident when the groups were compared. OA, osteoarthritis.

investigated further; therefore new challenges should be met such as experimental *ex vivo* research, allowing studying the interaction between subchondral bone and articular cartilage tissue. OA animal models can allow investigation of early disease progression and temporal changes in a relatively controlled environment, however, *ex vivo* research requires animal euthanasia at each desired interval. Future advances in non-invasive µCT imaging can allow *in vivo* imaging in small animal joints with isotropic resolution between 6-10 µm.

For the human TMJ samples, the required immersion time was determined by implementation of a cumulative immersion sequence. A minimal immersion time of one hour was determined, which is 30 minutes longer than the value used in the rat knee protocol [37]. Most probably the larger dimensions (*i.e.,* total volume) of the human TMJ might cause this difference. Another potentially relevant difference is that the fibrocartilage in the TMJ contains less sGAGs [280]. The result is a different FCD of the cartilage layers in jaw and knee joint, respectively. As EPIC-µCT attenuation is reversely proportional with this FCD, increased attenuation values in the human TMJ were expected. This likely caused the required adjustment of the immersion time for the human TMJ samples. Since we were only interested in possible adjustments of the protocol for human TMJ samples and the potential ability for (local) cartilage thickness measurements in both human and

mouse samples, cartilage changes such as GAG content was not evaluated in this study. Interestingly in the human samples, a significant increase in cartilage thickness was found between healthy joints and joints with early signs of OA (239.7 ± 50.5 and 414.2 ± 122.6 μm, respectively). A subsequent significant decrease was found in human joints with late signs of OA (197.4 ± 159.7). Increase in cartilage thickness during the earlier development of OA has been reported before [283]. It is hypothesized that in osteoarthritic cartilage the integrity of the collagen network is lost, leading to more water absorption due to the presence of the proteoglycans.

To study the aetiology and progression of TMJ-OA, conventional μCT can be applied for 3-D bone reconstruction of the complete TMJ including detailed morphology and the bone's mineral degree and distribution [275, 284]. Subsequently, EPIC-μCT provides the 3-D imaging of cartilage morphology and thickness measurements. As described before, the technique can also be used for measurements of relative sGAGs concentration and distribution [36, 38, 39, 285]; an indication of the healthy state of the cartilage. However, caution should be taken when using this technique for analysis of samples fixed in formalin. The mouse samples were stored in fixation fluid and the human samples were harvested from embalmed subjects. Kotwal and co-workers reported that a fixation procedure (pre-preservation versus post-preservation) does not influence the thickness or volume of the cartilage layer and, furthermore, no significant changes in attenuation in the intact joint surface of a mouse model were found [39]. In contradiction, Benders and co-workers reported "that formalin fixation decreases X-ray attenuation levels in ioxaglate-stained cartilage" in bovine osteochondral plugs [277]. Whether the fixation can influence the cartilage attenuation and thus sGAGs quantification is still on debate. In addition, no data is available on the influence of an embalming procedure on the attenuation levels.

In TMJ-OA, the mechanical overload has been suggested as a predominant initiator of the disease [267, 268, 272]. μCT-based biomechanical computational models (*i.e.*, finite element models) have become a standard tool to examine bone's mechanical properties and to predict its mechanical behavior [50]. Generally, when these dynamic models are used to examine the cartilage's mechanical behavior, a uniform articular cartilage thickness of 100 μm or 200 μm has been assumed [286, 287]. However, our results indicate a wider range including different thickness variances (**Figure 6**), more consistent with earlier findings in the human TMJ [288]. Morphological measurements of both bone and cartilage tissues via conventional μCT and EPIC-μCT could provide a more accurate future biomechanical models. Besides this advantage, the EPIC-μCT technique has the ability to determine the relative sGAGs concentration throughout the cartilage layer, since the attenuation values are considered inversely proportional to the distribution and average amount of sGAGs [36, 38]. These sGAGs concentrations

are linked to the biomechanical properties of the TMJ's cartilage layer [289] and can be implemented into a model further improving the input of material and/or tissue properties [290]. For example, it becomes possible to determine how changes in bone composition and structure affect the mechanical properties of the subchondral bone and thus whether these changes affect the overlying cartilage in a healthy or diseased joint using finite element analysis.

In conclusion, we established the *ex vivo* application of a semi-quantitative, high-resolution, 3-D imaging technique (*i.e.*, EPIC-μCT) to assess cartilage morphology in the mouse and human TMJ. For the human TMJ the original protocol provided by Xi *et al* [38] had to be adjusted and the immersion time was set to one hour. Conventional μCT and EPIC-μCT could allow for bone-cartilage interaction research in the initiation and progression of TMJ-OA in mouse and human models. The results in this study are encouraging for *ex vivo* research, however, *in vivo* application of the EPIC-μCT technique in the jaw joint is challenging and systematic further studies are needed to reveal if this technique has any clinical potential.

Acknowledgements

The authors thank Hans Korfage, Peter Brugman, Marion van Duin, and Ton Bronckers for their technical assistance. We thank Cindy Cleypool and Teun de Vries for providing help with sample collection. Furthermore, many thanks go to Denise Duijster for critically reading this manuscript. This work was funded by the Netherlands Organization for Scientific Research (NWO, grant number 021.001.050).

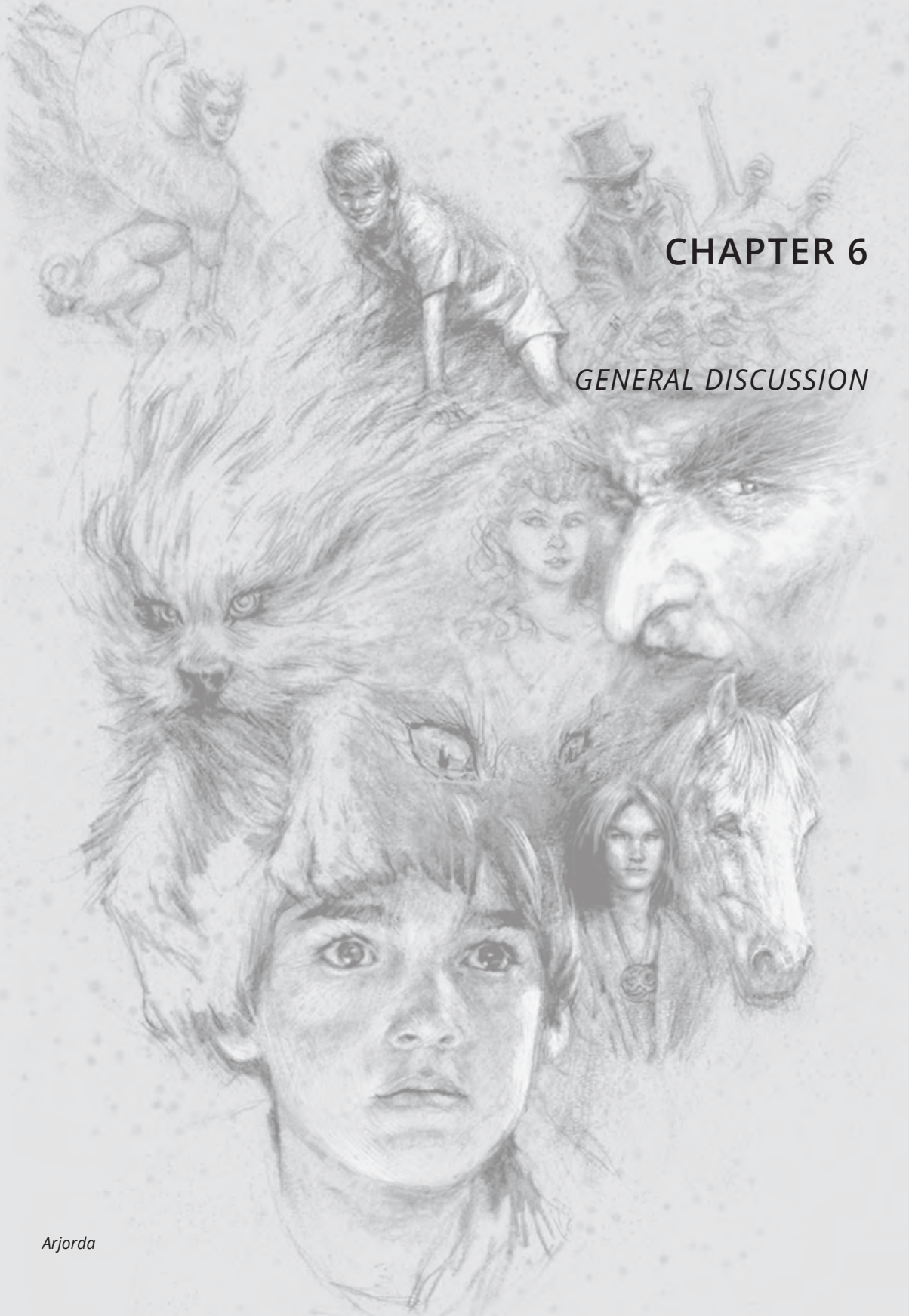

CHAPTER 6

GENERAL DISCUSSION

Arjorda

In this thesis we used: (i) conventional μCT to obtain fundamental data on bone parameters of the cortical and trabecular bone in the human mandibular condyle (**chapter 2**); (ii) MicroCT-based Finite Element (FE) modeling to determine the influence of the intratrabecular mineralization on several mechanical output parameters in the human mandibular condyle (**chapter 3**); (iii) conventional μCT imaging approach in a mouse model, and assessed the effect of bisphosphonate (BP) treatment in knee versus jaw joint and humerus versus mandible (**chapter 4**); and (iv) the EPIC-μCT technique for *ex vivo* 3D imaging and analysis of the articular cartilage in the human and mouse joint to produce μCT-based FE analyses of both joints (**chapter 5**).

Conventional μCT applied to the mandibular condyle

One of the questions that we attempted to tackle was: *Are regional differences in mineralization found within the mandibular condyle? If so, what are the possible functional implications of these differences?* Our study was the first one that examined the tissue mineral density (TMD) and its distribution in cortical and trabecular bone of the human mandibular condyle. Compared to the trabecular bone, the TMD is 25% higher in cortical bone. In addition, there were significant differences in TMD between cortical regions (subchondral >> posterior >> anterior). The largest variation of TMD distribution was found in the anterior cortex. Within the cortical bone, TMD decreased from the cortical canals to the periphery. Similarly, the TMD of trabecular bone increased from the surface of the trabeculae to their cores. Does the variation in TMD distribution indicate a difference in remodeling rate between condylar trabecular and cortical bone and between cortical regions? Does the differences in TMD between trabecular and cortical bone indicate differences in Young's modulus? What is the biological meaning of the variations in TMD distribution? Could it be adaptation to environment, function or pathology? And what about the relationship with cortical porosity?

The spatial variations of TMD and porosity are related to bone turnover [69, 291], which can be affected by the complex 3-D stress distribution in the condyle. The TMD in the condyle may reflect age and remodeling rate of the bone tissue. Quantification of the TMD facilitates a better understanding of possible effects on adaptive remodeling on mineralization of the condyle in the healthy and diseased joint and its possible consequences for mechanical properties. The changes in density and architecture of the subchondral bone have a profound effect on both the initiation and progression of cartilage degeneration in OA. For instance, the thickening of the subchondral plate is supposed to influence an increase in internal cartilage stress that leads to increased hardening of the subchondral bone or progressive thinning of the cartilage layer [1, 292-294].

Changes of bone mineralization may affect the mechanical properties of bone tissue at different scales such as the stiffness (*i.e.*, Young's modulus), the strength and the toughness [137, 143]. Both an increased and a decreased bone turnover have detrimental effects on bone quality, leading to a plastic but weak bone or to a stiff but brittle bone, respectively [291]. The lower TMD found in the trabecular region may be explained by a higher amount of remodeling in trabecular bone as a consequence of relatively more bone surface. Remodeling being initiated on the bone surface, a volume of bone with a large exposed surface will be remodeled more rapidly. The regional TMD variations in the cortical bone can be due to the adjustment of the condyle architecture during function. During jaw-closing the condyles are primarily subjected to compression forces in supero-inferior direction [52] and these dynamic loads vary in direction and magnitude [150, 295]. The condyle's architecture is adjusted to withstand this compressive loading in supero-inferior direction with the articular surface supported for the most part by vertically oriented trabeculae [186]. A previous study has shown that distribution of stress and strain in the mandibular condylar cortex has topographic characteristics with highest stress occurring in the posterior cortex and tension largely observed anteriorly and compression posteriorly [54].

To conclude, the range of daily loading patterns influences variations in TMD and cortical porosity, and therefore remodeling provides bone tissue a useful tool to adapt to changes in this loading patterns. In a healthy joint, articular cartilage and subchondral bone act together in transmitting load pressure through joints. Therefore, the integrity of both tissues is necessary for adequate joint function. When one element, such as the subchondral bone, becomes unbalanced due to TMD and/or porosity changes, it inevitability triggers multiple physiological, biochemical, and biomechanical responses from the other components as the joint system seek to rebalance itself.

MicroCT-based FE models of the mandibular condyle

Is there a relationship between the amount and degree of mineralization, and FE-based predicted biomechanical properties? We assume there is. The arguments supporting our assumption are the following: On a biomechanical level, the differences described suggests a large difference in Young's moduli. The incorporation of mineralization variation (heterogeneous model) decreased the apparent Young's and shear moduli by maximally 21% in comparison to the homogeneous model. The heterogeneous model apparent moduli correlated significantly with bone volume fraction and TMD. The refined FE models should provide more realistic estimations because the refined input provides a more realistic biological simulation. In the homogeneous model, the highest stresses were found at the surface with a significant decrease towards the core. Higher superficial

stresses could indicate a higher predicted fracture risk in the trabeculae simulating more brittle behavior. In the heterogeneous model this pattern was different. A significant increase in stress with increasing distance from the trabecular surface was found followed by a significant decrease towards the core. This suggests trabecular bending during compression. In both models a decrease in strain values from surface to core was predicted, which is consistent with trabecular bending. When mineral heterogeneity was taken into account, the predicted intratrabecular patterns of stress and strain are more consistent with the expected biomechanical behavior as based on mineral variations in trabeculae. *Does this indicate that we should always include mineral heterogeneity when performing biomechanical studies on topics such as the effects of antiresorptive treatments?* No. Including more parameters in a biomechanical model also makes the output more complex to read and to understand. Including all the mineral variables at once in a model can make it too complex. Depending on the research question a choice should be made which variable should be used. Furthermore, to really confirm the causality between the findings one should include real time mechanical testing.

In the case of osteoarthritis (OA), there is a growing awareness of a potential role for bone tissue in the disease progress. There is a recognition of OA as bone disease because OA involves the entire joint as an organ, not just the cartilage. The role of subchondral bone in the pathogenesis of osteoarthritic related cartilage damage has likely been underestimated. Subchondral bone is not only an important shock absorber, but may also be important for cartilage metabolism [7, 8]. It is generally accepted that the mutual feedback between the two tissues is required for their unique roles and functions with the joint organ. As such, bone and cartilage in the mature joint are independent, and are only capable of fulfilling their biomechanical functions with their mutual support from the macro-structural to the micro-structural level.

Implications of bisphosphonate treatment on bone tissue in knee versus jaw joint and humerus versus mandible

Due to our interest to investigate the interaction between bone and cartilage tissues in a joint, an animal model was designed in which mice were exposed to conditions known to experimentally induce bone changes. The underlying idea was to collect data on bone changes and measure possible cartilage changes as an outcome to predict tissue interaction. One of the chosen methods for the induced bone changes was the application of a bisphosphonate (BP). These drugs will probably be used more frequently in the clinical setting as a standard effective disease modifying osteoarthritis drug in the synovial joint of long bones [296]. In the BP treated animals, very intriguing and unexpected bone-site-specific changes were found in mineralization of the jaw joint.

Therefore, we focused on the implications of BP treatment on bone tissue in knee versus jaw joint and humerus versus mandible. *Are there differences in the response to BP treatment for long bone joints compared to the jaw joint?* Yes, there were. In the knee joint, zolendronic acid (ZA) treatment increased TMD, bone volume, and trabecular thickness but did not influence cortical thickness. In both control and ZA group, a higher trabecular TMD compared to cortical TMD was found. Unseen in the knee joint, ZA treatment in the jaw joint resulted in bone-site-specific changes in mineralization; a significant time-dependent higher TMD was evident in the subchondral bone compared to the most distal region of the mandibular condyle. MicroCT images revealed the presence of mineral in this region and histology showed that this region did not contain mature bone but cartilage-like tissue. *Does this mean that there is a possible detrimental effect of BP treatment on the jaw joint comparable to BP-related osteonecrosis of the jaw?* According to our data, this could be the case. The data suggest a possibility of site-specific negative side effects, *i.e.*, disturbing normal mandibular development under the influence of bisphosphonate therapy. From the literature, we do not have clinical (case) reports that describe such a finding in humans. In addition, it is important to realize that no studies have appeared that analyzed possible detrimental side effects in the jaw joint during antiresorptive treatment. Therefore, we do not know whether it also occurs in humans. Nor do we have knowledge about its biomechanical effect. *Were there also different implications found for long bone (humerus) versus mandible?* Yes, there were. Long-term treatment with ZA reduced the number of marrow cells in the mandible, without affecting the number of long-bone marrow cells. ZA treatment did not affect the number of osteoclasts *in vivo*. Yet, the bisphosphonate increased bone volume and TMD of both long bone and jaw. Interestingly, 6 months of treatment suppressed bone formation in long bones without affecting the jaw. Unexpectedly, we showed that bisphosphonates can cause molar root resorption, mediated by active osteoclasts. Taking all these findings together one should start to wonder what happens during the development and maturation of jawbone, jaw joints and the dentition in children undergoing high-dosage antiresorptive treatment.

EPIC-µCT applied to the jaw joint

Can we use EPIC-µCT for ex vivo 3D imaging and analysis of both bone and cartilage tissue in human and mouse jaw joint? Yes, we can. The contrast-enhancement protocol used by Xie and co-workers [37], can be used on mouse jaw joint samples. The measurements of cartilage thickness with EPIC-µCT provided similar results as histomorphometric measures. The protocol had to be adjusted for human jaw joint samples by increasing immersion time for 30 minutes to 60 minutes to allow 3D imaging of the cartilage layer. Three-dimensional imaging was successfully used to visualize the changes that occur

when a human jaw joint is affected by osteoarthritis. The EPIC-μCT technique is effective for *ex vivo* assessment of 3D cartilage morphology in the mouse as well as human jaw joint. This should allow for bone-cartilage interaction research in TMJ-OA and hopefully can be applied *in vivo*. If we can apply conventional and contrast-enhanced μCT techniques successfully to the jaw joint, our results could provide the means to produce μCT-based biomechanical computer models. In this thesis, the techniques were applied *ex vivo* to the complete human jaw joint. The dimension of the jaw joint is very suitable for this kind of research and was therefore our joint of interest. The combination of complimentary imaging techniques is promising for gaining more fundamental understanding of healthy and osteoarthritic joints as is permits the visualization of both bone and cartilage tissue. With the μCT-based biomechanical computer models that can be produced, it is possible to predict the biomechanical interaction of bone and cartilage tissue and the consequence of this interaction in a healthy and osteoarthritic human joint. Both tissues are important to the health of the complete joint, and when one tissue is comprised, it inevitably has an impact on the other. Furthermore, an animal experiment can be used to induce bone changes allowing for detailed investigations into the influence of specific bone changes on the overlying articular cartilage in the animal jaw joint. Combining both μCT techniques and an animal experiment will allow us to further investigate the influence of specific bone changes on the overlying cartilage *ex vivo*. The incidence of OA in the knee joint is high (Rijksinstituut voor Volksgezondheid & Milieu, January 2011). In many respects the knee joint is comparable to the jaw joint. However, the knee joint contains hyaline cartilage, whereas the jaw joint contains fibrous cartilage. Compared to fibrous cartilage hyaline cartilage is composed of different types of collagen and a different concentration of proteoglycans [229, 280]. These differences can play an important role in the initiation of pathological bone and/or cartilage changes in both joints and provide us with extra insight in the process of OA development and intervention. For this reason, we think for the future it will be very interesting to perform more studies on these two synovial joints in which they are compared. In this way we could try to figure out which factors can influence the delicate balance between bone and cartilage tissue when it triggers a cascade of (abnormal) physiological reactions.

Our data can be useful to find answers to more specific research questions: Is μCT a useful technique for quantitative bone research in the jaw joint? Is a μCT-based biomechanical model suitable for OA research in the jaw joint? Is μCT usable for cartilage assessment in the jaw joint of a human and murine model? Finding answers to these questions, we hope to contribute to the implementation of new methods and ways to understanding of OA development and the creation of effective treatments. One of the scopes in future OA research could be, for instance, to examine the complex interactions of different tissues in OA progression using methods provided in this thesis,

especially focusing on the importance of subchondral bone in the early stages of disease development.

To conclude, the results of this project described in this thesis can be useful for a wide range of future research. MicroCT techniques can be used for fundamental bone and cartilage research and also has the potential to be applicable for clinical purposes: (i) Several applications, improvements and comparisons of different CT techniques can be explored [297-301]; (ii) Tissue mineral density and heterogeneity in relation to anatomy [302] and biomechanical behavior parameters in jaw and long bones [303-309]; (iii) Influence of porosity on biomechanical behavior parameters [308, 310-313]; (iv) Mineralization parameters in relation to clinical conditions such as medicine usage [182, 193, 314-318] and clinical situations such as medical applications and pathology [319-324]; (v) Bioengineering research topics [325-329]; (vi) Biomechanical modeling [297, 330-338].

GENERAL SUMMARY

Vincent Jalkarese

In a healthy joint, articular cartilage and subchondral bone act together in transmitting load pressure through joints. Therefore, the integrity of both tissues is necessary for adequate joint function. When one element falls out of balance, it inevitably triggers multiple physiological, biochemical, and biomechanical responses from the other components as the joint system seek to rebalance itself. The close interaction between the two tissues is evident from their roots during development. Bone and cartilage were originally one tissue, and jointly differentiated into two distinct tissues to be found in the adult. It is generally accepted that the mutual feedback between the two tissues is required as they specialized and adapted to their unique roles and functions within the joint organ. As such, bone and cartilage in the mature joint are interdependent, and are only capable of fulfilling their biomechanical functions with their mutual support from a macro-structural to a micro-structural level. Furthermore, the intimate relationship between bone and cartilage involves multiple pathways of interaction; many of which were shown to regulate the metabolic and remodeling mechanisms of the tissues.

Our main research questions were: Is μCT a useful technique for quantitative bone research in the jaw joint? Is a μCT-based biomechanical model suitable for osteoarthritis (OA) research in the jaw joint? Is μCT usable for cartilage assessment in the jaw joint of a human and murine model? With obtaining answers to these questions, we hope to contribute to finding new methods and ways to improve our understanding of OA development and the creation of effective treatments. One of the scopes in future OA research could be, for instance, to examine the complex interactions of different tissues in OA progression using methods provided in this thesis, especially focusing on the importance of subchondral bone in the early stages of disease development.

Chapter 2 describes the application of conventional μCT to the mandibular component of the human jaw joint for quantitative measurements of bone structural (*e.g.*, cortical and trabecular morphology) and material parameters (*e.g.*, tissue mineral density and distribution). The dimension of the jaw joint is very suitable for this kind of research and was therefore our main joint of interest. Our study was the first one that examined the tissue mineral density (TMD) and its distribution in cortical and trabecular bone of the human mandibular condyle (**Chapter 2a**). The TMD in the mandibular condyle may reflect age and remodeling rate of the bone tissue. Quantification of the TMD facilitates a better understanding of possible effect on adaptive remodeling on mineralization of the condyle in the healthy and diseased joint and its possible consequences for mechanical properties. A conventional μCT system was used to measure TMD values. Mean TMD was higher in cortical than in trabecular bone and differed significantly between different cortical regions. The variation in TMD distribution was significantly larger in the anterior cortex than the posterior and subchondral cortex, indicating a larger amount

of heterogeneity of mineralization anteriorly. Within the cortical cortex, TMD increased with distance from the cortical canals to the periphery. Similarly, TMD of the trabecular bone increased with distance from the surface of the trabeculae to their cores. On a biomechanical level, the difference in TMD between condylar trabecular and cortical bone suggests a large difference in Young's moduli.

Another achievement of this thesis was high-resolution visualization of the cortical porosity network in 3D and providing further quantitative information via the conventional μCT technique (**Chapter 2b**). We were able to examine cortical porosity in relation to TMD, in order to get more information about the principal directions of stress and strains during loading. Quantification of porosity and tissue mineral density of bone facilitates a better understanding of possible effects of adaptive bone remodeling and possible consequences for its mechanical properties. The cortical canals in the subchondral cortex of the condyle were oriented in mediolateral direction, and in the anterior and posterior cortex in superoinferior direction. Cortical porosity (average 3.5%) did not differ significantly between the cortical regions. It correlated significantly with the diameter and number of cortical canals, but not with cortical tissue mineral density. In trabecular bone (average porosity 79.3%) a significant negative correlation was found between surface area of the trabeculae and tissue mineral density; such a correlation was not present between the surface area of the cortical canals and the tissue mineral density of cortical bone. No relationship between trabecular and cortical porosity or between trabecular tissue mineral density and cortical tissue mineral density was found, suggesting that adaptive remodeling is independent and different between trabecular and cortical bone. We conclude that the principal directions of stress and strains are primarily directed mediolaterally in the subchondral cortex and superoinferiorly in the anterior and posterior cortex, and that the amount of remodeling is larger in trabecular than in cortical bone of the mandibular condyle; in trabecular bone variation in the level of remodeling is related to the available surface area of the trabeculae.

Chapter 3 describes and discusses the use of μCT-based Finite Element (FE) analyses to determine the influence of the intratrabecular mineralization on several mechanical output parameters (*e.g.*, apparent elastic modulus and intratrabecular stress/strain patterns) of trabecular bone in the human mandibular condyle. Due to daily loading, trabecular bone is subjected to deformations (*i.e.*, strain), which lead to stress in the bone tissue. When stress and/or strain deviate from the normal range, the remodeling process leads to adaptation of the bone architecture and its tissue mineral density to effectively withstand the sustained altered loading. As the apparent mechanical properties of bone are assumed to depend on the degree and distribution of mineralization, the goal of our study in **Chapter 3a** was to examine the influences of mineral heterogeneity on the

biomechanical properties of trabecular bone in the human mandibular condyle. Two different sets of Finite Element (FE) models of trabecular samples were constructed; tissue stiffness was either scaled to the local tissue mineral density of bone as measured with μCT (heterogeneous) or tissue stiffness was assumed to be homogeneous. Compression and shear tests were simulated to determine the apparent elastic moduli in both model types (homogeneous vs. heterogeneous). The incorporation of mineralization variation decreased the apparent Young's and shear moduli by maximally 21% in comparison to the homogeneous model. The heterogeneous model apparent moduli correlated significantly with bone volume fraction and tissue mineral density of bone. It was concluded that disregarding mineral heterogeneity may lead to considerable overestimation of apparent elastic moduli in FE models.

Knowledge of the influence of mineral variations (*i.e.*, mineral heterogeneity) on biomechanical bone behavior at the trabecular level is limited. The aim of **Chapter 3b** was to investigate how this material property affects the intratrabecular distributions of stress and strain in human adult trabecular bone. The influence of intratrabecular mineral heterogeneity was analyzed by comparing the same models as constructed in **Chapter 3a**. Interesting effects were seen regarding intratrabecular stress and strain distributions. In the homogeneous model, the highest stresses were found at the surface with a significant decrease towards the core. Higher superficial stresses could indicate higher predicted fracture risk in the trabeculae. In the heterogeneous model this pattern was different. A significant increase in stress with increasing distance from the trabecular surface was found followed by a significant decrease towards the trabecular core. This suggests trabecular bending during a compression. In both models a decrease in strain values from surface to core was predicted, which is consistent with trabecular bending. When mineral heterogeneity was taken into account, the predicted intratrabecular patterns of stress and strain are more consistent with expected biomechanical behavior as based on mineral variations in trabeculae. Our findings indicate that mineral heterogeneity should not be neglected when performing biomechanical studies on topics such as the (long-term or dose dependent) effects of antiresorptive treatments.

Chapter 4 describes the different implications of high-dosage bisphosphonate treatment on bone tissue parameters (*e.g.,* mineral density, trabecular and cortical thickness) in the knee vs. jaw joint and mandible vs. humerus in a mouse model via μCT assessment and histological techniques. Bisphosphonates are bone antiresorptive agents traditionally used on a relatively large scale for treatment of bone metabolic diseases and on a smaller scale for bone metastasis treatment. A study on the effects of bisphosphonate treatment on healthy instead of diseased animals will give more insight into the basic mechanisms of bisphosphonates and their effects on different bone sites. In **Chapter 4a** we aimed to

assess the effect of BP on the mouse knee and jaw joint. At baseline and after treatment with zoledronic acid (ZA) for one, three or six months, we combined bone assessment via μCT and histology. Our results showed that, in the knee joint, ZA treatment increased TMD, bone volume, trabecular thickness but did not influence cortical thickness. In both control and the ZA group, a higher trabecular TMD compared to cortical TMD was seen. Unseen in the knee joint, ZA treatment in the jaw joint resulted in bone-site specific changes in mineralization; a significant time-dependent higher TMD was evident in the subchondral bone compared to the most distal region of the condyle. MicroCT images revealed the presence of mineral in this region and histology showed that this region did not contain mature bone tissue but cartilage-like tissue. Our data indicates the possibility of site-specific negative side effects, *i.e.* disturbing normal mandibular development under the influence of bisphosphonate therapy.

In **Chapter 4b** we investigated whether *in vivo* exposure to bisphosphonates has a different effect on long bone and jaw osteoclasts, and on the turnover of these different bones. The same animal experiment was used as described in **Chapter 4a**. The effects on the number of osteoclasts, bone mineralization, and bone formation were measured in the long bones and in the jaw. Long-term treatment with zoledronic acid reduced the number of jaw bone marrow cells, without affecting the number of long-bone marrow cells. Zoledronic acid treatment did not affect the number of osteoclasts *in vivo*. Yet, the bisphosphonate increased bone volume and mineral density of both long bone and jaw. Interestingly, six months of treatment suppressed bone formation in the long bones without affecting the jaw. Unexpectedly, we showed that bisphosphonates can cause molar root resorption, mediated by *active* osteoclasts. Our findings provide more insight into bone-site-specific effects of bisphosphonates and into the aetiology of osteonecrosis of the jaw. We demonstrated that bisphosphonates can stimulate osteoclast activity at the molar roots.

Chapter 5 describes the introduction of a novel μCT technique called EPIC-μCT. Both conventional μCT and EPIC-μCT are applied *ex vivo* to both human and mouse jaw joint for 3D assessment of bone and cartilage morphology. The temporomandibular joint (TMJ) is susceptible to the development of osteoarthritis (OA). More detailed knowledge of its development is essential to improve our insight into TMJ-OA. It is imperative to have a standardized, reliable 3-D imaging method that allows for detailed assessment of both bone and cartilage in healthy and diseased joints. We aimed to determine the applicability of a contrast-enhanced μCT technique for *ex vivo* research of mouse and human TMJ. Equilibrium Partitioning of an Ionic Contrast agent via μCT (EPIC-μCT) was previous applied for cartilage assessment in the knee joint. The method was *ex vivo* applied to the mouse TMJ and adapted for the human TMJ. EPIC-μCT (30' immersion time) was applied

to mouse mandibular condyles and 3-D imaging revealed average cartilage thickness measurements via EPIC-μCT comparable to histomorphometric measurements. For human healthy and OA-affected TMJ samples the protocol was adjusted to an immersion time of one hour. 3-D imaging revealed a significant thicker cartilage layer in joints with early signs of OA compared to healthy joints. A subsequent significant thinner layer was found in human joints with late signs of OA. The EPIC-μCT technique is effective for the *ex vivo* assessment of 3-D cartilage morphology in the mouse as well as human TMJ and allows bone-cartilage interaction research in TMJ-OA.

In this thesis, conventional and contrast-enhanced μCT techniques were applied *ex vivo* to the complete human jaw joint. The combination of complimentary imaging techniques is promising for gaining more fundamental understanding of healthy and osteoarthritic joints as it permits the visualization of both bone and cartilage tissue. The combination of conventional and EPIC-μCT methodology could furthermore allow future possibilities to study the cartilage-bone complex as a whole. The mechanical interaction between its different constituents and the dynamical loading patterns of the joint during habitual function and prolonged heavy loading conditions can be the central issues. The dimension of the joint at all its stages of development enables to assess the fine architecture of both the subchondral bone and trabecular bone by μCT techniques without fully disrupting its integrity. One goal of this approach could be to predict the changes in the subchondral and trabecular bone in the joint as a consequence of overloading conditions and compare these changes with the abnormal bone structure observed in OA. A second goal could be to predict changes in the loading history of the articular cartilage in the relation to the prerequisites for cartilage maintenance.

With the μCT-based biomechanical computer models that can be produced, it is possible to predict the biomechanical interaction of bone and cartilage tissue and the consequence of this interaction in a healthy and osteoarthritic human joint. Furthermore, an animal experiment can be used to induce bone changes allowing for detailed investigation into the influence of specific bone changes on the overlying articular cartilage in the animal jaw vs. knee joint. Combining both μCT techniques in an animal experiment will allow us to further investigate the influence of specific bone changes on the overlying cartilage *ex vivo*. Our data can be useful to find answers to the hypothesis: Bone changes precede cartilage changes and/or damage in the development of osteoarthritis. With the results of this thesis, we hope to contribute to the implementation of new methods and ways to understanding of OA development and the creation of effective treatments.

The results described add up to the following general conclusions:

- The range of daily loading patterns influences variations in tissue mineral density and cortical porosity, and therefore remodeling provides bone tissue a useful tool to adapt to changes in these loading pattern.
- A more specific input for a biomechanical model provides a more specific output and thus outcome. Depending on the research question a choice should be made which variable should be used.
- Responses to high-dosage bisphosphonate treatment are bone-sites-specific (jaw bone vs. long bones) and can additionally cause a possible detrimental and unknown effect on the jaw joint.
- The EPIC-μCT technique is effective for *ex vivo* assessment of 3D bone and cartilage morphology in the mouse as well as human jaw joint plausible useful for bone-cartilage interaction research in jaw joint osteoarthritis.

ALGEMENE SAMENVATTING

Soulstryder

In een gezond gewricht werken gewrichtskraakbeen en subchondraal bot samen om het krachtenspel in het gewricht goed te verdelen. Daarom is de integriteit van beide weefsels belangrijk voor een adequate functie. Als één van deze elementen uit balans raakt, zal het onvermijdelijk een cascade van fysiologische, biochemische en biomechanische reacties veroorzaken in de andere gewrichtscomponenten omdat het systeem zoekt naar een nieuwe balans. De intieme interactie tussen de twee weefsels komt voort uit de nauw geassocieerde ontstaanswijze van beide. Bot en kraakbeen ontstaat tijdens de ontwikkeling uit één weefsel en zijn naast elkaar gedifferentieerd in twee aparte weefsels. Het is algemeen geaccepteerd dat de wederzijdse feedback tussen deze weefsels nodig is tijdens hun verdere specialisatie op het gebied van ieders unieke rol en functies in een gewricht. Daarom zijn bot en kraakbeen in een volgroeid gewricht onderling van elkaar afhankelijk en alleen in staat om de verwachte biomechanische functies uit te voeren dankzij wederzijdse ondersteuning van elkaar op het niveau van macro-structuur tot aan micro-structuur. Aanvullend, deze intieme relatie tussen bot en kraakbeen omvat meerdere routes van interactie; waarvan er vele gerelateerd zijn aan regulatie van metabolisme en remodeleringsmechanismen van deze weefsels.

Onze belangrijkste onderzoeksvragen waren: Is µCT een bruikbare techniek voor kwantitatief botonderzoek in het kaakgewricht? Is een biomechanisch model gebaseerd op µCT bruikbaar voor osteoartritis (OA) onderzoek in het kaakgewricht? Is µCT bruikbaar voor kraakbeen analyse in het kaakgewricht van een menselijk of muizen model? Door het beantwoorden van deze vragen hopen wij bij te dragen aan het vinden van nieuwe methodes en manieren om OA ontwikkeling beter te begrijpen zodat er efficiëntere behandelingen ontworpen kunnen worden. Toekomstig OA onderzoek kan zich bijvoorbeeld richten op de complexe interacties tussen verschillende weefsels in OA progressie gebruikmakend van de technieken beschreven in dit proefschrift. Meer focus op de rol van het subchondrale bot in de vroege fases van deze ziekte, lijkt van belang.

Hoofdstuk 2 beschrijft de applicatie van de conventionele µCT methode op de mandibulaire component van het menselijke kaakgewricht voor kwantitatieve metingen van bot structuur parameters (bijv. corticale en trabeculaire morfologie) en materiaal parameters (bijv. mineralisatiegraad en mate van mineraalverdeling). De dimensies van het kaakgewricht zijn uitermate geschikt voor dit soort onderzoek en daarom werd dit gewricht gekozen als basisgewricht voor het onderzoek. In onze studie werd voor het eerst de mineralisatiegraad en de mate van mineraalverdeling onderzocht in het corticale en trabeculaire bot van de menselijke kaakkop (**Hoofdstuk 2a**). De mineralisatiegraad in de kaakkop kan een weerspiegeling zijn van leeftijd en mate van remodelering van het botweefsel. Kwantificering van deze mineralisatiegraad faciliteert een beter begrip van het mogelijke effect op adaptieve remodelering van mineralisatie in

de kaakkop van een gezond en ziek gewricht. Dit heeft mogelijk consequenties voor de mechanische eigenschappen van het bot. Een conventioneel µCT systeem werd gebruikt om mineralisatiegraad te bepalen. De gemiddelde mineralisatiegraad was hoger in het corticale bot in vergelijking tot het trabeculaire bot. Er werden ook verschillen gevonden tussen de verschillende gebieden van het corticale bot. De variatie van mineralisatiegraad was significant groter in de anterieure cortex dan in de posterieure en subchondrale cortex. Dit kan duiden op een grotere mate van heterogeniteit van de mineralisatiegraad in de anterieure cortex. Binnen de cortex nam de mate van mineralisatie toe met afstand tot de corticale kanalen. Overeenkomstig, de mineralisatiegraad in het trabeculaire bot nam toe van oppervlak naar de kernen van de botbalken. Op het biomechanische niveau suggereert een verschil in mineralisatiegraad tussen trabeculair en corticaal bot, een verschil tussen de elasticiteitsmoduli (Young's moduli: mate van stijfheid en starheid van een materiaal).

In dit proefschrift hebben we hoge resolutie visualisatie van het corticale porositeit netwerk in 3D kunnen weergeven. Daarnaast hebben we kwantitatieve informatie van dit netwerk kunnen verzamelen met behulp van conventionele µCT (**Hoofdstuk 2b**). We waren in staat om de corticale porositeit te onderzoeken in relatie tot de mineralisatiegraad om zo meer informatie te verkrijgen over de belangrijkste richting van trekbelasting en drukkracht. Kwantificering van porositeit en mineralisatiegraad van botweefsel verdiept het begrip van de mogelijke effecten op adaptieve bot remodelering en de mogelijke consequenties voor mechanische eigenschappen van bot. De corticale kanalen in de subchondrale cortex van de kaakkop bleken georiënteerd in mediolaterale richting, in de anterieure en posterieure cortex was dit in superoinferieure richting. Corticale porositeit (gemiddeld 3,5 %) was niet significant verschillend tussen de verschillende corticale regio's. Er was een significante correlatie met de diameter en aantal corticale kanalen, maar niet met corticale mineralisatiegraad. In het trabeculaire bot (gemiddeld porositeit 79,3 %) was een significante negatieve correlatie aanwezig tussen oppervlakte gebied van de trabeculae en mineralisatiegraad; deze correlatie was niet evident tussen oppervlakte gebied van de corticale kanalen en de corticale mineralisatiegraad. Er was geen relatie aanwezig tussen trabeculaire en corticale porositeit of tussen trabeculaire en corticale mineralisatiegraad, dit suggereert dat adaptieve remodelering onafhankelijk is en verschillend in trabeculair en corticaal bot. Wij concludeerden dat de belangrijkste richting van trekbelasting en drukkracht voornamelijk in mediolaterale richting is in de subchondrale cortex en superoinferieur in de anterieure en posterieure cortex. Verder is de mate van remodelering groter in het trabeculaire bot in vergelijking tot het corticale bot in de kaakkop; in trabeculair bot is variatie in de mate van remodelering gerelateerd aan het beschikbare oppervlak van de botbalken.

In **Hoofdstuk 3** wordt het gebruik van µCT-gebaseerde Finite Element (FE) analyses beschreven en bediscussieerd. Deze FE analyses worden gebruikt om de invloed van intratrabeculaire mineralisatie op verschillende mechanische output parameters (bijv. elasticiteitsmodulus en intratrabeculaire patronen van trekbelasting en drukkracht) te testen in het trabeculaire bot van de menselijke kaakkop. Door dagelijkse belasting ondervindt het trabeculaire bot vervormingen (dit is, drukkracht) die leiden tot trekbelasting in het botweefsel. Wanneer trekbelasting en/of drukkracht afwijken van de normale waarden, zal het remodeleringproces leiden tot adaptatie van de botarchitectuur en mineralisatiegraad om effectief om te gaan met het veranderende krachtenspel. Van de algemene mechanische eigenschappen van botweefsel wordt gedacht dat deze afhankelijk zijn van de verdeling en de hoeveelheid mineraal. Om deze reden was het doel van onze studie in **Hoofdstuk 3a** om te onderzoeken hoe mineralisatie heterogeniteit de biomechanische eigenschappen van het trabeculaire bot in de menselijke kaakkop kan beïnvloeden. Er werden twee sets FE modellen gemaakt van trabeculaire volumes; de weefselstijfheid werd geschaald naar de lokale mineralisatiegraad zoals gemeten met het µCT systeem (heterogene model) of er werd aangenomen dat deze homogeen was (homogene model). Compressie en schuiftesten werden gesimuleerd om de algemene elasticiteitsmodulus van beide modellen te bepalen (heterogeen model versus homogeen model). Het in acht nemen van de mineralisatiegraad zorgde voor afname van de algemene elasticiteitsmodulus en schuifmodulus met maximaal 21 % in vergelijking tot het homogene model. De algemene moduli in het heterogene model waren significant gecorreleerd met hoeveelheid bot volume en mineralisatiegraad van het bot. Er werd geconcludeerd dat het niet in acht nemen van deze mineralisatie heterogeniteit kan leiden tot aanzienlijke overschatting van algemene elasticiteitsmoduli in FE modellen.

Onze kennis van de invloed van mineralisatie variaties (dit is, mineralisatie heterogeniteit) op het biomechanische gedrag van bot op het trabeculaire niveau is beperkt. Om deze reden was het doel van **Hoofdstuk 3b** om te onderzoeken hoe deze materiaaleigenschap de intratrabeculaire verdeling van rekbelasting en drukkracht in het menselijke trabeculaire bot kan beïnvloeden. De invloed van intratrabeculaire mineralisatie heterogeniteit werd geanalyseerd door vergelijking van de eerder genoemde biomechanische modellen. Er werden interessante effecten gevonden als er werd gekeken naar intratrabeculaire verdelingen van rekbelasting en drukkracht. In het homogene model werden de hoogste trekbelastingen gevonden aan het oppervlak met een significante afname naar de kern van de botbalken. Hogere oppervlakkige trekbelastingen kan betekenen dat er een hogere kans op breukrisico is van de botbalken. In het heterogene model was de verdeling anders. Een significante toename van trekbelasting met toenemende afstand van het trabeculaire oppervlak werd gevonden gevolgd door een significante afname naar de kern van de botbalken. Dit suggereert

het buigen van de botbalken tussen compressie. In beide modellen werd een afname in drukkracht voorspeld van oppervlak naar kern, dit is overeenkomstig met trabeculair buigen. Wanneer er rekening werd gehouden met de mineralisatie heterogeniteit, waren de intratrabeculaire patronen van rekbelasting en drukkracht die voorspeld werden meer overeenkomstig met het te verwachten biomechanische gedrag zoals gebaseerd op mineralisatie variaties in de botbalken. Onze gegevens geven aan dat mineralisatie heterogeniteit niet verwaarloosbaar is bij het uitvoeren van biomechanische studies op het gebied van bijvoorbeeld (lange termijn of dosis afhankelijke) effecten van anti-resorptie behandelingen.

Hoofdstuk 4 beschrijft verschillende implicaties van een hoge dosis bisfosfonaat behandeling op botweefsel parameters (bijvoorbeeld mineralisatiegraad, trabeculaire en corticale dikte) in het kniegewricht versus kaakgewricht en onderkaak versus bovenarm in een muizenmodel met behulp van µCT assessment en histologie technieken. Bisfosfonaten (BF) zijn bot-anti-resorptie middelen die traditioneel gebruikt worden op relatief grote schaal voor behandeling van metabolische botziekten en op kleinere schaal voor behandeling van kanker in bot. Onderzoek naar de effecten van BF behandeling op gezonde, in plaats van ongezonde, dieren kan meer inzicht geven in de basale mechanismen van bisfosfonaten en hun effecten op verschillende bot regio's. In **Hoofdstuk 4a** hadden we als doel om het effect van BF behandeling op het knie- en kaakgewricht van de muis te onderzoeken. Aan het begin en aan het einde van een behandeling met zolendroninezuur (ZZ) gedurende één, drie of zes maanden, werd er een bot assessment uitgevoerd met µCT en histologie. Uit onze resultaten kwam naar voren dat, in het kniegewricht een ZZ behandeling een toename gaf van mineralisatiegraad, botvolume, en dikte van botbalken maar geen invloed had op de dikte van de cortex. In zowel de controle als in de experimentele groep werd een hogere mineralisatiegraad in het trabeculaire bot gevonden vergeleken tot het corticale bot. Wat nog nooit eerder waargenomen in het kaakgewricht was, was dat ZZ behandeling in dit gewricht resulteerde in een bot regio specifieke verandering van mineralisatie; een significant tijdsafhankelijke hoger mineralisatiegraad die duidelijk aanwezig was in het subchondrale bot. MicroCT beelden laten de aanwezigheid van mineralen in dit gebied zien en met behulp van histologie konden we aantonen dat deze regio niet bestaat uit volwassen botweefsel maar uit een kraakbeenachtig weefsel. Onze data duiden op mogelijke regio-afhankelijke negatieve bijwerkingen, bijvoorbeeld op verstoring van normale kaakkop ontwikkeling onder de invloed van bisfosfonaat.

In **Hoofdstuk 4b** hebben we onderzocht of *in vivo* blootstelling aan bisfosfonaten verschillende effecten kan hebben op botafbrekende cellen (osteoclasten) in de pijpbeenderen en in de kaak. Tevens is er gekeken naar de mate van botomzet in deze

verschillende botten. Er werd gebruik gemaakt van hetzelfde dierexperiment zoals beschreven in **Hoofdstuk 4a**. De effecten op het aantal osteoclasten, bot mineralisatie en botvorming werd gemeten in pijpbeenderen en kaak. Lange termijn behandeling van ZZ zorgde voor afname van het aantal beenmergcellen in de kaak, zonder beïnvloeding van het aantal beenmergcellen in de pijpbeenderen. Zolendroninezuur behandeling zorgde niet voor afname van het aantal osteoclasten *in vivo*. Toch zorgde BF voor toename van botvolume en mineralisatiegraad in zowel pijpbeenderen als kaakbot. Na zes maanden behandeling werd een remming van botvorming waargenomen in pijpbeenderen maar niet in het kaakbot. Daarbij werd onverwachts wortelresorptie van de molaren gevonden die gemedieerd werd door actieve osteoclasten. Onze bevindingen geven meer inzicht in bot-regio-afhankelijke effecten van bisfosfonaten en in de etiologie van osteonecrose van de kaak. Wij hebben kunnen demonstreren dat bisfosfonaten de osteoclast activiteit aan de wortels van molaren kan stimuleren.

Hoofdstuk 5 beschrijft de introductie van een nieuw µCT techniek genaamd EPIC-µCT. Beide technieken kunnen *ex vivo* toegepast worden in zowel een menselijk als muizen kaakgewricht voor 3D assessment van bot en kraakbeen morfologie. Het temporomandibulaire gewricht (TMG) is vatbaar voor ontwikkeling van osteoartritis. Meer gedetailleerde kennis van het ontstaan van de ziekte is essentieel om meer inzicht te krijgen van deze ziekte in het kaakgewricht (TMG-OA). Het is van belang om een gestandaardiseerde en betrouwbare 3D methodiek te hebben waarmee we in staat zijn om detailleerde assessment van bot en kraakbeen in gezonde en zieke gewrichten te bewerkstellingen. Het doel was om de toepasbaarheid van een contrast-versterkte µCT techniek te bepalen voor gebruik in *ex vivo* onderzoek in muizen en menselijk TMG. Equilibrium Partitioning of an Ionic agent via µCT (EPIC-µCT) werd al eens eerder toegepast voor kraakbeen analyse in het kniegewricht. De methode werd *ex vivo* toegepast op het muizen TMG en aangepast voor het menselijke TMG. EPIC-µCT (30 minuten inwerkingstijd) werd toegepast op muizen kaakkoppen en 3D beelden onthulden dat gemiddelde kraakbeen diktemetingen overeenkomstig waren met histomorfometrische metingen. Voor menselijke gezonde en OA-aangedane kaakkoppen werd het protocol aangepast met een inwerkingstijd van één uur. Driedimensionale beelden onthulden een significant dikkere kraakbeenlaag in gewrichten met vroege tekenen van OA in vergelijking tot gezonde gewrichten. Daaropvolgend werd een significant dunnere kraakbeenlaag gevonden in menselijke kaakkoppen met late tekenen van OA. De EPIC-µCT techniek bleek effectief voor de *ex vivo* analyse van 3D kraakbeen morfologie in kaakkoppen van muis en mens en kan bijdragen aan bot-kraakbeen interactie onderzoek in TMG-OA.

In dit proefschrift werden conventionele en contrast-versterkte µCT technieken *ex*

vivo toegepast op het complete menselijke kaakgewricht. De combinatie van beide bekrachtigende beeldvormende technieken is veelbelovend om een meer fundamenteel onderbouwd begrip te vormen van gezonde en osteoartritis aangedane gewrichten omdat het de visualisatie van zowel bot als kraakbeen toelaat. De combinatie van beide methodes kan in de toekomst ook zorgen voor meer mogelijkheden om het kraakbeen-bot complex als geheel te bestuderen. De mechanische interactie tussen beide onderdelen van het gewricht en het dynamische krachtenspel van een gewricht tijdens dagelijkse functie dan wel langdurig overbelasting kunnen centrale onderwerpen zijn. De dimensie van het gewricht tijdens alle stadia van ontwikkeling, stellen ons in staat om de fijne architectuur van zowel subchondraal als trabeculair bot te onderzoeken met behulp van µCT technieken zonder verstoring van de volledige integriteit van het gewricht. Een doel van deze benadering is om te achterhalen/voorspellen hoe veranderingen van het subchondrale en trabeculaire bot (ten gevolge van overbelasting) in het gewricht leiden tot abnormale botstructuur veranderingen, zoals in osteoarthritis. Een tweede doel kan zijn om te voorspellen hoe veranderingen in belasting van het articulaire kraakbeen gerelateerd zijn aan de vereiste veranderingen om het kraakbeen te onderhouden.

Met µCT-gebaseerde biomechanische computermodellen, die wij kunnen maken, is het mogelijk om de biomechanische interactie tussen bot en kraakbeen te voorspellen en te kijken naar de gevolgen van deze interactie in gezonde en osteoartritis aangedane gewrichten. Aanvullend kan een dierexperiment worden gebruikt om experimenteel geïnduceerde botveranderingen te onderzoeken door de invloed van specifieke botveranderingen op het kraakbeen in zowel knie- als kaakgewricht te bepalen. De combinatie van beide µCT technieken in een dierexperiment kan ervoor zorgen dat we onderzoek kunnen doen naar de invloed van specifieke botveranderingen op het kraakbeen *ex vivo*. Onze data kunnen gebruikt worden om de volgende hypothese te testen: Botveranderingen gaan vooraf aan kraakbeenveranderingen en/of –schade in de ontwikkeling van osteoartritis. Met de resultaten van dit proefschrift hopen wij bij te dragen aan de implementatie van nieuwe methodes en manieren om meer te begrijpen van de ontwikkeling van osteoartritis, en het ontwerpen van effectievere behandelingen.

De resultaten beschreven in dit proefschrift leiden tot de volgende algemene conclusies:

- De mate van het dagelijkse krachtenspel in botweefsel beïnvloedt de variaties van mineralisatiegraad en corticale porositeit, daarom kan remodelering een behulpzaam gereedschap zijn voor botweefsel om adaptaties te ondergaan passend bij dit krachtenspel.
- Een meer specifieke input voor een biomechanisch model zal leiden tot een meer specifieke output en uitkomst van dit model. Afhankelijk van de gekozen onderzoeksvraag dient er een keuze te worden gemaakt welke variabele gekozen wordt.
- Reacties op hoge-dosis bisfosfonaat behandeling zijn bot-regio-afhankelijk (kaakbot versus pijpbeenderen) en kunnen verder een mogelijk en onbekend schadelijk effect hebben op het kaakbot.
- De EPIC-µCT techniek is effectief voor *ex vivo* 3D analyse van bot en kraakbeen morfologie in kaakgewricht van muis en mens en is mogelijk bruikbaar voor bot-kraakbeen-interactie onderzoek in kaakgewricht osteoartritis.

REFERENCES

Vorace

1. Radin, E.L. and R.M. Rose, *Role of subchondral bone in the initiation and progression of cartilage damage.* Clinical Orthopaedics and Related Research, 1986. **213**: p. 34-40.
2. Day, J.S., et al., *Adaptation of subchondral bone in osteoarthritis.* Biorheology, 2004. **41**: p. 359-368.
3. Turner, C.H., *Three rules of bone adaptation to mechanical stimuli.* Bone, 1998. **23**(5): p. 399-407.
4. Ruimerman, R., et al., *A theoretical framework for strain-related trabecular bone maintenance and adaptation.* J Biomech, 2005. **38**(4): p. 931-41.
5. Woolf, A.D. and B. Pfleger, *Burden of major musculoskeletal conditions.* Bull World Health Organ, 2003. **81**(9): p. 646-56.
6. Poos, M.J.J.C., et al., *Kosten van ziekten in Nederland 2005. RIVM-rapport nr. 270751019.* Bilthoven: RIVM, 2008.
7. Imhof, H., et al., *Importance of subchondral bone to articular cartilage in health and disease.* Topics in Magnetic Resonance Imaging, 1999. **10**(3): p. 180-192.
8. Imhof, H., et al., *Subchondral bone and cartilage disease: a rediscovered functional unit.* Investigative Radiology, 2000. **35**(10): p. 581-588.
9. Lajeunesse, D. and P. Reboul, *Subchondral bone in osteoarthritis: A biological link with articular cartilage leading to abnormal remodeling.* Current Opinion in Rheumatology, 2003. **15**: p. 628-633.
10. Burr, D.B. and M.B. Schaffler, *The involvement of subchondral mineralized tissues in osteoarthrosis: quantitative microscopic evidence.* Microscopy research and technique, 1997. **37**: p. 343-357.
11. Dar, F.H. and R.M. Aspden, *A finite element model of an idealized diarthrodial joint to investigate the effects of variation in the mechanical properties of the tissues.* Proc Inst Mechn Eng, 2003. **217**: p. 341-348.
12. Carter, D.R., et al., *Mechanobiology of skeletal regeneration.* Clin Orthop Relat Res, 1998(355 Suppl): p. S41-55.
13. Hasler, E.M., et al., *Articular cartilage biomechanics: theoretical models, material properties, and biosynthetic response.* Crit Rev Biomed Eng, 1999. **27**(6): p. 415-88.
14. Radon, J. and P.C. Parks, *On the determination of functions from their integral values along certain manifolds.* IEEE Trans Med Imaging, 1986. **5**(4): p. 170-176.
15. Cormack, A.M., *Representation of a Function by Its Line Integrals, with Some Radiological Applications.* J Appl Physics, 1963. **34**: p. 2722-2727.
16. Cormack, A.M., *Representation of a Function by Its Line Integrals, with Some Radiological Applications. II.* J Appl Physics, 1964. **35**: p. 2908-2913.
17. Hounsfield, G.N., *Computerized transverse axial scanning (tomography). 1. Description of system.* Br J Radiol, 1973. **46**(552): p. 1016-22.

18. Feldkamp, L.A., et al., *The direct examination of three-dimensional bone architecture in vitro by computed tomography.* J Bone Miner Res, 1989. **4**(1): p. 3-11.
19. Ruegsegger, P., B. Koller, and R. Muller, *A microtomographic system for the nondestructive evaluation of bone architecture.* Calcified Tissue International, 1996. **58**: p. 24-29.
20. Kuhn, J.L., et al., *Evaluation of a microcomputed tomography system to study trabecular bone structure.* J Orthop Res, 1990. **8**(6): p. 833-42.
21. Laib, A., et al., *3D micro-computed tomography of trabecular and cortical bone architecture with application to a rat model of immobilisation osteoporosis.* Medical and Biological Engineering and Computing, 2000. **38**: p. 326-332.
22. Wachsmuth, L. and K. Engelke, *High-resolution imaging of osteoarthritis using microcomputed tomography.* Methods Mol Med, 2004. **101**: p. 231-48.
23. Zhang, J., et al., *Occlusal Effects on Longitudinal Bone Alterations of the Temporomandibular Joint.* J Dent Res, 2013.
24. Chen, J., et al., *Analysis of microarchitectural changes in a mouse temporomandibular joint osteoarthritis model.* Archives of Oral Biology, 2009. **54**(12): p. 1091-1098.
25. Chen, J., et al., *Altered functional loading causes differential effects in the subchondral bone and condylar cartilage in the temporomandibular joint from young mice.* Osteoarthritis Cartilage, 2009. **17**(3): p. 354-61.
26. Sobue, T., et al., *Murine TMJ loading causes increased proliferation and chondrocyte maturation.* J Dent Res, 2011. **90**(4): p. 512-6.
27. Wadhwa, S., et al., *Mice deficient in biglycan and fibromodulin as a model for temporomandibular joint osteoarthritis.* Cells Tissues Organs, 2005. **181**(3-4): p. 136-143.
28. Wadhwa, S., et al., *Accelerated osteoarthritis in the temporomandibular joint of biglycan/fibromodulin double-deficient mice.* Osteoarthritis Cartilage, 2005. **13**(9): p. 817-27.
29. Burstein, D., et al., *Protocol issues for delayed Gd(DTPA)(2-)-enhanced MRI (dGEMRIC) for clinical evaluation of articular cartilage*. 2001. p. 36-41.
30. Kurkijarvi, J.E., et al., *Evaluation of cartilage repair in the distal femur after autologous chondrocyte transplantation using T2 relaxation time and dGEMRIC.* Osteoarthritis Cartilage, 2007. **15**(4): p. 372-8.
31. Trattnig, S., et al., *Three-dimensional delayed gadolinium-enhanced MRI of cartilage (dGEMRIC) for in vivo evaluation of reparative cartilage after matrix-associated autologous chondrocyte transplantation at 3.0T: Preliminary results.* J Magn Reson Imaging, 2007. **26**(4): p. 974-82.
32. Goebel, J.C., et al., *New trends in MRI of cartilage: Advances and limitations in small animal studies.* Biomed Mater Eng, 2010. **20**(3): p. 189-94.

33. Widmalm, S.E., et al., *Limitation of the diagnostic value of MR images for diagnosing temporomandibular joint disorders.* Dentomaxillofacial Radiology, 2006. **35**: p. 334-338.
34. Obermann, W.R. and G.J. Kieft, *Knee arthrography: a comparison of iohexol, ioxaglate sodium meglumine, and metrizoate.* Radiology, 1987. **162**: p. 729-733.
35. Meijenhorst, G.C.H. and J.N.T.D. Bruin, *Hexabrix (Ioxaglate), a New Low Osmolality Contrast Agent for Lumbar Epidural Double-Catheter Venography.* Neuroradiology, 1980. **20**(1): p. 29-32.
36. Palmer, A.W., R.E. Guldberg, and M.E. Levenston, *Analysis of cartilage matrix fixed charge density and three-dimensional morphology via contrast-enhanced microcomputed tomography.* PNAS, 2006. **103**(51): p. 19255-19260.
37. Xie, L., et al., *Quantitative assessment of articular cartilage morphology via EPIC-microCT.* Osteoarthritis.Cartilage., 2009. **17**(3): p. 313-320.
38. Xie, L., et al., *Nondestructive assessment of sGAG content and distribution in normal and degraded rat articular cartilage via EPIC-microCT.* Osteoarthritis Cartilage, 2010. **18**(1): p. 65-72.
39. Kotwal, N., et al., *Initial Application of EPIC-uCT to Assess Mouse Articular Cartilage Morphology and Composition: Effects of Aging and Treadmill Running.* Osteoarthritis. Cartilage., 2012.
40. Stok, K.S., et al., *Revealing the interplay of bone and cartilage in osteoarthritis through multimodal imaging of murine joints.* Bone, 2009.
41. Xie, L., et al., *Quantitative imaging of cartilage and bone morphology, reactive oxygen species, and vascularization in a rodent model of osteoarthritis.* Arthritis Rheum., 2012. **64**(6): p. 1899-1908.
42. Piscaer, T.M., et al., *Imaging of experimental osteoarthritis in small animal models.* Biorheology, 2008. **45**(3-4): p. 355-364.
43. Piscaer, T.M., et al., *In vivo imaging of cartilage degeneration using microCT-arthrography.* Osteoarthritis.Cartilage., 2008. **16**(9): p. 1011-1017.
44. Siebelt, M., et al., *Clinically applied CT arthrography to measure the sulphated glycosaminoglycan content of cartilage.* Osteoarthritis.Cartilage., 2011. **19**(10): p. 1183-1189.
45. Thote, T., et al., *Localized 3D Analysis of Cartilage Composition and Morphology in Small Animal Models of Joint Degeneration.* Osteoarthritis Cartilage, 2013.
46. Willett, N.J., et al., *Intra-articular injection of micronized dehydrated human amnion/chorion membrane attenuates osteoarthritis development.* Arthritis Res Ther, 2014. **16**(1): p. R47.
47. Lau, S.F., et al., *Assessment of articular cartilage and subchondral bone using EPIC-microCT in Labrador retrievers with incipient medial coronoid disease.* Vet J, 2013.

198(1): p. 116-21.
48. Kok, A.C., et al., *No effect of hole geometry in microfracture for talar osteochondral defects.* Clin Orthop Relat Res, 2013. **471**(11): p. 3653-62.
49. Huiskes, R. and E.Y.S. Chao, *A survey of finite element analysis in orthopedic biomechanics: the first decade.* Journal of Biomechanics, 1983. **16**(6): p. 385-409.
50. Van Rietbergen, B., et al., *A new method to determine trabecular bone elastic properties and loading using micromechanical finite-element models.* Journal of Biomechanics, 1995. **28**(1): p. 69-81.
51. Korioth, T.W.P. and A. Versluis, *Modeling the mechanical behavior of the jaws and their related structures by finite element (FE) analysis.* Crit Rev Oral Biol Med, 1997. **8**(1): p. 90-104.
52. van Eijden, T.M., *Biomechanics of the mandible.* Crit Rev.Oral Biol.Med., 2000. **11**(1): p. 123-136.
53. van Ruijven, L.J., L. Mulder, and T.M. van Eijden, *Variations in mineralization affect the stress and strain distributions in cortical and trabecular bone.* J.Biomech., 2007. **40**(6): p. 1211-1218.
54. Cioffi, I., et al., *Regional variations in mineralization and strain distributions in the cortex of the human mandibular condyle.* Bone, 2007. **41**(6): p. 1051-1058.
55. Koolstra, J.H. and T.M. van Eijden, *Combined finite-element and rigid-body analysis of human jaw joint dynamics.* J.Biomech., 2005. **38**(12): p. 2431-2439.
56. Tanaka, M., et al., *Region-specific bone mass changes in rat mandibular condyle following ovariectomy.* J Dent Res, 2000. **79**(11): p. 1907-13.
57. Van Rietbergen, B., et al., *Trabecular bone tissue strains in the healthy and osteoporotic human femur.* J Bone Miner Res, 2003. **18**(10): p. 1781-8.
58. Fleisch, H., *Development of bisphosphonates.* Breast Cancer Res, 2002. **4**(1): p. 30-4.
59. Qvist, P., et al., *The disease modifying osteoarthritis drug (DMOAD): Is it in the horizon?* Pharmacol Res, 2008. **58**(1): p. 1-7.
60. Shapiro, H.H., *The anatomy of the temporomandibular joint. Structural relations and therapy.* Oral Surg Oral Med Oral Pathol, 1950. **3**(12): p. 1521-39.
61. Alomar, X., et al., *Anatomy of the temporomandibular joint.* Seminars in Ultrasound CT and MRI, 2007. **28**: p. 170-183.
62. Carter, D.R. and D.M. Spengler, *Mechanical properties and composition of cortical bone.* Clinical Orthopaedics and Related Research, 1978. **135**: p. 192-217.
63. Beek, M., et al., *Three-dimensional finite element analysis of the cartilaginous structures in the human temporomandibular joint*. 2001. p. 1913-1918.
64. Zarb, G.A. and G.E. Carlsson, *Temporomandibular disorders: osteoarthritis.* J Orofac Pain, 1999. **13**(4): p. 295-306.
65. Tanaka, E. and J.H. Koolstra, *Biomechanics of the temporomandibular joint.* J Dent

Res, 2008. **87**(11): p. 989-91.
66. Ericson, S. and M. Lundberg, *Structural changes in the finger, wrist and temporomandiblar joints. A comparative radiologic study.* Acta Odontol Scand, 1968. **26**(2): p. 111-26.
67. Axelsson, S., *Human and experimental osteoarthrosis of the temporomandibular joint. Morphological and biochemical studies.* Swed Dent J Suppl, 1993. **92**: p. 1-45.
68. Ong, T.K. and C.D. Franklin, *A clinical and histopathological study of osteoarthrosis of the temporomandibular joint.* British Journal of Oral & Maxillofacial Surgery, 1996. **34**(2): p. 186-192.
69. Currey, J.D., *The effect of porosity and mineral content on the Young's modulus of elasticity of compact bone.* Journal of Biomechanics, 1988. **21**(2): p. 131-139.
70. Meunier, P.J. and G. Boivin, *Bone mineral density reflects bone mass but also the degree of mineralization of bone: therapeutic implications.* Bone, 1997. **21**(5): p. 373-377.
71. Grynpas, M.D., *Age and disease-related changes in the mineral of bone.* Calcified Tissue International, 1993. **53**: p. S57-S64.
72. Reid, S.A. and A. Boyde, *Changes in the mineral density distribution in human bone with age: image analysis using backscattered electrons in the SEM.* Journal of Bone and Mineral Research, 1987. **2**(1): p. 13-22.
73. Gong, J.K., J.S. Arnold, and S.H. Cohn, *Composition fo trabecular and cortical bone.* The Anatomical Record, 1964. **149**: p. 325-332.
74. Hodgskinson, R., J.D. Currey, and G.P. Evans, *Hardness, an indicator of the mechanical competence of cancellous bone.* Journal of Orthopaedic Research, 1989. **7**(5): p. 754-758.
75. Mulder, L., et al., *Architecture and mineralization of developing cortical and trabecular bone of the mandible.* Anat.Embryol.(Berl), 2006. **211**(1): p. 71-78.
76. Loveridge, N., et al., *Bone mineralization density and femoral neck fragility.* Bone, 2004. **35**: p. 929-941.
77. Riggs, C.M., et al., *Mechanical implications of collagen fibre orientation in cortical bone of the equine radius.* Anat Embryol (Berl), 1993. **187**(3): p. 239-48.
78. Skedros, J.G., et al., *Analysis of a tension/compression skeletal system: possible strain-specific differences in the hierarchical organization of bone.* Anat Rec, 1994. **239**(4): p. 396-404.
79. Ciarelli, T.E., D.P. Fyhrie, and A.M. Parfitt, *Effects of vertebral bone fragility and bone formation rate on the mineralization levels of cancellous bone from white females.* Bone, 2003. **32**: p. 311-315.
80. Mulder, L., et al., *Architecture and mineralization of developing trabecular bone in the pig mandibular condyle.* Anat.Rec.A Discov.Mol.Cell Evol.Biol., 2005. **285**(1): p.

659-666.
81. Paschalis, E.P., et al., *FTIR microspectroscopic analysis of normal human cortical and trabecular bone.* Calcified Tissue International, 1997. **61**: p. 480-486.
82. Roschger, P., et al., *Bone mineralization density distribution in health and disease.* Bone, 2008. **42**(3): p. 456-66.
83. Paschalis, E.P., et al., *FTIR microspectroscopic analysis of human osteonal bone.* Calcified Tissue International, 1996. **59**: p. 480-487.
84. Mulder, L., J.H. Koolstra, and T.M. van Eijden, *Accuracy of microCT in the quantitative determination of the degree and distribution of mineralization in developing bone.* Acta Radiologica, 2004. **45**(7): p. 769-777.
85. Nuzzo, S., et al., *Quantification of the degree of mineralization of bone in three dimensions using synchrotron radiation microtomography.* Med Phys, 2002. **29**(11): p. 2672-81.
86. Boivin, G. and P.J. Meunier, *The degree of mineralization of bone tissue measured by computerized quantitative contact microradiography.* Calcified Tissue International, 2002. **70**(503): p. 511.
87. van Ruijven, L.J., et al., *Prediction of mechanical properties of the cancellous bone of the mandibular condyle.* J.Dent.Res., 2003. **82**(10): p. 819-823.
88. van Eijden, T.M., et al., *Structural and mechanical properties of mandibular condylar bone.* J.Dent.Res., 2006. **85**(1): p. 33-37.
89. van Eijden, T.M., L.J. van Ruijven, and E.B. Giesen, *Bone tissue stiffness in the mandibular condyle is dependent on the direction and density of the cancellous structure.* Calcif.Tissue Int., 2004. **75**(6): p. 502-508.
90. van Ruijven, L.J., et al., *The effect of bone loss on rod-like and plate-like trabeculae in the cancellous bone of the mandibular condyle.* Bone, 2005. **36**(6): p. 1078-1085.
91. Mulder, L., J.H. Koolstra, and T. Van Eijden, *Accuracy of microCT in the quantitative determination of the degree of distribution of mineralization in developing bone.* ACTA Radiologica, 2004. **45**: p. 769-777.
92. Yamauchi, M., T. Sugimoto, and K. Chihara, *Determinants of vertebral fragility: the participation of cortical bone factors.* Journal of Bone Mineral Metabolism, 2004. **22**: p. 79-85.
93. Bord, S., et al., *The effects of estrogen on osteoprotegerin, RANKL, and estrogen receptor expression in human osteoblasts.* Bone, 2003. **32**(2): p. 136-41.
94. Follet, H., et al., *The degree of mineralization is a determinant of bone strength: a study on human calcanei.* Bone, 2004. **34**: p. 783-789.
95. Kingsmill, V.J. and A. Boyde, *Mineralization density and apparent density of bone in cranial and postcranial sites in the aging human.* Osteoporos Int, 1999. **9**(3): p. 260-8.

96. Zysset, P.K., et al., *Elastic modulus and hardness of cortical and trabecular bone lamellae measured by nanoindentation in the human femur.* Journal of Biomechanics, 1999. **32**: p. 1005-1012.
97. Rho, J.Y., T.Y. Tsui, and G.M. Pharr, *Elastic properties of human cortical and trabecular lamellar bone measured by nanoindentation.* Biomaterials, 1997. **18**: p. 1325-1330.
98. Roschger, P., et al., *Validation of quantitative backscattered electron imaging for the measurement of mineral density distribution in human bone biopsies.* Bone, 1998. **23**(4): p. 319-326.
99. Crofts, R.D., T.M. Boyce, and R.D. Bloebaum, *Aging changes in osteon mineralization in the human femoral neck.* Bone, 1994. **15**(2): p. 147-152.
100. Sissons, H.A., *The microradiographic appearance of normal bone tissue at various ages. .* X-ray Microscopy and X-ray Microanalysis. Elsevier, Amsterdam 1960: p. 199-205.
101. Hoffler, C.E., et al., *Heterogeneity of bone lamellar-level elastic moduli.* Bone, 2000. **26**(6): p. 603-609.
102. Rho, J.Y., et al., *Variations in the individual thick lamellar properties within osteons by nanoindentation.* Bone, 1999. **25**(3): p. 295-300.
103. Borah, B., et al., *Three-dimensional microimaging (MRmicroI and microCT), finite element modeling, and rapid prototyping provide unique insights into bone architecture in osteoporosis.* The Anatomical Record, 2001. **265**: p. 101-110.
104. Carter, D.R. and W.C. Hayes, *The compressive behavior of bone as a two-phase porous structure.* J Bone Joint Surg Am, 1977. **59**(7): p. 954-62.
105. Giesen, E.B., et al., *Changed morphology and mechanical properties of cancellous bone in the mandibular condyles of edentate people.* J.Dent.Res., 2004. **83**(3): p. 255-259.
106. Jordan, G.R., et al., *Spatial clustering of remodeling osteons in the femoral neck cortex: a cause of weakness in hip fracture?* Bone, 2000. **26**(3): p. 305-313.
107. McCalden, R.W., et al., *Age-related changes in the tensile properties of cortical bone.* The Journal of Bone and Joint Surgery, 1993. **75A**(8): p. 1193-1205.
108. Schaffler, M.B. and D.B. Burr, *Stiffness of compact bone: effects of porosity and density.* J Biomech, 1988. **21**(1): p. 13-6.
109. Bell, K.L., et al., *Regional differences in cortical porosity in the fractured femoral neck.* Bone, 1999. **24**(1): p. 57-64.
110. Giesen, E.B. and T.M. van Eijden, *The three-dimensional cancellous bone architecture of the human mandibular condyle.* J.Dent.Res., 2000. **79**(4): p. 957-963.
111. Skedros, J.g., S.C. Su, and R.D. Bloebaum, *Biomechanical implications of mineral content and microstructural variations in cortical bone of horse, elk, and sheep calcanei.* The Anatomical Record, 1997. **249**: p. 297-316.

112. Thomas, C.D., S.A. Feik, and J.G. Clement, *Regional variation of intracortical porosity in the midshaft of the human femur: age and sex differences.* J Anat, 2005. **206**(2): p. 115-25.
113. Hert, J., P. Fiala, and M. Petrtyl, *Osteon orientation of the diaphysis of the long bones in man.* Bone, 1994. **15**(3): p. 269-277.
114. Lai, Y.M., et al., *Regional differences in cortical bone mineral density in the weigth-bearing long bone shaft - a pQCT study.* Bone, 2005. **36**: p. 465-471.
115. Renders, G.A., et al., *Degree and distribution of mineralization in the human mandibular condyle.* Calcif.Tissue Int., 2006. **79**(3): p. 190-196.
116. Beaupre, G.S., T.E. Orr, and D.R. Carter, *An approach for time-dependent bone modeling and remodeling-application: a preliminary remodeling simulation.* J Orthop Res, 1990. **8**(5): p. 662-70.
117. Bousson, V., et al., *CT of the middiaphyseal femur: cortical bone mineral density and relation to porosity.* Radiology, 2000. **217**: p. 179-187.
118. Wachter, N.J., et al., *Correlation of bone mineral density with strength and microstructural parameters of cortical bone in vitro.* Bone, 2002. **31**(1): p. 90-95.
119. Van Eijden, T., et al., *Structural and mechanical properties of mandibular condylar bone.* Journal of Dental Research, 2006. **85**(1): p. 33-37.
120. Cooper, D.M.L., et al., *Quantitative 3D analysis of the canal network in cortical bone by micro-computed tomography.* The Anatomical Record Part B, 2003. **274B**: p. 169-179.
121. Harrigan, T.P. and R.W. Mann, *Characterization of micro-structural anisotrophy in orthotropic materials using a second rank tensor.* J Mater Sci, 1984. **19**: p. 761-767.
122. Bousson, V., et al., *Cortical bone in the human femoral neck: Three-dimensional appearance and porosity using synchontron radiation.* Journal of Bone Mineral Research, 2004. **19**(5): p. 794-801.
123. Martin-Badosa, E., et al., *A method for the automatic characterization of bone architecture in 3D mice microtomographic images.* Comput Med Imaging Graph, 2003. **27**(6): p. 447-58.
124. Matsumoto, T., et al., *Monochromatic synchrotron radiation muCT reveals disuse-mediated canal network rarefaction in cortical bone of growing rat tibiae.* J Appl Physiol, 2006. **100**(1): p. 274-80.
125. Cohen, J. and W.H. Harris, *The three-dimensional anatomy of haversian systems.* J Bone Joint Surg Am, 1958. **40-A**(2): p. 419-34.
126. Petrtyl, M., J. Hert, and P. Fiala, *Spatial organization of the haversian bone in man.* Journal of Biomechanics, 1996. **29**(2): p. 161-169.
127. Hara, T., et al., *Mechanical properties of buccal compact bone of the mandibular ramus in human adults and children: relationship of the elastic modulus to the*

direction of the osteon and the porosity ratio. Bulletin Tokyo Dental College, 1998. **39**(1): p. 47-55.
128. Verna, C., B. Melsen, and F. Melsen, *Differences in static cortical bone remodeling parameters in human mandible and iliac crest.* Bone, 1999. **25**(5): p. 577-583.
129. Stein, M.S., et al., *An automated analysis of intracortical porosity in human femoral bone across age.* J Bone Miner Res, 1999. **14**(4): p. 624-32.
130. Dempster, W.T. and D.H. Enlow, *Patterns of vascular channels in the cortex of the human mandible.* The Anatomical Record, 1959. **135**: p. 189-205.
131. Bousson, V., et al., *Distribution of intracortical porosity in human midfemoral cortex by age and gender.* Journal of Bone and Mineral Research, 2001. **16**(7): p. 1308-1317.
132. Feik, S.A., C.D.L. Thomas, and J.G. Clement, *Age-related changes in cortical porosity of the midshaft of the human femur.* Journal of Anatomy, 1997. **191**: p. 407-416.
133. Seeman, E., *Pathogenesis of bone fragility in women and men.* The Lancet, 2002. **359**: p. 1841-1850.
134. Currey, J.D., *What determines the bending strength of compact bone.* The Journal of Experimental Biology, 1999. **202**: p. 2495-2503.
135. Cooper, D.M.L., et al., *Comparison of microcomputed tomographic and microradiographic measurements of cortical bone porosity.* Calcified Tissue International, 2004. **74**: p. 437-447.
136. Wachter, N.J., et al., *Prediction of strength of cortical bone in vitro by microcomputed tomography.* Clinical Biomechanics, 2001. **16**: p. 252-256.
137. Currey, J.D., *The many adaptations of bone.* Journal of Biomechanics, 2003. **36**: p. 1487-1495.
138. Van Eijden, T.M.G.J., *Biomechanics of the mandible.* Critical Reviews in Oral Biology and Medicine, 2000. **11**(1): p. 123-136.
139. Frost, H.M., *Wolff's Law and bone's structural adaptations to mechanical usage: an overview for clinicians.* Angle Orthod, 1994. **64**(3): p. 175-88.
140. Wolff, J., *Das Gesetz der Transformation der Knochen. (Translated as: The law of bone remodeling).* Maquet P, Furlong R. Berlin, 1892. **Springer Verlag 1986**.
141. Roux, W., *Der zu¨chtende Kampf der Teile, oder die "Teilauslee" im Organismus (Theorie der "funktionellen Anpassung").* Leipzig: Wilhelm Engelmann., 1881.
142. Mulder, L., et al., *Relationship between tissue stiffness and degree of mineralization of developing trabecular bone.* Journal of Biomedical Materials Research, 2008. **84**(2): p. 508-515.
143. Currey, J.D., *Effects of differences in mineralization on the mechanical properties of bone.* Philosophical Transactions of the Royal Society of London, Series B: Biological Sciences, 1984. **304**(1121): p. 509-518.

144. Kopperdahl, D.L. and T.M. Keaveny, *Yield strain behavior of trabecular bone.* Journal of Biomechanics, 1998. **31**: p. 601-608.
145. Mulder, L., et al., *Biomechanical consequences of developmental changes in trabecular architecture and mineralization of the pig mandibular condyle.* J.Biomech., 2007. **40**(7): p. 1575-1582.
146. Van der Linden, J.C., et al., *Trabecular bone's mechanical properties are affected by its non-uniform mineral distribution.* Journal of Biomechanics, 2001. **34**: p. 1573-1580.
147. Ulrich, D., et al., *The abiltity of three-dimensional structural indices to reflect mechanical aspects of trabecular bone.* Bone, 1995. **25**(1): p. 55-60.
148. Van Rietbergen, B., *Micro-FE analyses of bone: State of the art.* Advanced Experimental Medical Biology, 2001. **496**: p. 21-30.
149. Muller, M., et al., *Prediction of bone mechanical properties using QUS and pQCT: Study of the human distal radius.* Medical engineering and Physics, 2007. **in press**.
150. van Ruijven, L.J., E.B. Giesen, and T.M. van Eijden, *Mechanical significance of the trabecular microstructure of the human mandibular condyle.* J.Dent.Res., 2002. **81**(10): p. 706-710.
151. Bourne, B.C. and M.C.H. Van der Meulen, *Finite element models predict cancellous apparent modulus when tissue modulus is scaled from specimen CT-attenuation.* Journal of Biomechanics, 2004. **37**: p. 613-621.
152. Renders, G.A., et al., *Porosity of human mandibular condylar bone.* J.Anat., 2007. **210**(3): p. 239-248.
153. Ding, M., A. Odgaard, and I. Hvid, *Accuracy of cancellous bone volume fraction measured by micro-CT scanning.* Journal of Biomechanics, 1999. **32**: p. 323-326.
154. Hollister, S.J., J.M. Brennan, and N. Kikuchi, *A homogenization sampling procedure from calculating trabecular bone effective stiffness and tissue level stress.* Journal of Biomechanics, 1994. **27**(4): p. 433-444.
155. Van Rietbergen, B., et al., *Direct mechanics assessment of elastic symmetries and properties of trabecular bone architecture.* Journal of Biomechanics, 1996. **29**(12): p. 1653-1657.
156. Yeh, O.C. and T.M. Keaveny, *Biomechanical effects of intraspecimen variations in trabecular architecture: a three-dimensional finite element study.* Bone, 1999. **25**(2): p. 223-228.
157. Jaasma, M.J., et al., *Biomechanical effects of intraspecimen variations in tissue modulus for trabecular bone.* Journal of Biomechanics, 2002. **35**: p. 237-246.
158. Chevalier, Y., et al., *Validation of a voxel-based FE method for prediction of the uniaxial apparent modulus of human trabecular bone using macroscopic mechanical tests and nanoindentation.* Journal of Biomechanics, 2007. **40**: p. 3333-3340.
159. Liu, X.S., et al., *Quantification of the roles of trabecular microarchitecture and*

trabecular type in determining the elastic modulus of human trabecular bone. Journal of Bone and Mineral Research, 2006. **21**(10): p. 1608-1617.
160. Martin, R.B., *The importance of mechanical loading in bone biology and medicine.* Journal of Musculoskeletal Neuronal Interaction, 2007. **7**(1): p. 48-53.
161. Rubin, C.T. and L.E. Lanyon, *Regulation of bone mass by mechanical strain magnitude.* Calcified Tissue International, 1985. **37**: p. 411-417.
162. Turner, C.H. and F.M. Pavalko, *Mechanotransduction and functional response of the skeleton to physical stress: the mechanisms and mechanics of bone adaptation.* Journal of Orthopaedic Science, 1998. **3**: p. 346-355.
163. Zioupos, P. and J.D. Currey, *Comments on 'On the relationship between the microstructure of bone and its mechanical stiffness'.* J Biomech, 1994. **27**(7): p. 993-5.
164. Kosmopoulos, V., C. Schizas, and T.S. Keller, *Modeling the onset and propagation of trabecular bone microdamage during low-cycle fatigue.* Journal of Biomechanics, 2008. **41**: p. 515-522.
165. Martin, R.B., *Fatigue microdamage as an essential element on bone mechanics and biology.* Calcified Tissue International, 2003. **73**: p. 101-107.
166. Choi, K. and S.A. Goldstein, *A comparison of the fatigue behavior of human trabecular and cortical bone tissue.* Journal of Biomechanics, 1992. **25**(12): p. 1371-1381.
167. Lee, T.C., A. Staines, and D. Taylor, *Bone adaptation to load: microdamage as a stimulus for bone remodelling.* Journal of Anatomy, 2002. **201**: p. 437-446.
168. Mullender, M., et al., *Effect of mechanical set point of bone cells on mechanical control of trabecular bone architecture.* Bone, 1998. **22**(2): p. 125-131.
169. Turner, C.H., I. Owan, and Y. Takano, *Mechanotransduction in bone: role of strain rate.* American Journal of Physiology, 1995. **269**: p. 438-442.
170. Van der Meulen, M.C.H., et al., *Cancellous bone adaptation to in vivo loading in a rabbit model.* Bone, 2006. **38**(6): p. 871-877.
171. Ruffoni, D., et al., *The bone mineralization density distribution as a fingerprint of the mineralization process.* Bone, 2007. **40**: p. 1308-1319.
172. Batiste, D.L., et al., *Ex vivo characterization of articular cartilage and bone lesions in a rabbit ACL transection model of osteoarthritis using MRI and micro-CT.* Osteoarthritis and Cartilage, 2004. **12**: p. 986-996.
173. Botter, S.M., et al., *Quantification of subchondral bone changes in a murine osteoarthritis model using micro-CT.* Biorheology, 2006. **43**: p. 379-388.
174. Burr, D.B., *Anatomy and physiology of the mineralized tissues: Role in the pathogenesis of osteoarthrosis.* Osteoarthritis and Cartilage, 2004. **12**: p. S20-S30.
175. Renders, G.A., et al., *Biomechanical effect of mineral heterogeneity in trabecular bone.* J.Biomech., 2008. **41**(13): p. 2793-2798.
176. Boyde, A., J.C. Elliot, and S.J. Jones, *Stereology and histogram analysis of backscattered*

electron images: age changes in bone. Bone, 1993. **14**: p. 205-210.
177. Roschger, P., et al., *Constant mineralization density distribution in cancellous human bone.* Bone, 2003. **32**: p. 316-323.
178. Nuzzo, S., et al., *Synchrotron radiation microtomography allows the analysis of three-dimensional microarchitecture and degree of mineralization of human iliac crest biopsy specimens: effects of etidronate treatment.* Journal of Bone and Mineral Research, 2002. **17**(8): p. 1372-1382.
179. Roschger, P., et al., *Alendronate increases degree and uniformity of mineralization in cancellous bone and decreases the porosity in cortical bone of osteoporotic women.* Bone, 2001. **29**(2): p. 185-191.
180. Roschger, P., et al., *Bone mineralization density distribution in health and disease.* Bone, 2006. **42**(3): p. 456-466.
181. Roy, M.E., et al., *Mechanical and morphological variation of the human lumbar vertebral cortical and trabecular bone.* Journal of Biomedical Materials Research, 1999. **44**: p. 191-197.
182. Easley, S.K., et al., *Contribution of the intra-specimen variations in tissue mineralization to PTH- and raloxifene-induced changes in stiffness of rat vertebrae.* Bone, 2010. **46**(4): p. 1162-1169.
183. Fratzl, P., et al., *Structure and mechanical quality of the collagen-mineral nano-composite in bone.* Journal of Materials Chemistry, 2004. **14**: p. 2115-2123.
184. Verhulp, E., et al., *Micro-finite element simulation of trabecular-bone post-yield behaviour - effects of material model, element size and type.* Computer Methods in Biomechanics and Biomedical Engineering, 2008. **11**(4): p. 389-395.
185. Mulder, L., et al., *The influence of mineralization on intratrabecular stress and strain distribution in developing trabecular bone.* Ann.Biomed.Eng, 2007. **35**(10): p. 1668-1677.
186. Giesen, E.B., et al., *Mechanical properties of cancellous bone in the human mandibular condyle are anisotropic.* J.Biomech., 2001. **34**(6): p. 799-803.
187. Giesen, E.B., et al., *Architectural measures of the cancellous bone of the mandibular condyle identified by principal components analysis.* Calcif.Tissue Int., 2003. **73**(3): p. 225-231.
188. Kabel, J., et al., *The role of an effective isotropic tissue modulus in the elastic properties of cancellous bone.* Journal of Biomechanics, 1999. **32**: p. 673-680.
189. Koolstra, J.H., *Dynamics of the human masticatory system.* Critical Reviews in Oral Biology and Medicine, 2002. **13**(4): p. 366-376.
190. Fratzl, P., et al., *Evidence that treatment with risedronate in women with postmenopausal osteoporosis affects bone mineralization and bone volume.* Calcified Tissue International, 2007. **81**: p. 73-80.

191. Bourrin, S., et al., *Recovery of proximal tibia bone mineral density and strength, but not cancellous bone architecture, after long-term bisphosphonate or selective estrogen receptor modulator therapy in aged rats.* Bone, 2002. **30**: p. 195-200.
192. Day, J.S., et al., *Bisphosphonate treatment affects trabecular bone apparent modulus through micro-architecture rather than matrix properties.* Journal of Orthopaedic Research, 2004. **22**: p. 465-471.
193. Gourion-Arsiquaud, S., et al., *Bisphosphonate treatment modifies canine bone mineral and matrix properties and their heterogeneity.* Bone, 2010. **46**(3): p. 666-672.
194. Mashiba, T., et al., *Effects of high-dose etidronate treatment on microdamage accumulation and biomechanical properties in beagle bone before occurrence of spontaneous fractures.* Bone, 2001. **29**: p. 271-278.
195. Misof, B.M., et al., *Differential effects of alendronate treatment on bone from growing osteogenesis imperfecta and wild-type mouse.* Bone, 2005. **36**: p. 150-158.
196. Perez-Lopez, F.R., *Postmenopausal osteoporosis and alendronate.* Maturitas, 2004. **48**(3): p. 179-92.
197. Roschger, P., et al., *Mineralization of cancellous bone after alendronate and sodium fluoride treatment: a quantitative backscattered electron imaging study on minipig ribs.* Bone, 1997. **20**: p. 393-397.
198. Renders, G.A., et al., *Mineral heterogeneity affects predictions of intratrabecular stress and strain.* J.Biomech., 2011. **44**(3): p. 402-407.
199. Ding, M., et al., *Age variations in the properties of human tibial trabecular bone.* J Bone Joint Surg Br, 1997. **79**(6): p. 995-1002.
200. Hernandez, C.J., et al., *The influence of bone volume fraction and ash fraction on bone strength and modulus.* Bone, 2001. **29**(1): p. 74-8.
201. Day, J.S., *Bone quality: The mechanical effects of microarchitecture and matrix properties.* Ph.D. thesis. Department of Orthopaedics, Erasmus MC, Rotterdam, the Netherlands, 2005.
202. O'Flaherty, E.J., *Physiologically based models for bone-seeking elements. I. Rat skeletal and bone growth.* Toxicol Appl Pharmacol, 1991. **111**(2): p. 299-312.
203. Boivin, G., et al., *Influence of remodeling on the mineralization of bone tissue.* Osteoporosis International, 2009. **20**: p. 1023-1026.
204. Labrinidis, A., et al., *Zoledronic acid inhibits both the osteolytic and osteoblastic components of osteosarcoma lesions in a mouse model.* Clin Cancer Res, 2009. **15**(10): p. 3451-61.
205. Pozzi, S., et al., *High-dose zoledronic acid impacts bone remodeling with effects on osteoblastic lineage and bone mechanical properties.* Clin Cancer Res, 2009. **15**(18): p. 5829-39.
206. Hayami, T., et al., *The role of subchondral bone remodeling in osteoarthritis: reduction*

of cartilage degeneration and prevention of osteophyte formation by alendronate in the rat anterior cruciate ligament transection model. Arthritis Rheum, 2004. **50**(4): p. 1193-206.
207. Lories, R.J. and F.P. Luyten, *The bone-cartilage unit in osteoarthritis.* Nat Rev Rheumatol, 2011. **7**(1): p. 43-9.
208. Rodan, G.A. and H.A. Fleisch, *Bisphosphonates: mechanisms of action.* J Clin Invest, 1996. **97**(12): p. 2692-6.
209. Filleul, O., E. Crompot, and S. Saussez, *Bisphosphonate-induced osteonecrosis of the jaw: a review of 2,400 patient cases.* J Cancer Res Clin Oncol, 2010. **136**(8): p. 1117-24.
210. Migliorati, C.A., et al., *Managing the care of patients with bisphosphonate-associated osteonecrosis: an American Academy of Oral Medicine position paper.* J Am Dent Assoc, 2005. **136**(12): p. 1658-68.
211. Bradaschia-Correa, V., et al., *Effect of alendronate on endochondral ossification in mandibular condyles of growing rats.* Eur J Histochem, 2012. **56**(2): p. e24.
212. Migliorati, C.A., M.A. Siegel, and L.S. Elting, *Bisphosphonate-associated osteonecrosis: a long-term complication of bisphosphonate treatment.* Lancet Oncol, 2006. **7**(6): p. 508-14.
213. Bouxsein, M.L., et al., *Guidelines for assessment of bone microstructure in rodents using micro-computed tomography.* J Bone Miner Res, 2010. **25**(7): p. 1468-86.
214. Bab, I., et al., *Micro-tomographic atlas of the mouse skeleton.* Springer Science & Business Media, 2007.
215. De Rossi, A., L.B. Rocha, and M.A. Rossi, *Application of fluorescence microscopy on hematoxylin and eosin-stained sections of healthy and diseased teeth and supporting structures.* Journal of Oral Pathology & Medicine, 2007. **36**(6): p. 377-81.
216. Renders, G.A., et al., *Contrast-enhanced microCT (EPIC-muCT) ex vivo applied to the mouse and human jaw joint.* Dentomaxillofac Radiol, 2014. **43**(2): p. 20130098.
217. Boivin, G. and P.J. Meunier, *Changes in bone remodeling rate influence the degree of mineralization of bone.* Connective Tissue Research, 2002. **43**: p. 535-537.
218. Bala, Y., et al., *Time sequence of secondary mineralization and microhardness in cortical and cancellous bone from ewes.* Bone, 2010. **46**(4): p. 1204-12.
219. Fuchs, R.K., et al., *Bisphosphonates do not alter the rate of secondary mineralization.* Bone, 2011. **49**(4): p. 701-5.
220. Gamsjaeger, S., et al., *Bone material properties in actively bone-forming trabeculae in postmenopausal women with osteoporosis after three years of treatment with once-yearly Zoledronic acid.* J Bone Miner Res, 2011. **26**(1): p. 12-8.
221. Allen, M.R. and D.B. Burr, *Mandible matrix necrosis in beagle dogs after 3 years of daily oral bisphosphonate treatment.* J Oral Maxillofac Surg, 2008. **66**(5): p. 987-94.

222. Allen, M.R., D.J. Kubek, and D.B. Burr, *Cancer treatment dosing regimens of zoledronic acid result in near-complete suppression of mandible intracortical bone remodeling in beagle dogs.* J Bone Miner Res, 2010. **25**(1): p. 98-105.
223. Burr, D.B. and M.R. Allen, *Mandibular necrosis in beagle dogs treated with bisphosphonates.* Orthodontics & Craniofacial Research, 2009. **12**(3): p. 221-8.
224. Vermeer, J.A., et al., *Jaw bone marrow-derived osteoclast precursors internalize more bisphosphonate than long-bone marrow precursors.* Bone, 2013. **57**(1): p. 242-51.
225. Huja, S.S. and F.M. Beck, *Bone remodeling in maxilla, mandible, and femur of young dogs.* Anat Rec (Hoboken), 2008. **291**(1): p. 1-5.
226. Furstman, L., *The early development of the human temporomandibular joint.* Am J Orthod 1963. **49**(9): p. 672-682.
227. Brighton, C.T., *Structure and function of the growth plate.* Clin Orthop Relat Res, 1978(136): p. 22-32.
228. Schenk, R., et al., *Effect of ethane-1-hydroxy-1,1-diphosphonate (EHDP) and dichloromethylene diphosphonate (Cl 2 MDP) on the calcification and resorption of cartilage and bone in the tibial epiphysis and metaphysis of rats.* Calcif Tissue Res, 1973. **11**(3): p. 196-214.
229. Delatte, M., et al., *Primary and secondary cartilages of the neonatal rat: the femoral head and the mandibular condyle.* Eur J Oral Sci, 2004. **112**(2): p. 156-62.
230. Brooks, R.A. and G. Di Chiro, *Beam hardening in x-ray reconstructive tomography.* Phys Med Biol, 1976. **21**(3): p. 390-8.
231. Burghardt, A., et al., *Quantitative Assessment of Bone Tissue Mineralization with Polychromatic Micro-Computed Tomography.* Calcified Tissue International, 2008. **83**(2): p. 129-138.
232. Kazakia, G.J., et al., *Assessment of bone tissue mineralization by conventional x-ray microcomputed tomography: Comparison with synchrotron radiation microcomputed tomography and ash measurements.* Medical Physics, 2008. **35**(7): p. 3170-3179.
233. Deuerling, J.M., et al., *Improved accuracy of cortical bone mineralization measured by polychromatic microcomputed tomography using a novel high mineral density composite calibration phantom.* Med Phys, 2010. **37**(9): p. 5138-45.
234. Sebestyen, J.F., T. Srivastava, and U.S. Alon, *Bisphosphonates use in children.* Clin Pediatr (Phila), 2012. **51**(11): p. 1011-24.
235. Khosla, S., et al., *Bisphosphonate-associated osteonecrosis of the jaw: report of a task force of the American Society for Bone and Mineral Research.* J Bone Miner Res, 2007. **22**(10): p. 1479-91.
236. Reid, I.R., *Osteonecrosis of the jaw: who gets it, and why?* Bone, 2009. **44**(1): p. 4-10.
237. Marx, R.E., et al., *Bisphosphonate-induced exposed bone (osteonecrosis/osteopetrosis) of the jaws: risk factors, recognition, prevention, and treatment.* J Oral Maxillofac Surg,

2005. **63**(11): p. 1567-75.
238. Allen, M.R. and D.B. Burr, *The pathogenesis of bisphosphonate-related osteonecrosis of the jaw: so many hypotheses, so few data.* J Oral Maxillofac Surg, 2009. **67**(5 Suppl): p. 61-70.
239. Bi, Y., et al., *Bisphosphonates cause osteonecrosis of the jaw-like disease in mice.* Am J Pathol, 2010. **177**(1): p. 280-90.
240. Kikuiri, T., et al., *Cell-based immunotherapy with mesenchymal stem cells cures bisphosphonate-related osteonecrosis of the jaw-like disease in mice.* J Bone Miner Res, 2010. **25**(7): p. 1668-79.
241. Aghaloo, T.L., et al., *Periodontal disease and bisphosphonates induce osteonecrosis of the jaws in the rat.* J Bone Miner Res, 2011. **26**(8): p. 1871-82.
242. Aguirre, J.I., et al., *Oncologic doses of zoledronic acid induce osteonecrosis of the jaw-like lesions in rice rats (Oryzomys palustris) with periodontitis.* J Bone Miner Res, 2012. **27**(10): p. 2130-43.
243. Pozzi, S., et al., *High-Dose Zoledronic Acid Impacts Bone Remodeling with Effects on Osteoblastic Lineage and Bone Mechanical Properties.* Clinical Cancer Research, 2009. **15**(18): p. 5829-5839.
244. Ersan, N., et al., *Teriparatide and the treatment of bisphosphonate-related osteonecrosis of the jaw: a rat model.* Dentomaxillofac Radiol, 2013. **43**(1): p. 20130144.
245. Bauss, F., T. Pfister, and S. Papapoulos, *Ibandronate uptake in the jaw is similar to long bones and vertebrae in the rat.* J Bone Miner Metab, 2008. **26**(4): p. 406-8.
246. Wen, D., et al., *Anatomic site variability in rat skeletal uptake and desorption of fluorescently labeled bisphosphonate.* Oral Dis, 2011. **17**(4): p. 427-32.
247. de Souza Faloni, A.P., et al., *Jaw and long bone marrows have a different osteoclastogenic potential.* Calcif.Tissue Int., 2011. **88**(1): p. 63-74.
248. Cornish, J., et al., *Bone-bound bisphosphonate inhibits growth of adjacent non-bone cells.* Bone, 2011. **49**(4): p. 710-6.
249. Coxon, F.P., et al., *Visualizing mineral binding and uptake of bisphosphonate by osteoclasts and non-resorbing cells.* Bone, 2008. **42**(5): p. 848-60.
250. Hokugo, A., et al., *Equilibrium-dependent bisphosphonate interaction with crystalline bone mineral explains anti-resorptive pharmacokinetics and prevalence of osteonecrosis of the jaw in rats.* Bone, 2013. **53**(1): p. 59-68.
251. Pazianas, M., *Osteonecrosis of the jaw and the role of macrophages.* J Natl Cancer Inst, 2011. **103**(3): p. 232-40.
252. Roelofs, A.J., et al., *Fluorescent risedronate analogues reveal bisphosphonate uptake by bone marrow monocytes and localization around osteocytes in vivo.* J Bone Miner Res, 2010. **25**(3): p. 606-16.
253. Hoefert, S., et al., *Altered macrophagic THP-1 cell phagocytosis and migration in*

bisphosphonate-related osteonecrosis of the jaw (BRONJ). Clin Oral Investig, 2015.
254. Katsarelis, H., et al., *Infection and Medication-related Osteonecrosis of the Jaw.* J Dent Res, 2015. **94**(4): p. 534-539.
255. Hoefert, S., et al., *Importance of microcracks in etiology of bisphosphonate-related osteonecrosis of the jaw: a possible pathogenetic model of symptomatic and non-symptomatic osteonecrosis of the jaw based on scanning electron microscopy findings.* Clin Oral Investig, 2010. **14**(3): p. 271-84.
256. Mashiba, T., et al., *Suppressed bone turnover by bisphosphonates increases microdamage accumulation and reduces some biomechanical properties in dog rib.* J Bone Miner Res, 2000. **15**(4): p. 613-20.
257. Fujimura, Y., et al., *Influence of bisphosphonates on orthodontic tooth movement in mice.* Eur J Orthod, 2009. **31**(6): p. 572-7.
258. Igarashi, K., et al., *Inhibitory effect of the topical administration of a bisphosphonate (risedronate) on root resorption incident to orthodontic tooth movement in rats.* J Dent Res, 1996. **75**(9): p. 1644-9.
259. Sirisoontorn, I., et al., *Orthodontic tooth movement and root resorption in ovariectomized rats treated by systemic administration of zoledronic acid.* Am J Orthod Dentofacial Orthop, 2012. **141**(5): p. 563-73.
260. Kozloff, K.M., et al., *Near-infrared fluorescent probe traces bisphosphonate delivery and retention in vivo.* J Bone Miner Res, 2010. **25**(8): p. 1748-58.
261. Adachi, H., et al., *Effects of topical administration of a bisphosphonate (risedronate) on orthodontic tooth movements in rats.* J Dent Res, 1994. **73**(8): p. 1478-86.
262. Storey, E., *The nature of tooth movement.* Am J Orthod, 1973. **63**(3): p. 292-314.
263. Kanzaki, H., et al., *Periodontal ligament cells under mechanical stress induce osteoclastogenesis by receptor activator of nuclear factor kappaB ligand up-regulation via prostaglandin E2 synthesis.* J Bone Miner Res, 2002. **17**(2): p. 210-20.
264. de Vries, T.J., et al., *Myeloid blasts are the mouse bone marrow cells prone to differentiate into osteoclasts.* J.Leukoc.Biol., 2009. **85**(6): p. 919-927.
265. Kanzaki, H., et al., *Dual regulation of osteoclast differentiation by periodontal ligament cells through RANKL stimulation and OPG inhibition.* J Dent Res, 2001. **80**(3): p. 887-91.
266. Henrotin, Y., L. Pesesse, and C. Sanchez, *Subchondral bone in osteoarthritis physiopathology: State-of-the-art and perspectives*. 2009. p. 311-316.
267. Tanaka, E., M.S. Detamore, and L.G. Mercuri, *Degenerative disorders of the temporomandibular joint: etiology, diagnosis, and treatment.* Journal of Dental Research, 2008. **87**(4): p. 296-307.
268. Dijkgraaf, L.C., et al., *The structure, biochemistry, and metabolism of osteoarthritic cartilage: a review of the literature.* Journal of Oral and Maxillofacial Surgery, 1995.

53: p. 1182-1192.
269. Shen, G. and M.A. Darendeliler, *The adaptive remodeling of condylar cartilage---a transition from chondrogenesis to osteogenesis.* J Dent Res, 2005. **84**(8): p. 691-9.
270. Embree, M., et al., *Role of Subchondral Bone during Early-stage Experimental TMJ Osteoarthritis.* J.Dent.Res., 2011. **90**(11): p. 1331-1338.
271. Jiao, K., et al., *Subchondral bone loss following orthodontically induced cartilage degradation in the mandibular condyles of rats.* Bone, 2011. **48**(2): p. 362-71.
272. Huang, Q., et al., *Experimentally induced unilateral tooth loss: histochemical studies of the temporomandibular joint.* Journal of Dental Research, 2002. **81**(3): p. 209-213.
273. Trattnig, S., et al., *Three-dimensional delayed gadolinium-enhanced MRI of cartilage (dGEMRIC) for in vivo evaluation of reparative cartilage after matrix-associated autologous chondrocyte transplantation at 3.0T: Preliminary results*. 2007. p. 974-982.
274. Kurijarvi, J.E., et al., *Evaluation of cartilage repair in the distal femur after autologous chondrocyte transplantation using T2 relaxation time and dGEMRIC*. 2007. p. 372-378.
275. Kameoka, S., et al., *Diagnostic accuracy of microcomputed tomography for osseous abnormalities in the rat temporomandibular joint condyle.* Dentomaxillofac Radiol, 2009. **38**(7): p. 465-9.
276. Chen, J., et al., *Analysis of microarchitectural changes in a mouse temporomandibular joint osteoarthritis model.* Arch Oral Biol, 2009. **54**(12): p. 1091-8.
277. Benders, K.E., et al., *Formalin fixation affects equilibrium partitioning of an ionic contrast agent-microcomputed tomography (EPIC-muCT) imaging of osteochondral samples.* Osteoarthritis.Cartilage., 2010. **18**(12): p. 1586-1591.
278. Liang, G., J. Vanhouten, and C.M. Macica, *An atypical degenerative osteoarthropathy in Hyp mice is characterized by a loss in the mineralized zone of articular cartilage.* Calcif Tissue Int, 2011. **89**(2): p. 151-62.
279. Moyer, H.R., et al., *A new animal model for assessing cartilage repair and regeneration at a nonarticular site.* Tissue Eng Part A, 2010. **16**(7): p. 2321-2330.
280. Kuroda, S., et al., *Biomechanical and biochemical characteristics of the mandibular condylar cartilage.* Osteoarthritis.Cartilage., 2009. **17**(11): p. 1408-1415.
281. Byers, P.D., C.A. Contepomi, and T.A. Farkas, *A post mortem study of the hip joint. Including the prevalence of the features of the right side.* Annals of the Rheumatic Diseases, 1970. **29**: p. 15-31.
282. Hildebrand, T. and P. Ruegsegger, *A new method for the model independent assessment of thickness in three-dimensional images.* J Microsc, 1997. **185**: p. 67-75.
283. Cotofana, S., et al., *Cartilage thickening in early radiographic human knee osteoarthritis - within-person, between-knee comparison.* Arthritis Care Res (Hoboken), 2012.
284. Renders, G.A.P., et al., *Degree and distribution of mineralization in the human*

mandibular condyle. Calcified Tissue International, 2006. **79**: p. 190-196.
285. Joshi, N.S., et al., *Effect of contrast agent charge on visualization of articular cartilage using computed tomography: exploiting electrostatic interactions for improved sensitivity.* J.Am.Chem.Soc., 2009. **131**(37): p. 13234-13235.
286. Hu, K., et al., *Effects of condylar fibrocartilage on the biomechanical loading of the human temporomandibular joint in a three-dimensional, nonlinear finite element model.* Medical engineering and Physics, 2003. **25**: p. 107-113.
287. Beek, M., et al., *Dynamic properties of the human temporomandibular joint disc.* J.Dent.Res., 2001. **80**(3): p. 876-880.
288. Hansson, T., et al., *Thickness of the soft tissue layers and the articular disk in the temporomandibular joint.* Acta Odontologica Scandinavica, 1977. **35**(2): p. 77-83.
289. Lu, X.L., V.C. Mow, and X.E. Guo, *Proteoglycans and mechanical behavior of condylar cartilage.* Journal of Dental Research, 2009. **88**(3): p. 244-248.
290. Bansal, P.N., et al., *Contrast enhanced computed tomography can predict the glycosaminoglycan content and biomechanical properties of articular cartilage.* Osteoarthritis.Cartilage., 2010. **18**(2): p. 184-191.
291. Peel, N., *Bone remodelling and disorders of bone metabolism.* Surgery (Oxford), 2009. **27**(2): p. 70-74.
292. Radin, E.L., I.L. Paul, and R.M. Rose, *Role of mechanical factors in pathogenesis of primary osteoarthritis.* Lancet, 1972. **1**(7749): p. 519-22.
293. Radin, E.R., I.L. Paul, and R.M. Rose, *Pathogenesis of primary osteoarthritis.* Lancet, 1972. **1**(7765): p. 1395-6.
294. Shimizu, M., et al., *Morphometric analysis of subchondral bone of the tibial condyle in osteoarthrosis.* Clin Orthop Relat Res, 1993(293): p. 229-39.
295. Herring, S.W. and Z.J. Liu, *Loading of the temporomandibular joint: anatomical and in vivo evidence from the bones.* Cells Tissues Organs, 2001. **169**(3): p. 193-200.
296. Spector, T.D., *Bisphosphonates: potential therapeutic agents for disease modification in osteoarthritis.* Aging Clin Exp Res, 2003. **15**(5): p. 413-8.
297. Wagner, D.W., D.P. Lindsey, and G.S. Beaupre, *Deriving tissue density and elastic modulus from microCT bone scans.* Bone, 2011. **49**(5): p. 931-8.
298. Cooper, D.M., et al., *Visualization of 3D osteon morphology by synchrotron radiation micro-CT.* J Anat, 2011. **219**(4): p. 481-9.
299. Swain, M.V. and J. Xue, *State of the art of Micro-CT applications in dental research.* Int J Oral Sci, 2009. **1**(4): p. 177-88.
300. Hasslinger, P., et al., *Coupling multiscale X-ray physics and micromechanics for bone tissue composition and elasticity determination from micro-CT data, by example of femora from OVX and sham rats.* International Journal for Computational Methods in Engineering Science and Mechanics, 2016. **17**(3): p. 222-244.

301. Gross, T., et al., *Mineral heterogeneity has a minor influence on the apparent elastic properties of human cancellous bone: a SRmuCT-based finite element study.* Comput Methods Biomech Biomed Engin, 2012. **15**(11): p. 1137-44.
302. Cioffi, I., et al., *Degree of mineralization at the attachment of lateral pterygoid.* Anat. Rec.(Hoboken.), 2010. **293**(8): p. 1387-1392.
303. Brennan, O., et al., *Biomechanical properties across trabeculae from the proximal femur of normal and ovariectomised sheep.* Journal of Biomechanics, 2009. **42**: p. 498-503.
304. Zioupos, P., M. Gresle, and K. Winwood, *Fatigue strength of human cortical bone: age, physical, and material heterogeneity effects.* J Biomed Mater Res A, 2008. **86**(3): p. 627-36.
305. Tanaka, E., et al., *Effect of food consistency on the degree of mineralization in the rat mandible.* Ann.Biomed.Eng, 2007. **35**(9): p. 1617-1621.
306. Skedros, J.G., et al., *Do regional modifications in tissue mineral content and microscopic mineralization heterogeneity adapt trabecular bone tracts for habitual bending? Analysis in the context of trabecular architecture of deer calcanei.* J Anat, 2012. **220**(3): p. 242-55.
307. Lloyd, A.A., Z.X. Wang, and E. Donnelly, *Multiscale contribution of bone tissue material property heterogeneity to trabecular bone mechanical behavior.* J Biomech Eng, 2015. **137**(1).
308. Rasoulian, R., et al., *Reference point indentation study of age-related changes in porcine femoral cortical bone.* J Biomech, 2013. **46**(10): p. 1689-96.
309. Busse, B., et al., *Increased calcium content and inhomogeneity of mineralization render bone toughness in osteoporosis: mineralization, morphology and biomechanics of human single trabeculae.* Bone, 2009. **45**(6): p. 1034-43.
310. Cardoso, L., et al., *Advances in assessment of bone porosity, permeability and interstitial fluid flow.* J Biomech, 2013. **46**(2): p. 253-65.
311. Tonar, Z., et al., *Quantification of compact bone microporosities in the basal and alveolar portions of the human mandible using osteocyte lacunar density and area fraction of vascular canals.* Ann Anat, 2011. **193**(3): p. 211-9.
312. Dvorak, G., et al., *Cortical porosity of the mandible in an osteoporotic sheep model.* Clin Oral Implants Res, 2011. **22**(5): p. 500-5.
313. Britz, H.M., et al., *3D visualization and quantification of rat cortical bone porosity using a desktop micro-CT system: a case study in the tibia.* J Microsc, 2010. **240**(1): p. 32-7.
314. Brennan, O., et al., *The effects of estrogen deficiency and bisphosphonate treatment on tissue mineralisation and stiffness in an ovine model of osteoporosis.* J Biomech, 2011. **44**(3): p. 386-90.

315. Kim, D.G., et al., *Effect of estrogen deficiency on regional variation of a viscoelastic tissue property of bone.* J Biomech, 2013. **46**(1): p. 110-5.
316. Brennan, M.A., et al., *Effects of ageing, prolonged estrogen deficiency and zoledronate on bone tissue mineral distribution.* J Mech Behav Biomed Mater, 2014. **29**: p. 161-70.
317. Bartlow, C.M., et al., *PTH(1-34) and zoledronic acid have differing longitudinal effects on juvenile mouse femur strength and morphology.* J Orthop Res, 2016.
318. Jiang, L., et al., *Effects of bisphosphonates on mandibular condyle of ovariectomized osteoporotic rats using micro-ct and histomorphometric analysis.* J Oral Pathol Med, 2016.
319. Karssemakers, L.H., et al., *Microcomputed tomographic analysis of human condyles in unilateral condylar hyperplasia: increased cortical porosity and trabecular bone volume fraction with reduced mineralisation.* Br J Oral Maxillofac Surg, 2014. **52**(10): p. 940-4.
320. Ames, M.S., et al., *Estrogen deficiency increases variability of tissue mineral density of alveolar bone surrounding teeth.* Arch Oral Biol, 2010. **55**(8): p. 599-605.
321. Brennan, M.A., et al., *Site specific increase in heterogeneity of trabecular bone tissue mineral during oestrogen deficiency.* Eur Cell Mater, 2011. **21**: p. 396-406.
322. Forlino, A., et al., *New perspectives on osteogenesis imperfecta.* Nat Rev Endocrinol, 2011. **7**(9): p. 540-57.
323. Edwards, B.J., et al., *Bisphosphonates and nonhealing femoral fractures: analysis of the FDA Adverse Event Reporting System (FAERS) and international safety efforts: a systematic review from the Research on Adverse Drug Events And Reports (RADAR) project.* J Bone Joint Surg Am, 2013. **95**(4): p. 297-307.
324. Burket, J.C., et al., *Variations in nanomechanical properties and tissue composition within trabeculae from an ovine model of osteoporosis and treatment.* Bone, 2013. **52**(1): p. 326-36.
325. Fradique, R., et al., *Production of new 3D scaffolds for bone tissue regeneration by rapid prototyping.* J Mater Sci Mater Med, 2016. **27**(4): p. 69.
326. Cook, D., M. Julias, and E. Nauman, *Biological variability in biomechanical engineering research: Significance and meta-analysis of current modeling practices.* J Biomech, 2014. **47**(6): p. 1241-50.
327. Mailhiot, S.E., et al., *Non-Invasive Quantification of Cartilage Using a Novel In Vivo Bioluminescent Reporter Mouse.* PLoS One, 2015. **10**(7): p. e0130564.
328. Delecourt, C., et al., *Cartilage morphology assessed by high resolution micro-computed tomography in non OA knees.* Osteoarthritis Cartilage, 2016. **24**(3): p. 567-71.
329. Boerckel, J.D., et al., *Microcomputed tomography: approaches and applications in bioengineering.* Stem Cell Res Ther, 2014. **5**(6): p. 144.

330. Blanchard, R., et al., *Intravoxel bone micromechanics for microCT-based finite element simulations.* J Biomech, 2013. **46**(15): p. 2710-21.
331. Topolinski, T., et al., *The relationship between trabecular bone structure modeling methods and the elastic modulus as calculated by FEM.* ScientificWorldJournal, 2012. **2012**: p. 827196.
332. Yeni, Y.N., et al., *Variability of trabecular microstructure is age-, gender-, race- and anatomic site-dependent and affects stiffness and stress distribution properties of human vertebral cancellous bone.* Bone, 2011. **49**(4): p. 886-94.
333. Chang, P.C., et al., *Functional apparent moduli as predictors of oral implant osseointegration dynamics.* J Biomed Mater Res B Appl Biomater, 2010. **94**(1): p. 118-26.
334. Dejaco, A., et al., *Micro CT-based multiscale elasticity of double-porous (pre-cracked) hydroxyapatite granules for regenerative medicine.* J Biomech, 2012. **45**(6): p. 1068-75.
335. Oftadeh, R., et al., *Biomechanics and mechanobiology of trabecular bone: a review.* J Biomech Eng, 2015. **137**(1).
336. Nyman, J.S., et al., *Predicting mouse vertebra strength with micro-computed tomography-derived finite element analysis.* Bonekey Rep, 2015. **4**: p. 664.
337. Depalle, B., et al., *Finite element dependence of stress evaluation for human trabecular bone.* J Mech Behav Biomed Mater, 2013. **18**: p. 200-12.
338. Chen, Y., et al., *Large-scale finite element analysis of human cancellous bone tissue micro computer tomography data: a convergence study.* J Biomech Eng, 2014. **136**(10): p. 101013.

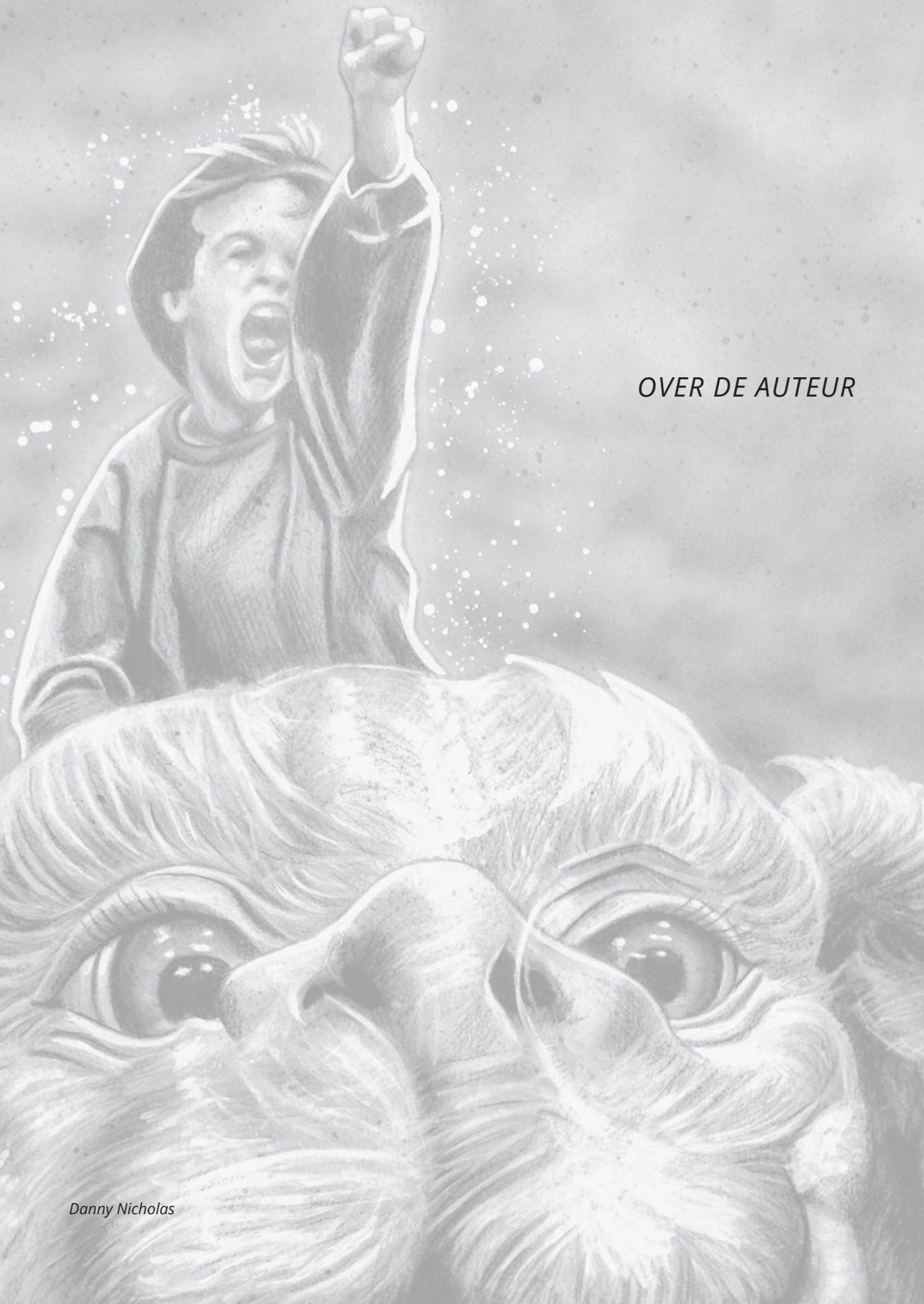

OVER DE AUTEUR

Danny Nicholas

Over de auteur

Geschreven door mijn moeder

Ons Greetje, geboren op 21 oktober 1979 als derde dochter op een zondag. Ze was precies met 40 weken om 9:30, woog 3000 gram en 50cm lang. Toen was ze al precies in alles en dit is altijd zo gebleven.

Ze was een bijzonder kindje, altijd vrolijk, kon zich goed vermaken in haar eentje, maar ook met andere kinderen en haar zusjes. Ze had ook haar eigen wereldje en was erg handig. Ze speelde graag met technische lego en bouwde altijd moeilijke dingen weer tot een geheel. Ze hield erg veel van dieren, reed paard en verzorgden ze ook helemaal zelf. Ze was ook een onderzoeker, wat zit er in dat ei? Hoelang kan een kuikentje blijven leven als ik ze opsluit…? Ze sleutelde met haar papa aan de tractor en bouwden er een nieuwe motor in. Ze bouwde konijnenhokken en dergelijke. Haar interesses waren breed. Ze heeft bijvoorbeeld jaren voor een roofvogelasiel gewerkt.

Op driejarige leeftijd was ze kwijt waardoor iedereen in paniek was. Na een half uur werd ze gevonden. Ze was aan het proberen hoe het water uit de drinkbakjes kwam bij de koeien. Verder had ze een knuffel, Woefje, en sliep niet zonder dat hondje. Ze liet Woefje soms ergens in de tuin liggen en we moesten dan zoeken tot ze het weer in haar bedje had. Pfffff…

Met haar 3 à 4 jaar peuterde ze schedeltjes vanuit allerlei diertjes en verzamelde deze schedeltjes. Ontdekken en onderzoeken zo klein als ze was. Kleren vond ze niet zo belangrijk, als het maar fijn zat om in te werken en spelen. Ze was een bezige bij. Ze wordt niet snel boos, maar als ze boos is, is ze een tijger…

Greetje was erg leergiering, precies en een onderzoeker. Hoe zit dit, hoe zit dat?

Zo, een kort verhaaltje

Mama en Papa†

Tot op heden is Greetje werkzaam in Amersfoort als tandarts. En, met uitzondering van een korte periode, is zij nog altijd werkzaam op ACTA. Sinds augustus 2014 als klinisch docent. Met deze uitdaging zal zij in augustus van dit jaar stoppen om verder te gaan naar het volgende avontuur: De differentiatie Orale Kinesiologie.